Enhanced Flotation of Ultramafic Nickel Ores Using Carbon Dioxide as a Flotation Gas and Sodium Tripolyphosphate as a Serpentine Depressant

by

Nzubechukwu Chukwuebuka Ezeonyi

A thesis submitted in partial fulfillment of the requirements for the degree of

Master of Science
in
Chemical Engineering

Department of Chemical and Materials Engineering
University of Alberta

Abstract

Challenges in the processing of minerals have been on the rise due to increasing low-grade ores which require to be finely ground to liberate valuable minerals. Low-grade ores like the ultramafic ores contain large amounts of gangue minerals which impacts recovery of the valuable pentlandite minerals. In ultramafic nickel ores, serpentine (MgO-bearing mineral) slime-coats and decreases the recovery of the nickel-bearing pentlandite. To improve the recovery of pentlandite and subsequently suppress serpentine in ultramafic nickel ores, CO_2 gas (either as a depressant or a flotation gas) and sodium tripolyphosphate (STPP) as a reagent for serpentine depression are used in this study. Phosphate groups in STPP chelate magnesium ions and can facilitate serpentine depression in flotation systems. CO_2 can also precipitate divalent cations like magnesium cations, and due to the high solubility of CO_2 gas, it can form fine bubbles on hydrophobic valuable minerals to improve their recovery. The surface charge on the serpentine samples were completely reversed upon either the introduction of STPP at above 10 mg/L or by conditioning the suspension with CO_2 gas during zeta potential measurements. The resulting negative charge of the serpentine minerals indicates that the heterogeneous agglomeration with pentlandite surface is weakened, which should allow for a more pentlandite floatability. Subsequently, an optimum concentration of 50 mg/L was obtained which was then used to perform XPS analysis and flotation tests. Flotation benefits were achieved as serpentine depression and enhanced pentlandite recovery was observed for both STPP and CO_2 cases. STPP was more effective in depressing serpentine by 5%, while the highest pentlandite recovery of 88% was obtained when CO_2 was used as a flotation gas, which is a 20% increase in recovery from the baseline case. The more effective STPP depressing ability was validated by XPS results and provides an opportunity to explore the combination of STPP and CO_2 in future studies. Results from this study further re-emphasizes the need to explore

the decarbonization strategy of using CO_2 in flotation circuits and in mineral processing in general, while simultaneously improving recovery. This research also provides some information about the progress of CO_2 in the mining industry and will serve as a guide for researchers to perform more experiments in the direction of CO_2-assisted flotation.

Preface

This thesis is an original work conducted by Nzubechukwu Chukwuebuka Ezeonyi.

The thesis especially Chapters 3, 4, and 5 is planned to be published in International Mineral Processing Congress (IMPC) 2024 conference proceedings. The abstract for the paper titled "Enhanced flotation of ultramafic nickel ores using CO_2 as a flotation gas and sodium tripolyphosphate (STPP) as serpentine depressant", has been accepted under the abstract number 4300. The authors are listed as Nzubechukwu C. Ezeonyi, Omar B. Wani, Erin R. Bobicki, and Farzaneh Sadri. The manuscript has been submitted and I have been assigned a poster presentation for the conference taking place from September 29 to October 3, 2023, at the National Harbor, Washington, DC.

I was responsible for experiment execution, editing, data collection, and analysis of the generated data as well as the manuscript composition. Dr. Bobicki and Dr. Farzaneh Sadri were the supervisory authors and assisted with the conceptualization, manuscript composition and revisions. Dr. Omar Wani assisted with the conceptualization, experimental ideas, manuscript composition, and editing.

Acknowledgement

I would like to express my sincere gratitude to my supervisor Dr. Erin Bobicki for granting me opportunity to be part of her bubble group at the University of Alberta and all the support she provided me during the course of my program. I would like to specially express my profound gratitude to Dr. Farzaneh Sadri for accepting me to be under her review as my co-supervisor, and also for her keen interest in my work and well-being, scholarly advice, scientific approach, and great communication of information which were essential towards accomplishing this thesis work. I also extend an acknowledgement to the departmental leadership especially Dr. Vinay Prasad and Dr. Hao Zhang for their timely intervention and support to ensure the successful completion of my program. I am grateful to the department of Chemical and Materials Engineering for all the financial support during my program and to the Graduate and Postdoctoral Studies (GPS) for awarding me Graduate Student Engagement Scholarships for two consecutive terms.

I owe a deep sense of gratitude to my former bubble group members Dr. Omar Wani and Caroline da Costa Gonçalves for their great involvements, timely suggestions, contributions, meaningful discussions, and great scientific/literature idea that were pivotal in this thesis research. I am also grateful for all the valuable contributions and meaningful discussions from Dr. Chao Qi and Dr. Mingda Li, and for all the lab supports received from Jim Skwarok and Shiraz Merali. I am thankful to the nanoFAB staff members especially to Peng Li for introducing me to the lab procedures/trainings, to XueHai Tan for performing the XRD analysis, and to Shihong Xu for conducting the XPS analysis. I would like to give a special acknowledgment to Allan Harm from the Renewable Resources Department for performing all ICP-OES measurements. I would like to specially thank Dr. Hongbo Zeng for always authorizing me to use his lab facilities; and Dr. Qi Liu for providing me the CO_2 gas cylinder that was used for this thesis work. I would like to give a special mention to Youngxiang Sun and Lin Yang from Dr. Hongbo Zeng's group for always making their labs accessible to me even during weekends. Same special mention also goes to Kaipeng Wang and Hanyu Zhang from Dr. Qi Liu's group for their assistance with delivering the CO_2 gas cylinder and other accessories.

Furthermore, I would like to thank my parents, siblings, friends, and other members of Dr. Bobicki's group (Rebecca Achina-Obeng, Inês Luís, and Chris Zerr) that supported me throughout

my study program through prayers, moral encouragements, social support, and scientific contributions. Most specially, I am very grateful to my fiancé Chinaza for her unconditional love and support. She was always comforting especially when it becomes very stressful, and I am grateful for that. Finally, I would like to thank the Almighty God for life, strength, and the ability to carry out this thesis successfully.

Table of Contents

List of Tables

List of Figures

1. Introduction

1.1. Background

Heavy industrial processes like burning of fossil fuels, mining, construction, etc., are the leading causes of climate change, greenhouse gas emissions and high levels of atmospheric carbon dioxide. These impacts continue to rise due to modernization, increased global population and increased demand for raw materials. As a result, there has been a continuous depletion of high-grade ores and an increased shift towards processing of low-grade ores in order to meet the demand for raw materials, especially the critical metals. Data has shown (**1**) that critical metals are found in low-grade and finely disseminated ores either as the product or by-product which have opened discussions (**2-5**) about a possible depletion of mineral resources. In low-grade ores like the ultramafic nickel ores which generates a lot of fine particles in the comminution stage, the valuable pentlandite (which contains the critical nickel metal) is slime-coated by the fibrous/gangue serpentine mineral, thereby impacting the recovery of nickel-pentlandite in flotation systems (**6**).

One main parameter that has been recognized as a booster for the recovery of fine particles in flotation systems is the presence of small bubbles which promotes particle aggregation, improving the overall performance of the process. In the last decades, it has been proven that the addition of fine bubbles promotes improvements in fine mineral flotation recovery (**7, 8**). In terms of fine bubbles for froth flotation, CO_2 tends to produce finer or smaller bubbles when compared to other gasses/air because of its increased solubility (**9-11**). The fine bubbles can be generated by different methods and spargers and are often called nanobubbles and microbubbles. Although small bubbles are a potential solution to process fine low-grade ores, the fundamental understanding of how they perform and their efficiency at more complex flotation systems are still lacking, especially due to technological limitations regarding in-situ measurements and observations of bubble-particle aggregation. The benefits claimed by recent research in laboratory scale using what is currently known about froth flotation cannot yet support industrial operations, and divergences are common. This explains the quick growth of scientific research with terms such as fines, microbubbles, and nanobubbles which follow the same trend for the term low-grade ore (**Figure 1**). In addition to

promoting fine mineral aggregation, fine bubbles can also be used to facilitate removal of slimes from the surface of valuable minerals (**12**).

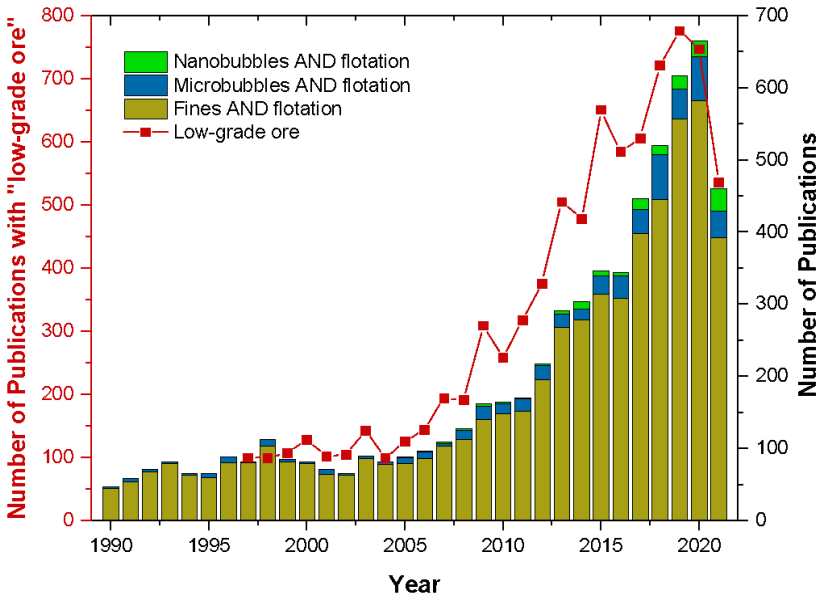

Figure 1: Comparison of the number of publications from 1990 to 2021 showcasing low-grade ores, fines, flotation and micro-/nano-bubbles, using the database Web of Science from Clarivate.

Liberating valuable minerals in low-grade ores requires the ore to be finely ground which result in challenging issues. The gangue minerals which are also finely ground, slime-coat the valuable minerals thereby increasing the slurry viscosity and decreasing the recovery of the valuable minerals in the flotation process (**6,13**). To address the issue of poor flotation kinetics of low-grade ores like the ultramafic nickel ores, the use of CO_2 fine bubbles as a flotation gas will be used to both facilitate the removal of the gangue minerals from the valuable minerals' surface and improve the aggregation of the valuable minerals to the froth phase. This research will also explore the use of sodium tripolyphosphate (STPP) as a reagent for suppressing serpentine (**14**), which has never been applied in ultramafic nickel ores or pentlandite-serpentine mineral mixtures.

Understanding interactions of CO_2 with mineral surfaces are necessary towards its wide acceptance in the mineral processing and mining industry. CO_2 interactions involve investigating parameters like contact angle, bubble size, particle size, surface tension, slurry and flotation pH, and zeta potential. The proper understanding of the behaviour of CO_2 with respect to these

parameters are required to explain their interactions with mineral surfaces and subsequent application in mining operations. In mineral processing, CO_2 has been used as a flotation gas (**15-17**). It can be used for other purposes such as a depressant (**18,19**), or a pH regulator (**20,21**). It has also been used for pre-conditioning prior to flotation with other gasses (**22**). These studies mostly focused only on improving the flotation kinetics of other sulphide minerals but not pentlandite. The closest study to explore the use of CO_2 gas in ultramafic nickel ores was performed by Wani and Co-workers, where they used CO_2 in a preconditioning stage prior to air flotation to improve pentlandite recovery (**23**). Their results provided a good background to further explore the use of CO_2 as a flotation gas instead of air in the processing of ultramafic nickel ores which is presented in this study.

By exploring the use of CO_2 as a flotation gas and STPP as a serpentine depressant, they present the advantage of interacting with the divalent cations (Mg^{2+} from the Mg-Silicate gangue minerals and any Ca^{2+} from the process water) and facilitating their removal (**14,24**), thereby reducing slime coating and slurry viscosity while enhancing the recovery of valuable nickel mineral (pentlandite). This research also aims to highlight the importance of commercializing CO_2 for flotation recovery improvements and for decarbonization purposes by simultaneously storing carbon/CO_2 in mineral form, a climate change mitigation strategy that will not only benefit the mining industry in terms of obtaining carbon credits but will generally benefit Canada in terms of reduction of its greenhouse emissions.

1.2. Hypothesis

CO_2 can exhibit both aggregation and dispersion abilities. As already mentioned, MgO bearing minerals and divalent cations are known to have impact on the separation and rheology of ultramafic nickel ores under ordinary conditions (i.e., with air as a flotation gas). Introducing CO_2 as a flotation gas in the processing of ultramafic nickels has the potential of depressing serpentine and decreasing the slime coating of pentlandite. By injecting CO_2 gas in the flotation system, charge reversal of serpentine should occur and any divalent cations (Mg^{2+} and Ca^{2+}) present should precipitate to form the mineral carbonates, $MgCO_3$ and $CaCO_3$ respectively. These carbonates or reversed serpentine surfaces have similar negative surface charges as pentlandite and do not slime-

coat pentlandite. Dispersion of the serpentine particles will occur, and by precipitating out the divalent cations from solution as carbonates, slurry viscosity is reduced as well as enhanced recovery and grade of the nickel mineral. Moreover, the more soluble and hydrophobic CO_2 bubbles can attach better to the valuable pentlandite minerals and enhance their aggregation to the froth phase. On the other hand, STPP can depress serpentine by complexing the magnesium cations with its phosphate groups, thereby enhancing the flotation of pentlandite in ultramafic nickel ores.

1.3. Research objectives

The main purpose of this research is to investigate the use of CO_2 as a flotation gas in comparison to air flotation. The research focuses on CO_2 flotation of a sulphide mineral, pentlandite. CO_2 gas is employed as both a flotation gas and as a depressant in separate experiments. STPP is solely investigated as serpentine depressant while following expected flotation benefits. Hence, the study of the interactions of CO_2 gas and STPP with mineral surfaces will be performed. The objectives are summarized under two broad categories as follows:

1.3.1. Surface study of mineral surfaces and their interactions with CO_2 and STPP reagents.

These studies involve zeta potential measurements and XPS analysis. These studies are necessary to demonstrate how CO_2 bubbles or STPP can alter surface charge or composition of mineral surfaces, thereby enhancing dispersion of the gangue minerals and facilitating slime coating removal, resulting in improved hydrophobicity and floatability of the valuable minerals.

1.3.2. Investigating the effect of CO_2 and STPP on the flotation recovery of pentlandite ($(Fe,Ni)_9S_8$).

The study here involves exploring the flotation benefits (*i.e.* improved pentlandite recovery) that should be achieved by potential suppression of serpentine using either CO_2 gas or STPP reagent. This objective explores both air and CO_2 as flotation gases while STPP is utilized solely as a depressant in a microflotation setup. In addition to being used as a flotation gas, the depressing capabilities of CO_2 gas is investigated as well. Common flotation reagents like the potassium amyl

xanthate (PAX) collector and methyl isobutyl carbinol (MIBC) frother are used to perform the experiments.

1.4. Scope of thesis

This thesis is divided into five chapters or sections, and they cover the following aspects summarized below.

- Chapter 1 introduces the main challenges and reasons for the study, followed by explicit statement of the hypotheses and objectives of the study.
- In Chapter 2, detailed literature review encompassing the fundamental aspects of froth flotation; fine bubble and CO_2 flotation; discussion about complexity of ultramafic nickel ores and the role of CO_2, and an introduction to the effect of STPP as a flotation depressant are conducted.
- Chapter 3 involves detailed description of all the methods and materials employed in the study.
- Chapter 4 presents the results of the experiments performed in this study. It starts with mineral sizes determination for zeta potential measurements, followed by three different zeta potential measurements under different conditions/reagents. Thereafter, flotation studies using different gasses, different serpentine depressants, and detailed comparisons of each of the experimental cases are performed. This chapter also explores XPS analyses using different reagents, expands further to discuss these experimental types under different reagents/conditions, and provides underlying mechanisms of reactions.
- Chapter 5 puts together the main conclusions of the study and provides recommendations for further studies.

2. Literature review

2.1. Introduction to mineral processing and froth flotation

Minerals are homogeneous substances with a solid three-dimensional crystalline structure (at 25ºC), specific chemical composition, and commonly inorganic that naturally occur as a result of geological processes. They are classified according to their constituents (**25**) and three criteria must be met to form a mineral (**26**). They include sufficient abundance and appropriate proportions of elements, favourable physical and chemical conditions (temperature, pressure, available oxygen, pH, or the presence of water), and sufficient time for the atoms to arrange into a crystalline structure. Rocks, on the other hand, are solid masses of geological materials that may include minerals, fossils, or non-mineral substances like glass. When these minerals are concentrated to the point of being economically viable for recovery with the available technology, a rock mass becomes an ore deposit (**26**).

Some authors emphasize the scarcity and exhaustion of our mineral resources (**27**) based on the drop of grades of processed ores (**1**) and newly discovered deposits over the years. High-grade ores might deplete since they can be exhausted before being renewed by natural processes (**4**). Due to the depletion of high-grade ores, attention has been shifted to low-grade ores to address scarcity of mineral resources. Opposingly, other authors (**2,3**) advocate for a broader analysis of the term "low-grade ore" which should consider several factors such as demand, price, geopolitics, and deposit type. High commodity prices allow the exploration of lower grade ores, changing the cut-off grade (**3,28**). Including low-grade deposits resulted in a slight increase of mineral reserves of copper and zinc overtime due to new mining methods and mineral processing technologies that allow the exploitation of low-grade ores (**29**). For instance, it is known the average copper grade of processed ores is decreasing but the high demand and price stimulate the optimization of current processing strategies, and this becomes clear when major copper production originates from operations considered of low-grade (**28**). In those cases, higher amounts of ore have to be processed to yield the same amount of final product.

Mineral processing involves the liberation and separation of valuable minerals contained in an ore. Mineral liberation is achieved by a given number of size reduction and classification unit

operations, which involve, generally, crushing and grinding operations (**30-32**). Lotter and co-workers explained that when a mineral particle is completely detached from other substances, it is said to be "free", meaning that 100% liberation or almost was achieved, otherwise, a mineral particle is considered locked when surrounded by gangue particles (**32**). In real systems, different degrees of liberation will occur between these two extremes. The main reason is that mineralogy and texture of an ore can greatly differ from one deposit to another, even if the ore type is the same. In the situation where a valuable mineral is fully liberated, adequate particle size reduction is required to achieve liberation which can further reduce the particle size of the valuable mineral and can be significantly costly (**32**). Fine and ultrafine grinding is therefore necessary to liberate valuable sulphides in composite particles (**30**). However, the liberation of ores of low-grade and complex mineralogy poses a different level of challenges to their comminution but also to mineral concentration or separation stages due to the generation of fine and ultrafine particles.

Mineral concentration stages allow the separation of gangue (waste minerals) from valuable minerals contained in a deposit, concentrating them into a smaller volume. This volume is easier and more economic to transport, and it also facilitates further refining processes (as needed). Most of the concentration techniques rely on the difference of physical and surface chemistry properties between different minerals (**33-36**) such as sensor-based ore sorting (optical properties, conductivity, or differential heating), gravity methods (differential densities), magnetic concentration (magnetic susceptibility), and froth flotation (differential surface wettability). Moreover, the applicability and performance of each method (and equipment) depends on the particle size range and on how liberated those particles are. Each mineral processing technique has a particle size optimal range to achieve the best possible results. The limit size range for a particular technique is also highly dependent on each ore type and mineralogy. Froth flotation appears to cover a wider range of particle sizes, but its optimum range lies within 10 and 300 μm (**33-36**). Due to the impact of the presence of fine and ultrafine particles on froth flotation processes some basic principles of this concentration technique are reviewed in the following section.

2.2. Principles of froth flotation

Froth flotation is a common mineral separation technique employed in the mining and mineral processing industry that depends on the differences in the surface properties of minerals. The surface property in which froth flotation relies on is the differential surface wettability or hydrophobicity of the valuable minerals (**36**). Froth flotation involves three phases: solid phase, liquid phase, and gas phase (**36, 41**). The hydrophobic valuable minerals (solid phase) attach to gas bubbles (gas phase) and are collected as froth, while the gangue minerals (solid phase) are hydrophilic or wetted and remain in the liquid phase. Mouat (**39**) describes froth flotation as "the greatest single metallurgical improvement in the modern era", due to its versatility, wide applicability, and ability to process large volumes of ore. This technique has allowed the processing of lower grade ores since the beginning of the 20th century (**40**). It is also the most interesting mineral processing technique from an economical point of view. Klimpel (**41**) considers there are three major components of a flotation system: chemistry, equipment, and operational components (**Figure 2**). Ultimately, these components incorporate a number of factors (some interdependent) which can be controlled in order to achieve the desired performance. According to the author (**41**), "the nature of flotation is that many of the factor settings involved with the various components are either self-compensating or capable of strongly reinforcing desired or undesired system performance".

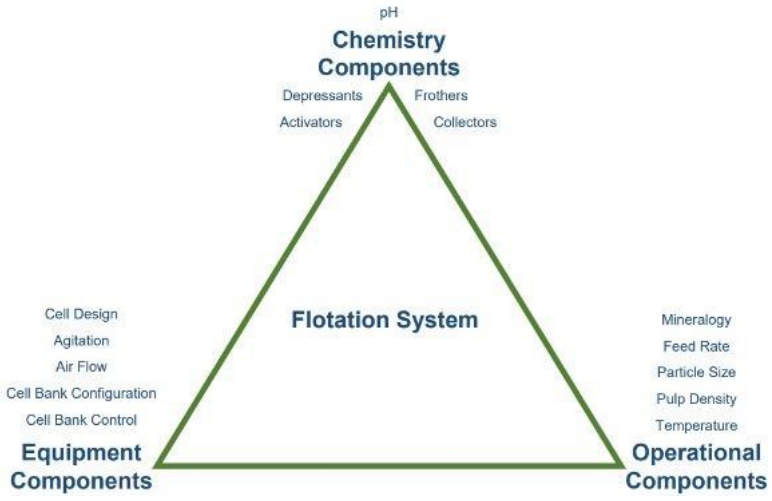

*Figure 2: Major components of a flotation system. Adapted from (**41**).*

As previously stated, froth flotation relies on the difference of surface wettability (natural or induced) of distinct minerals usually given in terms of the contact angle (θ) (**Figure 3**). Some minerals are wetted by water (hydrophilic minerals), while others are repelled by it (hydrophobic minerals) (**35**). Thus, the greater the contact angle, the higher the hydrophobicity degree of the mineral particle.

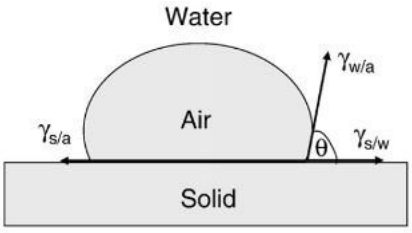

*Figure 3: Schematic description of the contact angle of an air bubble attached to a solid particle in water. Modified from (**42**).*

The angle formed between the solid surface and the air bubble is due to the tensile forces in this system. At equilibrium, these forces can be described by the Young's equation as

$$\gamma_{solid/air} = \gamma_{solid/water} + \gamma_{water/air} \cos\theta \quad (1)$$

where γ represents the surface tension (or surface energy in the case of solid/air interface) between elements of the system, and θ is the contact angle between the solid surface and the water. Once a bubble and a particle attach, the force necessary for the detachment to occur is called work of adhesion (**36, 42**) given by

$$W_{solid/air} = \gamma_{water/air} + \gamma_{solid/water} - \gamma_{solid/air} \quad (2)$$

Combining the two equations above **(Equations (1) and (2))**, the Young-Dupré expression (**Equation 3**) is obtained as

$$W_{solid/air} = \gamma_{water/air} (1 - \cos\theta) \quad (3)$$

2.2.1. Flotation reagents

The surface chemistry of a mineral particle can be modified by flotation reagents such as collectors, depressants, and activators. Collectors are organic substances that increase the hydrophobicity of the minerals or turn hydrophilic minerals hydrophobic (**35**). Excluding the non-ionizing collectors (used with naturally hydrophobic minerals like coal), collectors are heteropolar compounds constituted by a hydrocarbon chain with a polar functional group – that adsorbs onto the mineral surface – which can be negatively or positively charged (**36**). Thus, they divided ionizing collectors into two large groups: anionic and cationic, depending on the charge of the functional group attached to the hydrocarbon chain. For example, most sulphide minerals in the operational flotation pH range (2-11) present a negative zeta potential (chalcopyrite, galena, pentlandite etc.). Anionic collectors, specifically compounds from the sulfydryl (thiol) group such as xanthate adsorb onto sulphide minerals and help to increase their recovery. Adsorption of thiol collectors are specific (*i.e.,* chemisorption). Another collector adsorption can be physisorption. The oxyhydryl type of anionic collectors and cationic collectors are mostly used in the flotation of non-sulphide minerals.

Modifiers on the other hand, also known as regulators, help to target the collectors' effect, either by rendering some minerals hydrophilic (depressants), or by improving the hydrophobicity of the mineral surface (activator) and have been extensively reviewed by (**43**). Modifiers can also function as dispersants or assist by adjusting the pH of the flotation slurry (**36**). Will and Finch described depressants as a class of modifiers used to limit or prevent the flotation recovery of uninterested or gangue minerals by making them more hydrophilic and unable to attach to gas bubbles (**36, 37**). They highlighted that depressants' mechanisms can act either independently or interdependently and they include: "adsorption of hydrophilic species; blocking of collector adsorption sites; removal (desorption) of activating species (deactivation); and removal of hydrophobic sites (desorption/destruction of adsorbed collector)". Nagaraj and Ravishankar 2007 (**43**), classified the depressants into small organics, organic polymers, and inorganics. Inorganic depressants have wide applications in the flotation of sulphide minerals and typical examples are sulfur dioxides, cyanides, phosphates etc. STPP is an inorganic depressant used in this thesis work to depress serpentine and is further discussed in **Section 2.10.** STPP reagent and its role in addressing the complexity of nickel bearing minerals. Additionally, there is a class of flotation reagents called frothers which do not alter the surface chemistry but helps to form and stabilize the

froth (discussed further in **Section 2.5.1.** Frothers), thus improving the efficiency of the process (36).

The use of reagents has such a paramount significance that Nagaraj and Farinato (**44**) divided the evolution of froth flotation in five phases consisting of the early period, discovery and expansion, rational and targeted design, new optimization methods, and the emerging phase. The transition from the early period to the discovery and expansion (1920-1950) occurred when the mineral processing industry started to adopt chemicals such as xanthates, dextrin, and short chain alcohols previously employed in other industries. From 1950 to the beginning of 2000's, several reagents were manufactured specifically for flotation applications. However, the authors (**44**) established a fourth phase at the beginning of the 90's which was also marked by new methodologies and approaches for the optimization and reagent selection in plant practices, and an increasing interest for mineralogical aspects. Furthermore, the emerging phase began approximately 13 years ago, when topics such as mining sustainability started to appear more frequently and problems such as low-grade ore processing started to be addressed (**Figure 1**).

2.2.2. Flotation devices

The understanding of the kinetic factors becomes more evident in a flotation mechanical cell where air or any other gas is injected and released at the bottom of the cell, creating bubbles that disperse within the pulp (**35**). The hydrophobic minerals tend to attach to these bubbles and rise (concentrate), being collected in the froth, and the hydrophilic minerals sink (tailings) (36). When aggregates of mineral particles with bubbles reach the top of the cell, mineral particles remain attached to them if the froth is stable enough, otherwise the bubble collapses and "drop" the mineral particles (**36,37**). However, mechanical cells have shown in the past their inefficiency regarding the processing of fine particles due to their low probability of collision with air bubbles and entrainment tendency (**35**). In a flotation column, a similar process happens. Nevertheless, some hydrodynamic differences, caused by geometric and manufacturing variations, make column cells a better solution for the recovery of fine particles (**35**). The impeller is replaced by a sparger placed at the bottom of the cell. Together with the long geometry of the column, a longer flotation time is allowed for the particles, promoting bubble-particle interactions, and decreasing their detachment probability (**35**). Wash water sprinkles are usually installed on the top, reducing

gangue entrainment. Along with the deeper froth bed, this reduces entrainment of undesirable particles, increasing the overall concentrate grade, rendering this type of cells a great solution for cleaning stages (**45**).

The flotation process is determined by three distinct phenomena that directly affect recovery which are particle-bubble collision, particle attachment to the bubble, and particle detachment from the bubble (**46, 47**). The probability of collision and attachment models are reviewed in several papers (**47, 48**), and a more fundamental analysis of those topics regarding the froth flotation of fine particles is discussed in subsequent sections.

2.3. Flotation mechanism

2.3.1 Froth flotation fundamentals

Low-grade and finely disseminated ores often require fine grinding to liberate valuable minerals, which generate fine particles. There is no consensus about the size interval to describe a fine mineral particle in terms of diameter, and it is often interchangeably used with ultrafines. The main reason is that the floatability of fine particles seems to be related to the mineral's properties such as density (**49**) and morphology. As briefly stated by Ralston (**50**), coal particles considered fines have a size varying from 100 to 200 μm, while for some sulphides, fines are fractions below 5 μm. Overall, the flotation behavior of fine particles can also be partially clarified by studying all subprocesses, namely, particle-bubble collision, attachment, and stability (detachment). However, if a fine or ultrafine particle successfully collides and attaches to a conventional size air bubble, the probability of detachment is negligible (**48**). Therefore, detachment is not considered in the literature review for this thesis because it seems an issue more related to the flotation of coarser mineral particles which occurs when the particle's kinetic energy is the same or superior to its detachment energy (**51**).

2.3.2. Particle-bubble interaction

2.3.2.1. Particle-bubble collision

For simplification, particle-bubble interactions are based on the analysis of forces present in the three-zone particle collection model proposed by Derjaguin and Dukhin in 1961 (**48**, **50, 52, 53**) for a rising bubble and a falling particle (**Figure 4**a).

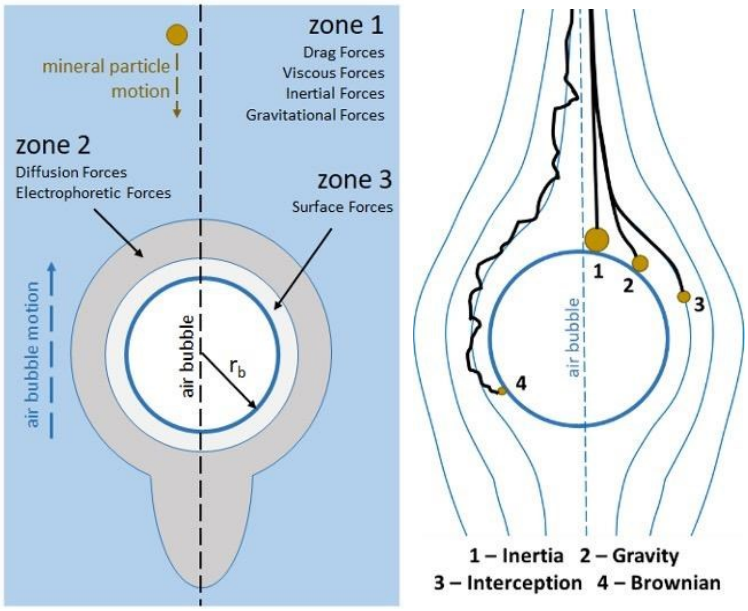

*Figure 4: Schematic representation of the three-zone model for the interaction between small to medium size mineral particles and air bubbles (a). Main forces in the collision mechanisms according to particle size (b). Note: the thickness of all zones, bubble size and particle size do not correspond to reality and are only considered for illustration. Modified from (**52,53, 62**].*

A mineral particle in zone 1 is subjected to hydrodynamic forces which are those that do not favor collisions such as drag forces (particle sweeping motion) and viscous forces (relative deceleration). Favoring forces include particle inertial and gravitational forces which pull the particle in the bubble direction. However, for small particles, some of these forces may not be applied as their collision is mostly governed by interception forces (**52**) (**Figure 4**b particle 3). Hence, when modeling, pathlines of small particles are considered to be the same as the fluid streamlines

(**Figure 4**b particle 3) (**53**). Due to their small mass, fine particles are also under Brownian motion (**50)** (**Figure 4**b particle 4), indicating that particle collisions might be analyzed as a probability distribution. In addition, bubble film thinning forces were mentioned by Wang and Liu (**48**) as part of the hydrodynamic forces in zone 1. A drop in velocity of a small particle (~120 μm) approaching a regular size bubble (~1.3 mm), which remains when the particle slides around the bubble, was observed by Verrelli et al. (**54**) who attributed it to a resistance force by the intervening liquid drainage. The low inertia of fine particles (**53**) adversely affects the liquid film rupture which can potentially inhibit bubble-particle collision.

Forces in zone 2 (**Figure 4**a) are highly influenced by bubble surface mobility and size (**53**). They are described as diffusional and electrophoretic forces that arise from a heterogeneous (and concentrated) distribution of surfactants around the bubble rear. The distribution is affected by the stream direction generating an electrical field between particles and a concentrate region with surfactants (**52**). Forces in zone 2 are often neglected in particle-bubble interaction studies, although its thickness can be considerable (**53**). In those studies, the bubble surface is mobile (no contamination), which is an acceptable condition to 'sufficiently large bubbles' since they cannot be fully retarded exactly due to the non-uniform distribution of surfactants (**52**). However, these restrictions impose inconsistencies with the application of models in industrial systems, and just more recently, Chen et al. (**55**) attempted to study the interaction between particles (90 to 106 μm) and bubbles (1.05 to 1.9 mm) in the presence of a cationic collector.

In zone 3 (**Figure 4**a), surface forces such as electrostatic (F_e), van der Waals (F_{vdw}), and hydrophobic forces (F_h) (**56**) equilibrated with the hydrodynamic forces (**54**) to regulate the speed of the liquid film rupture which is part of the attachment process. The extended Derjaguin, Landau, Vervey, and Overbeek (DLVO) theory defined as the sum of the electrostatic double layer (V_e), van der Waals (V_{vdw}), and hydrophobic (V_h) interaction energies given by (**57**),

$$V_{ext\text{-}DLVO} = V_e + V_{vdw} + V_h \quad (4)$$

can be a good approach to calculate particle-bubble interactions in zone 3. An extensive theoretical approach for the calculation of forces exerting in all zones for particles <50 μm is provided by Derjaguin and Dukhin (**53**).

The impact of particle size on flotation recovery was tested by Senior et al. (**58**). Using a modified Denver stainless steel cell, the authors demonstrated that pentlandite ($(Fe,Ni)_9S_8$) below 10 µm has poor floatability (< 60%) (**Figure 5**). The recovery drop is more significant when 2 µm particles are floated (< 40%), while intermediate particles ranging from 15 to 80 µm were completely (or almost) recovered. For complex sulphide ores (Merensky and UG2 deposits, South Africa), a similar trend in which fine particles are poorly floated and intermediate particles (+64-90 µm) showed a higher sulphur (S) recovery (> 90%) was observed by Feng and Aldrich (**59**).

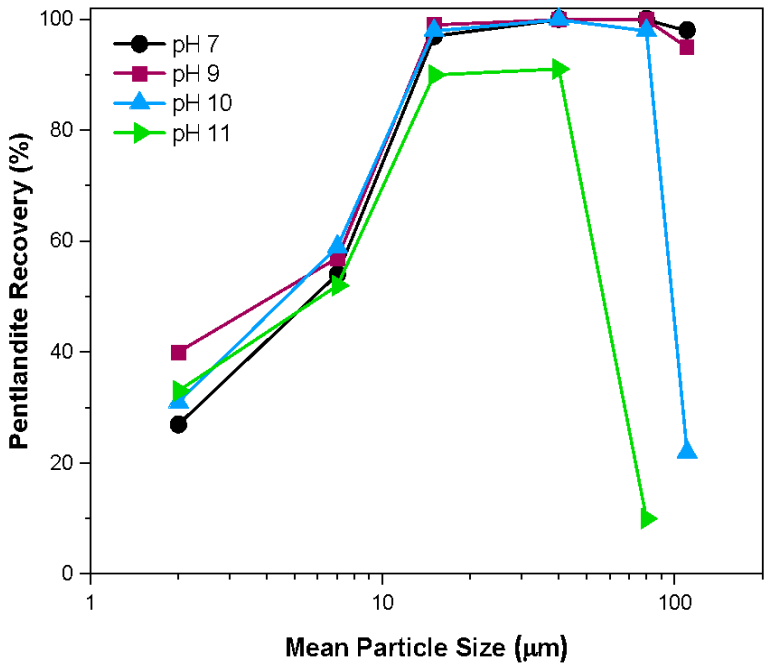

*Figure 5: Effect of particle size on pentlandite recovery in a pentlandite-quartz mixture at pH 7, 9, 10, and 11 using potassium ethylxantate (KEX). Modified from (**58**).*

This behavior is not a unique characteristic of sulphide fines and can therefore be extended to other minerals (**60, 61**). It is related to the low probability of collision (P_c) between fine particles and air bubbles (**47, 59, 62**). Low P_c is the reason for slow flotation rates of fine particles, confirmed by most developed particle-bubble collision models. Several assumptions and restrictions are imposed to build these models (e.g., quiescent conditions, no particle inertia, mobile bubble surface, homogeneous collision) but the efficiency of collision (E_c) is either a direct (or indirect)

function of particle and bubble sizes. For illustrating this relationship, Yoon and Luttrell model (1989) (**52**) is used. The authors considered three main flow conditions according to the bubble Reynolds number (R_{eb}) defined as

$$R_{eb} = \left(\rho_f V_b d_b\right)/\mu \tag{5}$$

in which ρ_f is the fluid density, V_b is the bubble rising velocity, d_b is the bubble diameter, and μ is the fluid dynamic viscosity. R_{eb} values determine the flow regime (fluid flow at the bubble surface), *i.e.,* R_{eb}<1 refers to the Stoke regime, R_{eb} 1 denotes the potential (or streamline) flow regime, and intermediate values of Reb indicate an intermediate flow regime. In the case of R_{eb} 1, the efficiency of collision (E_C) is

$$E_C = \frac{3}{2}\left(\frac{d_p}{d_b}\right)^2 \tag{6}$$

where d_p is the particle diameter. For an intermediate R_{eb}, E_C is calculated according to

$$E_C = \left(\frac{d_p}{d_b}\right)^2 \left(\frac{3}{2} + \frac{4R_{eb}^{0.72}}{d_b}\right) \tag{7}$$

Finally, for R_{eb} 1, the efficiency is given by

$$E_C = \frac{3d_p}{d_b} \tag{8}$$

also known as the Sutherland model (1948) (**Equation** 8). In summary, **equations 6 - 8** show that E_c increases when particle size increases (to a certain limit) and bubble size decreases. Collision models are reviewed in detail in Tao (**47**), Dai et al. (**52**), Miettinen et al., (**62**), and Nguyen et al. (**63**).

2.3.2.2. Particle-bubble attachment

The collision process is only one of the sub processes influencing flotation rates (**49**) and flotation efficiency (or efficiency of collection) (E_F) (**50, 52, 64**) can be calculated as

$$E_F = E_C * E_A * E_S \quad (9)$$

in which E_A is the attachment efficiency, and E_S refers to the efficiency of particle-bubble aggregate stability (or detachment). The attachment subprocess starts with thinning and rupture of the liquid film followed by the establishment of a wetting perimeter (**51, 54, 64**) and it is defined as induction time (t_i) (**48**). The 'wetting perimeter' is formed from the instability of the thin film (**53**) and as a consequence of the motion of the three-phase contact line (tpcl). With the tpcl motion, the liquid phase recedes from the solid surface while the gas phase advances (**51**). Independently of particle or bubble sizes, attachment is successful when the induction time does not exceed the contact time (impact and sliding) (**56**).

A few attachment models have been developed (**48,54**) in comparison with the collision models (**Figure 6**), even though in the last 21 years, other particle-single bubble attachment experiments (**65 – 68**) and mathematical modeling (**69**) were reported. An example is the kinetic model proposed by Dobby and Finch (**70**) for flotation columns. To calculate E_A, some parameters are considered such as the distribution of particle collision angle (α) with the bubble, and the maximum angle (αm) above which no particle-bubble contact occurs. This model assumes that bubbles are rigid spheres as well as mineral particles. Usually, αm is considered to be 90°, highly influencing the attachment efficiency. The maximum collision angle restriction (< 90°) was disproven by Verrelli et al. (**54**) who recorded a particle jump-in event in a bubble's sub equator. In other words, particle (d_p~130 μm) attachment occurred at the lower half of a bubble (d_b = 1.3 mm). They attributed this behavior to particle surface heterogeneities, and bubble surface deformation. It is important to note that single fine particles may not have enough kinetic energy to deform a bubble surface (bouncing).

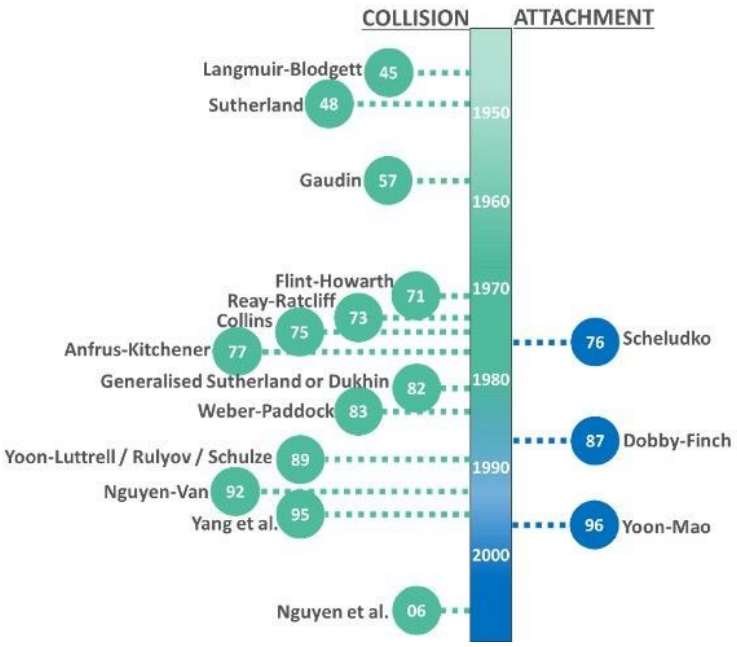

*Figure 6: Timeline comparison between some collision and attachment models developed from 1940 to 2010. Compiled from (**52, 62, 63**).*

Attachment efficiency depends on pondering hydrodynamics (e.g., agitation) and surface properties (**54**). Surface properties include particle and bubble charges, particle hydrophobicity and particle shape as well as bubble and mineral particle sizes (**51, 64**) (**Figure 7**). Some of these properties have a connection with surface forces in zone 3 (**Figure 4**a) and can modulate the collection process when a particle is sufficiently close to a bubble. As the distance between mineral particles and bubbles reduces, an electrostatic force (F_e) is generated due to their electrical double layer superposition, depending on their surface charges. Although small, Fe can promote the 'pick-up' of hydrophilic particles by bubbles with opposite charges (**71**) which could lower concentrate grades. Surface charges, measured in terms of zeta potential (at the shear plane), may be modified by the adsorption of surfactants/collectors/depressants, presence of electrolytes, changes in pH (H^+ and OH^- adsorption), or surface dissolution/oxidation (for particles only). For instance, sulphide minerals undergo dissolution by releasing metal ions in solution which precipitate as hydroxides on the same mineral and/or activate/deactivate another mineral surface. Details about the hydrolysis reactions undergone by sulphide minerals can be consulted in (**36, 72**). The attractive hydrophobic force (F_h) is often the principal contribution to particle-bubble attachment which is

expressed in terms of particle hydrophobicity (natural or induced). The higher the F_h, the faster the induction time (**Figure 7**). Modifications of particle hydrophobicity require the use of reagents such as collectors, and more recently, the use of micro/nanobubbles (**56**). In addition, investigations regarding the influence of shape in particle-bubble attachment (**73 – 75**) proved that, generally, a lower induction time on a rough surface is a consequence of a more rapid thin film rupture compared with a smooth spherical particle.

Attachment has also shown dependence on bubble sizes (**Figure 7**) as mentioned by Hewitt et al. (**64**). The authors calculated that E_A (**Equation 9**) is higher for smaller bubbles due to a faster establishment of a wetting perimeter when comparing air bubbles sizing 0.75, 1.2, and 2.0 mm. This faster induction time for smaller bubbles was recently confirmed to be the opposite in the presence of flotation reagents such as collectors due to more significant retardation of small bubble surfaces (**55**). This shows the importance of further research on particle interactions with small bubbles in the presence of reagents (immobile surface) since fine bubbles may not behave in the same manner as conventional and/or 'sufficiently large' bubbles. Regarding particle size, under constant conditions, finer particles (**Figure 7**) may also show a higher EA due to a longer contact time around the bubble (**51, 70**) measured in terms of the angular speed (**56**). Others argue that the low inertia of small particles results in lower attachment probability due to difficulties in rupturing the liquid film (**76**).

Much can be learned from the aforementioned trends. However, they usually account for particles colliding and sliding around a bubble surface (**Figure 4**a) which might not be comparable to the flotation of fine particles **Figure 4**b particle 4) with small bubbles. Also, particle-bubble attachment studies (**55, 64, 77, 78**) use static bubbles sizing above nano/micro scales, and data is often reported about medium to coarse particles (100 - 200 μm) (**54, 56**) likely due to limitations on measurements (**78**). Understanding bubbles' behavior could be the basis for further improvements in flotation processes and the next barrier to be broken in the sector. In the following section (Section **2.4.** Fine bubbles in froth flotation), aspects related to small bubble formation, stability, and properties (size and charge) are reported.

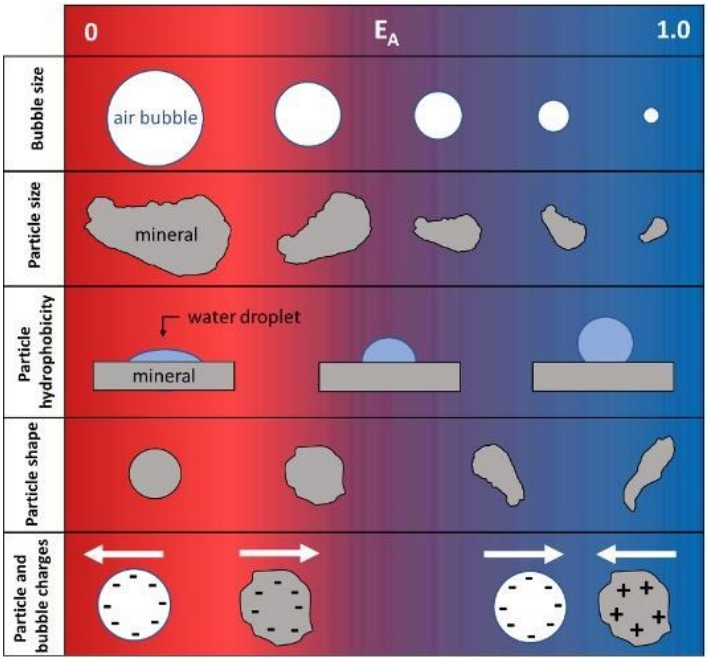

*Figure 7: The efficiency of particle-bubble attachment (EA) as a function of some surface properties. Compiled from (**62, 64**).*

2.4. Fine bubbles in froth flotation

The importance of studying bubbles in froth flotation was earlier stated by Rickard in 1916 (**79**) when he said, 'we know that the key…is to be found not in the oil, not in the acid, or in the apparatus, but in the bubbles'. Conversely to fine particles, bubble classification is regulated according to the International Organization for Standardization ISO 20480-1:2017 (**80**). It is a size-based classification that is not specific to the mineral processing sector, and it was defined due to the growing interest in small bubble technologies for other applications such as cleaning, medicine, and agriculture. According to the diagram (**Figure 8**), fine bubbles generally have a volume equivalent diameter ≤0.01 to 100 µm. Microbubbles range from 1 to 100 µm while ultrafine bubbles range from ≤0.01 to 1 µm, respectively. To this date, in the literature, the most used term to describe ultrafine bubbles is nanobubbles, and no publication was found including "ultrafine bubbles" AND "flotation" according to the Web of Science (Clarivate) database (consultation in February 2022) (**Figure 1**). Several recent research and reviews focus on generating,

characterizing, measuring, understanding the stability (see **Section 2.4.2.** On the stability of surface and bulk nanobubbles), and proving the existence of nanobubbles (**81 – 85**).

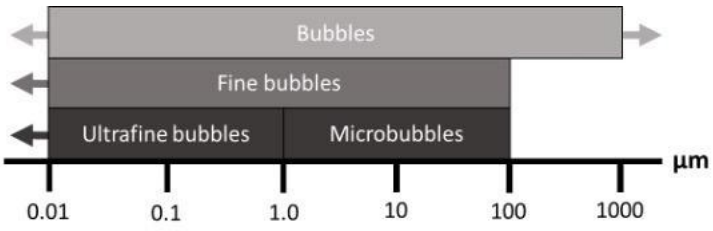

*Figure 8: Definition of bubble, fine bubble, microbubble, and ultrafine bubble according to size. Reproduced from (**80**).*

The positive impact of fine bubbles on fine particle flotation has been well documented in the literature for a variety of ores/minerals (**7, 8, 12, 86**), for not only improving the recovery of targeted particles but also reducing the consumption of frother and collector (**87**). The use of small bubbles seems obvious to boost collection efficiencies (**Equations 6 - 8**) **(49, 59)** and relevant attention has been given to develop a method that could generate the finest bubbles possible (**88**). However, Chipakwe et al. (**89**) recently discussed the gap in assessing nanobubble usage in complex systems in terms of metallurgical performance as this could be problematic for the industry. They showed for a Pb-Cu ore that mass recovery was greatly improved by the presence of nanobubbles with methyl isobutyl carbinol (MIBC) compared to nanobubbles without MIBC and conventional size bubbles. High mass recoveries using nanobubbles with MIBC were readily associated with better recovery of – 38 µm fractions, but the selectivity Pb-Cu vs Zn for that same particle size decreased considerably. Therefore, flotation selectivity using fine bubbles seems to be sensitive to several factors including the presence of reagents (see **Section 2.5.** Chemical factors affecting bubble properties). Additionally, selectivity may be a result of the presence of fine surface bubbles on targeted mineral surfaces, demonstrating the importance of ore surface characteristics and how bubbles are formed. This is discussed in the following section (see **Section 2.4.1.** Formation of bulk and surface bubbles).

2.4.1. Formation of bulk and surface bubbles

The formation of bubbles or cavitation inception (independently of the size) starts with a subprocess called nucleation (**90**). Considering a highly pure liquid, temperature and supersaturation levels trigger nucleation due to local pressure fluctuations and phase separation (to reach equilibrium), respectively (**91**). For froth flotation, investigations with different levels of dissolved gas are pertinent. To model a spherical bubble being formed in an air supersaturated liquid, Takahashi and co-workers (**92**) assumed that no vapor nuclei was present, the dissolved air could be considered an ideal gas, and Henry's law given by

$$P_D = H_E x_D \tag{10}$$

could be applied. In **Equation 10**, P_D refers to dissolved pressure, H_E is Henry's law constant, and x_D, the gas solubility (after changes in the equilibrium concentration). Henry's law shows a direct relationship between air solubility in water and pressure at a constant temperature. As a bubble nucleates due to pressure release from P_D to P_O (atmospheric pressure), similarly, to dissolved air flotation (DAF), a change in free energy (ΔF) using Gibbs' approach can be calculated as (**92**)

$$\Delta F = \left(P_O + \frac{2\gamma}{r}\right)\frac{4}{3}\pi r^3 l\, n\left(\frac{P_O + \frac{2\gamma}{r}}{P_D}\right) + \frac{4}{3}\pi r^2 \gamma \tag{11}$$

in which γ = surface tension (dyne/cm), and r is the bubble radius (cm). For cavitation inception, the energy barrier that must be overcome is defined as the 'cohesive/tensile strength of the liquid' (**93, 94**), and it is highly dependent on concentrations of dissolved gas and type of nucleation. High dissolved gas concentrations decrease the tensile strength of the liquid which can culminate in spontaneous bubble growth at pressures above the liquid vapor pressure (**95**). Dissolved gas concentrations also correlated with the critical radius of nucleation (**92, 93**). According to the classic theory, a bubble evolves only with values above critical radius (r_c) given by (**92**)

$$r_c = \frac{2\gamma}{(P_D - P_o)} \tag{12}$$

which is also the definition of the Laplace pressure for a spherical bubble (**96**). Bubble evolution includes the subprocesses of nucleation, bubble growth (gas diffusion and coalescence), bubble

detachment (from surfaces, for instance), and bubble break-up. The type of nucleation can be homogeneous and/or heterogeneous (**Figure 9**a), as described in detail elsewhere (**90, 91, 93, 97**). In this review, heterogeneous nucleation occurs due to the presence of tiny solid particles, free gas and/or vapor cavity nuclei as well as pre-existing gas air pockets in a solid surface crevasse (Harvey nuclei).

In a system completely free of contaminations (e.g., solid particles and reagents), formed homogenous nuclei (**Figure 9**.a.1) in the bulk phase have the highest nucleation energy barrier and demand high air saturation levels, usually exceeding 100 (**91, 93, 94**). However, due to the short lifetime (10 – 12 s) and outstanding internal pressure (~1440 atm), homogeneous nuclei formation appears unlikely (**90**), which automatically imposes questions about the inception and stability of bulk fine bubbles. The presence of tiny suspending solid particles or a substrate cavity lowers the necessary energy for nucleation (**Figure 9**.a.2), although it still requires high levels of saturation (**93**). High levels of saturation do not apply to the nucleation described in **Figure 9**.a.3 which occurs at pre-existing gas cavities in the bulk solution or on a substrate surface (93). If the radius of pre-existing gas cavities (r_1) is smaller than the critical radius (r_c) (**Equation 12**), then the energy barrier is lower than that in cases 1 and 2 (**91**). In the last type of nucleation (non-classical), no energy barrier exists since the radius of pre-existing gas nuclei (r_2) is larger than r_c (**Figure 9**.a.4) (**91, 93**). For Yang et al. (**98**) who tested carbon dioxide (CO_2) nucleation on a TMCS (trimethylchlorosilane) modified gold surface using Quartz Crystal Microbalance (QCM), the nucleation stage comprised of slowly adsorption of gas molecules dissolved in solution onto the 'pre-existing gas cavities' (Harvey model), followed by a stage in which bubbles rapidly grow, according to dissolved gas availability. Albeit bubble growth may be affected by different parameters such as viscous forces, surface tension, convection forces, and inertial forces, it is usually approached in terms of the diffusion of gas molecules and their motion across the liquid-gas interface (**93, 98**).

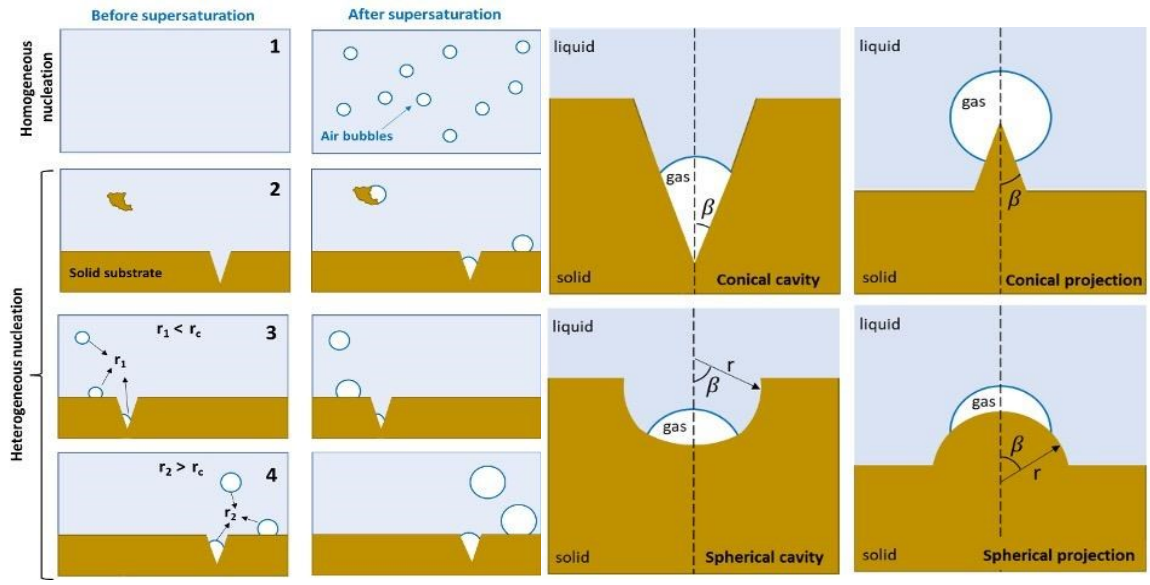

*Figure 9: Homogeneous versus heterogeneous nucleation (a). Note: in case 3, bubbles may or may not grow. Modified from (**93**). Schematic representation of the four cavities shapes used for theoretical calculations of heterogeneous nucleation (b). Note: r refers to the spherical cavity and its projection radius. Modified after (**99**).*

The existence of pre-gas cavities in a liquid is supported by a mismatch between calculations of nucleation rates using the classical theory and experimentally observed values (**93**). Zhou (**100**) showed that a decrease in light transmittance in a Venturi tube due to bubble formation and growth is a consequence of the expansion of pre-existing nuclei. Besides, when pre-existing gas nuclei were removed from the water by boiling or heating, almost no nucleation was observed even on hydrophobic surfaces such as bitumen (**101**). However, some authors calculated the existence of micro-sized free gas nuclei in water (**102**). No ratio or limit defining differences between the size of a nuclei (free gas and vapor cavity) and the size of fine bubbles has been found in the literature, and nanobubbles have been suggested to enable nucleation (**91, 103, 104**). A distinction between fine bubbles and free gas/vapor nuclei in terms of size, stability, or nature might be relevant due to the growing interest in this area.

Another condition for heterogeneous nucleation on suspending solid particles and/or flat surfaces (**Figure 9**.a.2 and **Figure 9**.a. 3) is hydrophobicity (**91, 95, 98, 105 – 107**). The energy barrier for nuclei formation on a hydrophilic surface with a contact angle (θ) close to 0º can be as significant as in homogeneous nucleation (**91, 106**) (**Figure 9**.a. 1) (91). In a hydrophobic surface (θ = 180º),

no nucleation energy barrier exists (**91**). This process of surface nucleation could promote particle aggregation, increasing the apparent size of fine particles, and, consequently, enhancing the efficiency of collision of particle-bubble aggregates to conventional size bubbles (0.8 – 3.0 mm) (**Equations 6-8**) (**82**). If gas nucleation can selectively occur on a specific mineral, manipulations of surface hydrophobicity of a valuable mineral may improve separability.

However, there are some controversies whether surface hydrophobicity has to be paired with surface roughness to enable heterogeneous nucleation. Ryan and Hemmingsen (**108**) demonstrated that nucleation was minimal on smooth polystyrene microspheres ($\theta = 129 \pm 4^{o}$) even at high levels of saturation. Although it is possible to qualitatively visualize the smoothness of polystyrene microspheres by Scanning Electron Microscope (SEM) (**108**), it is difficult to compare with later research which employed more sophisticated techniques (**105, 106**). Yang et al. (**106**) clearly revealed the presence of nanobubbles on a hydrophobized silica wafer ($\theta_A = 74^{o}$ and $\theta_R = 67^{o}$) with 0.1 nm roughness via tapping mode atomic force microscopy (TMAFM) imaging. Bremond et al. (**105**) also presented microscope images of heterogeneous cavitation on a smooth hydrophobic silica wafer ($\theta_A = 106 \pm 1^{o}$) with a roughness of less than 2 nm. Li et al. (**107**), comparing powdered silica particles and smooth glass beads, proved that surface roughness is not a condition for cavitation inception.

On the other hand, Xu et al. (**109**) stated that roughness is one of the main factors affecting bubble nucleation on a graphite surface. Other parameters are hydrodynamic conditions and the degree of air saturation (**109**). When surface roughness is mentioned, there are no clear criteria defining limits for it, i.e., if surfaces can be considered rough when nano and/or microscopic crevasses are present. Considering that surface roughness is not a condition for heterogeneous nucleation, how does it take place on a perfectly smooth surface? How are the nucleation sites distinct in a naturally vs. chemically induced hydrophobic mineral surface? Studies on smooth mineral samples such as muscovite (**110**) with induced hydrophobicity showed differences in the contact angle of samples at various dodecylamine (DDA) dosages. The authors (**110**) believe that high DDA dosage assists with the stability of bulk nanobubbles which could then be adsorbed on the muscovite surface. Similarly, Xiao et al. (**111**) showed the absence of surface nanobubbles on mica surfaces in deionized water in comparison with high sodium oleate (NaOl) solutions by AFM imaging. Available literature lacks an approach to explain the raised questions. It still remains unknown

whether the presence of frosted fine bubbles is a result of surface nucleation or adsorption of bulk fine bubbles (or both), and how this could change according to the substrate used.

In some of those experiments (**98, 105, 107, 108**) the authors used very controlled and smooth surfaces such as silica wafer, glass beads, and polystyrene microspheres. The presence of air pockets on real mineral surfaces is not an odd assumption due to heterogeneities and microfractures generated by their proper nature (e.g., cleavage, defects, and vacancies). Grinding, friction, oxidation, and dissolution are also examples of processing effects that can generate and alter mineral surface roughness and texture. However, some authors (**99, 105**) argue that air pockets present and formed on solid surfaces are dependent on the shape of the crevice. Wilt (**99)** compared the nucleation of a CO_2 bubble in a conical crevasse, a conical projection, a spherical cavity, and a spherical projection (Figure 6.b) by calculations based on the traditional nucleation theory (**93**). The author reported that those bubbles only nucleate in a hydrophobic ($\theta = 94 – 130^o$) conical crevasse. This phenomenon, however, may occur at specific β values which was later indirectly proved by Bremond et al. (**105**). Note that β is a function of the cavity width.

While topics related to the importance of bulk nanobubbles in froth flotation have been extensively reviewed (**81**) contributions as Xu et al. (**109**) and Li et al. (**107**) regarding the nucleation of fine air bubbles on natural mineral surfaces are scarce, especially for dynamic systems (**101**). Usually, fine surface bubbles are formed via solvent exchange or temperature difference and evaluated for mineral samples or for fabricated samples (e.g., Highly Ordered Pyrolytic Graphite - HOPG) using AFM (**112 – 114**). Zhou et al. (**90**) mentioned that in hydrodynamic cavitation, small gas structures (air pockets) located in the crevices of mineral particles might grow due to the negative pressures achieved during the fluid flow. In any of those circumstances, bulk and surface fine bubbles have to be stable to endure the hydrodynamics conditions of flotation cells/columns.

2.4.2. On the stability of surface and bulk nanobubbles

Due to the exponential growth in research about fine bubbles, a short analysis of factors affecting the stability of surface and bulk nanobubbles is given. Several research in mineral processing have attempted to prove/measure, and also showed their benefits in froth flotation for the recovery of fine particles (**81, 83, 84, 109**), and coarse particles (**115**). Most research, however, relies on data and models for larger bubbles with extrapolation to nanobubbles. Those correlations certainly have

a limitation, and this is why the existence of nanobubbles is still a topic of discussions and no universal explanation has been fully accepted (**103, 105, 116**). It is not intended to critically assess those theories but rather provide some examples that may be applied to froth flotation in terms of gas saturation levels, presence of reagents, and the type of solid surface (i.e., hydrophobicity and heterogeneity). More details have already been provided in a recent review by Zhang et al. (**117**) and (**118**).

The basis of those discussions starts with the diffusion theory which indicates that bubbles have a permeable interface allowing gas exchange with the surrounding liquid (**103**). As a consequence, spherical gas bubbles would be unstable at usual conditions over time (t) as given by the Epstein and Plesset solution (**103**)

$$\frac{dR}{dt} = - \frac{D}{\rho_g}\left(\frac{P_o}{H_E} + \frac{2\gamma}{H_E r} - C_\infty\right)\left(\frac{1}{r} + \frac{1}{\sqrt{\pi}Dt}\right) \quad (13)$$

in which r refers to the bubble radius, ρ_g corresponds to the gas density, H_E is the Henry's law constant (**Equation 10**), D is the diffusion constant, c is the concentration field, and γ is the surface tension. The intern pressure of a nanobubble given by the Laplace pressure (ΔP) would be extremely high "forcing" the bubble to dissolve in less than milliseconds (**82, 83**). Most of the stability theories for bulk and surface nanobubbles intend to "balance" the Laplace pressure in order to provide some explanation for the low rates of dissolution.

For bulk nanobubbles, the assumption that homogeneous nuclei stability results from the existence of an organic layer or surfactant given by (**119, 120**) is still found in the literature (**103**). Organic reagents/contamination would form a protective layer reducing the bubble surface tension and, consequently, the Laplace pressure. This assumption could be applied to froth flotation as the use of organic reagents such as collectors, frothers, and depressants is a routine for most circuits (see **Section 2.5.** Chemical factors affecting bubble properties). Other factors for nanobubble stability may include those of hydrodynamic nature as mentioned by Zhou (**100**) who defined stirring as an important condition in a solution with available dissolved air. It is common to focus on characterizing fine bubble generators but how the shear conditions affect the size distribution of fine bubbles in flotation cells and columns is still to be clarified. Additionally, the stability of bulk nanobubbles is often associated with the action of high repulsive forces of the bubbles' double

layers which prevents their coalescence (**82, 121**). According to Tan et al. (**103**), the electrostatic stabilization, also called the Akulichev's model, considers an electrostatic pressure (P_e) generated by the bubble surface charge density (σ) acting oppositely to the Laplace pressure. The electrostatic pressure is defined as (**103**)

$$P_e = \frac{\sigma^2}{2\varepsilon_r \varepsilon_0} \tag{14}$$

where ε_r is the relative permittivity of water and ε_0 is the permittivity of space. However, the electrostatic stabilization model does not account for other factors common in froth flotation such as dissolved gas concentration (**103**).

There is no substantial evidence that the stability of surface nanobubbles would be even partially influenced by the bubble surface charge (**103**). Instead, in the last two decades, several researchers have attempted to develop a satisfactory model by considering factors such as dynamic gas influx and outflux (dynamic equilibrium theory) (**122**) and the contact line pinning (**123**). In the dynamic equilibrium theory, the gas influx and outflux on the nanobubble surface are mostly maintained by a gas enriched layer close to the hydrophobic surface. This assumption considers that hydrophobic surfaces can interact with dissolved gas molecules generating a concentrated area (**124**). For the contact line pinning between a solid surface and a nanobubble has been correlated to chemical heterogeneities and surface roughness by many authors as described in Lohse and Zhang's review (**125**). On the experimental side, Bremond et al. (**105**) reported that surface nanobubbles (~37 nm) were not stable on a smooth hydrophobic surface and dissolved within a two hour interval. On the other hand, stable nanobubbles (15 hours) nucleated on an etched surface with cylindrical cavities (15 μm deep and 2-4 μm wide) were reported (**105**) which would be related to the stability provided by the cavity's sharp edge (**Figure 9**) and similar pressures values inside and outside the bubble. The presence of crevasses on solid surfaces may not only promote bubble nucleation as previously discussed (Section **2.4.** Fine bubbles in froth flotation) but it appears to assist with their stabilization. Bubble stability in terms of preventing coalescence and break-up is also a function of the presence of reagents such as frother and collectors as well as chemical species such as ions which are reviewed in the following section.

2.5. Chemical factors affecting bubble properties

Several factors can influence the size and charge of bubbles in aqueous media. They may be divided into those related to the bubble surface tension and shear conditions. No distinction between conventional and fine bubbles is provided unless stated. The main purpose of this section is to inquire if fine bubbles' properties might be affected in a similar manner by showing supporting information of what is known about conventional bubbles. Although research has reported nanobubble size changes by the addition of reagents such as frothers (**126**), other phenomena such as bubble coalescence and break-up may not follow the same trend and need further investigation. Regarding shear conditions, mechanical energy input, air flow rate, and bubble generation method, for instance, have been extensively reviewed in the context of conventional and fine bubbles (**48**). Frother (concentration and type), electrolyte species, and collector substantially affect bubble properties which in turn impact flotation recoveries and are further discussed.

2.5.1. Frothers

Frothers are surface-active reagents known to help produce smaller bubbles and stabilize froths, but their mechanisms of action are still in debate. The main discussion refers to if surface tension reduction due to frother addition could be used to justify the generation of smaller bubbles. According to Pan et al. (**127**), this is not possible, while other authors have justified their experimental results using the opposite argument (**126**). Pourkarimi et al. (**126**) related the bubble size reduction to surface tension by applying the Young Laplace equation (**Equation 12)** to six different frothers under identical conditions. They stated that the formation of fine bubbles was because of the notable decrease in the water's surface tension and better foamability. However, some authors argued that there is no direct relationship between a decrease in surface tension and bubble size reduction (**127, 128**), especially at low frother concentration (**129**). The reason is that the surface tension is not able to equilibrate in real systems (**127**). Additionally, the surface tension only started to reduce at higher frother concentrations which might not apply to all froth flotation systems (**127,130**).

Atrafi and Malik (**131**) explained bubble size reduction differently. They found that reduction of bubble size by long-chain fatty acids solution was related to the generation of a surface tension

gradient (Marangoni effect) and prevention of coalescence. Similarly, Finch et al. (**129**) described that frothers are able to reduce bubble size by either hindering coalescence (due to the Gibbs elasticity and Marangoni effect) or by enhancing the break-up of the air stream. Bubble coalescence mechanism appears to provide an effective approach to determining how frothers affect bubble size (**128, 129**). On the other hand, the air stream break-up occurs as a consequence of surface perturbations and surface break-away force generated when a frother molecule is introduced, thereby causing a tearing action resulting in surface instabilities and tendencies of bubbles to break up (**128**). Kracht and Finch (**130**) studied bubble break-up and coalescence prevention mechanisms by investigating bubble size distribution measurement/modelling in the presence and absence of frothers. It was demonstrated that the presence of frothers significantly diminished the tendency of bubbles to coalesce. Frother effects were also observed to some extent in bubble break-up. The effect was more pronounced in less than 10% volume fraction break-up. These further re-states the non-uniform/unequal distribution of frother molecules on bubble surface prior to breakage i.e., surface tension gradient. To complement the study of Kracht and Finch (**130**), Chu et al. (**132**) showed how frothers reduce bubble size in a break-up mechanism separately from the coalescence event. They were able to achieve this by considering only the first bubble breakage. In their findings, the presence of frothers enhanced bulge deformation by creating a variation in the surface tension, leaving a force in the direction of higher surface tension. Thus, a surface tension gradient-driven stress is generated which provides an extra energy to the mechanical stress arising from the flotation's device geometry, thereby increasing instabilities at the air/water interface and enhancing smaller bubble size break-up.

2.5.1.1. Frother concentration

Factors such as frother concentration and type also play a vital role in determining bubble sizes (**133**). The addition of high frother dosages reduced the mean Sauter bubble size (d_{32}) generated using jets in a flotation column (**134**). The authors measured a d_{32} change from 3.2 mm to 2.4 mm using 75 ppm of frother, but this led to uncontrolled frothing which can be detrimental to the operation in many aspects. The effect of frother concentration was also investigated by Kracht and Finch (**130**), and contrary to the observations of Finch et al. (**129**), the authors found that increasing the concentration did not favor coalescence prevention but decreased bubbles breakage. Regarding the mechanism, Chu et al. (**135**) further investigated if surface tension gradients are minimized by higher frother concentrations. Their findings showed that at high frother concentration, there is a

sufficient rate of mass transfer which causes frother saturation at the air/water interface, thereby dampening the surface tension gradient. A diminishing surface tension gradient implies highly reduced surface instabilities and a low tendency of the frothers to produce small bubbles. It was already stated that the mass transfer rate is also dependent on the size of the frother molecule (**132**).

2.5.1.2. Frother types

Chu and co-workers demonstrated how different frothers act to reduce bubble size formed by the break-up mechanism and how these frothers affect the rate of mass transfer (**135**). They introduced the concept of critical break-up concentration (CBC), defined as "effective concentration for producing the smallest bubble at break-up", which was also used to describe the actions of different frothers (MIBC, DF20, F160-13, F150). Although there was no significant difference among all frothers tested (as they showed a similar trend of initial decrease and subsequent increase of bubble size), the shorter hydrocarbon chain frothers had a faster mass transfer rate (owing to its short-chain and less hydrophilic sites to H-bond with water molecules) which translates to lower CBC. Thus, MIBC requires a low concentration to produce the smallest bubble size, but because of a high mass transfer rate, a uniform surface concentration is quickly achieved, and the surface tension gradient is dampened. Hence, the production of small bubbles was hindered when CBC was achieved, and the bubble size began to increase (a similar behavior was achieved when the high concentrations of frothers were used). This shows that high frother concentrations and short hydrocarbon chain frothers are limiting to fine bubble production and are described by the mass transfer rate concept. Furthermore, Chu et al. (**135**) established a relationship between CBC (for single bubbles) and the critical coalescence concentration (CCC) (**128**). It was observed that frothers with high CCC tend to have low CBC and vice versa. The break-up strength follows MIBC < DF250 < F150. When considering both mechanisms of bubble size determination, short hydrocarbon chains are effective in causing break-up at low concentrations but would require high concentrations to preserve the bubble size from coalescing. In terms of long hydrocarbon chain frothers, the prevention of coalescence occurs at low concentrations and would require high concentrations to reduce bubble size in the break-up mechanism. When different frothers were compared, some appeared to be more surface-active than others, a different observation from (**130**). Di ethoxy-mono propoxy hexanol and mono propoxy-di ethoxy hexanol achieved CCC faster at a lower concentration than hexanol, di ethoxy hexanol, and MIBC. In a different study by Corona-Arroyo et al. (**136**), frothers decreased bubble size at concentrations below and up to CCC. Above

CCC, there was no observed further decrease in the bubble size, suggesting a uniform surface distribution of the surfactant at the bubble surface (surface saturation).

2.5.2. Electrolyte species

Sovechles and Walters (**137**) concluded in their experiments with different salts that their effect on bubble size is determined by the ionic strength of the solution, an extension of frother's CCC. Thus, the higher the ionic strength, the smaller the bubble size. Hence using saline solutions would decrease bubble size in the absence of frothers, a phenomenon reported by different authors (**137, 138**), and already applied in the industry with sufficient bubble reduction and good frothing characteristics (**139**). However, by combining MIBC with a saline solution (where concentrations are high enough and coalescence is inhibited), the bubble size was found to increase (**138**). It is suspected that both frother and electrolyte solution would increase the total concentration and thus, high mass transfer rate, thereby creating a uniform surface concentration or interface saturation and causing surface tension dampening, as explained by Chu et al. (**135**). In a recent study of frother and ionic strength combined effect, Corin et al. (**140**) found that at high concentrations of both parameters, a stable froth was observed, but the recoveries of copper and nickel were mostly unaffected, and their grade decreased. Since these studies have demonstrated the effect of high ionic strength on bubble size reduction (hence improved flotation recovery), regulating frother usage in such high electrolyte solutions makes sense. This observation is important in operations that utilize recycled process water and in high saline water regions, as frother consumption should be reduced. Pan et al., (**127**) investigated the interaction of different flotation reagents such as MIBC, potassium amyl xanthate (PAX), and sodium hydrosulphide (NaHS) on the properties of the air-liquid interface. They found that the combined effect of these three reagents provided more stability to the bubbles by preventing bubble coalescence, which was determined by the coalescence time experiments and measurement of the Sauter mean diameter of the bubbles.

2.5.3. Effects of electrolyte species (salts) on bubble zeta potential

As some authors appear to agree with the fact that bulk nanobubbles are electrostatically stabilized (**Section 2.4.2.** On the stability of surface and bulk nanobubbles), the discussion is extended to the study of their zeta potential (**82, 121**). Bubble zeta potential is essential in mineral flotation as their charge can determine their interaction with reagents, mineral particles, and other bubbles. In

froth flotation operations, similarly to large bubbles and microbubbles, the zeta potential of nanobubbles can also be modulated by various factors such as presence of the salts, surfactants, and polyvalent cations. When possible, a parallel comparison with microbubbles is given as most available spargers often generate a broad size range of fine bubbles (**141**). Some analogous trends exist as negative values of zeta potential of bulk nanobubbles at alkaline pH have been confirmed by authors who used different bubble generation techniques with no surfactants or salts (**82, 121, 142, 143**). However, this is far from real flotation systems as different kinds of salts are introduced by the use of recycled process water (**144**), sea water (**145**), pulp viscosity modifiers (**146**), and pH regulators (**147**). By increasing salt concentration, the magnitude of zeta potential decreases which reduces the repulsion and stability of bulk nanobubbles (**121**). The instability can be explained by the increasing ionic strength of the solution and quantified in terms of the Debye length (κ^{-1}) as (**121**)

$$\kappa^{-1} = \sqrt{\frac{\varepsilon k_B T}{e^2 I}} \tag{15}$$

where I refers to salt ionic strength, ε to the medium permittivity, T to temperature, e to the density of electrons, and k_B to the Boltzmann constant. By adding salt into a solution with nanobubbles, the Debye length reduces. Whereas the adsorption of monovalent ions such as monovalent ions such as Na^+ did not impact the zeta potential (reference to the blank test) (**143**), the presence of polyvalent cations/metal ions poses an interesting trend which is particularly relevant for sulphide flotation due to mineral oxidation and dissolution, and the addition of activation agents. The presence of Mg^{2+} was shown to reverse the zeta potential of air bubbles at alkaline pH values due to the precipitation of magnesium hydroxide ($Mg(OH)_2$) species at the gas liquid interface, whereas the decrease in the magnitude at acidic pH values was attributed to specific adsorption of Mg^{2+} (**148**). An example is the effect of trivalent ions such as Fe^{3+} which kept nanobubble zeta potential positive for the entire pH range tested (**143**). The adsorption of Fe^{3+}, $Fe(OH)^{2+}$, and $Fe(OH)^{++}$ at pH 7 resulted in a net positive value when the negative inner nanobubble charge was summed to the positive Fe^{3+} cation species on the outside of the bubble surface. Li and Somasundaran (**149**) also observed for microbubbles a charge reversal in the presence of trivalent aluminium cations which was attributed to the specific adsorption of Al^{3+} and its hydroxo complexes at the gas liquid interface. These studies (**143,149, 148**) have shown that pristine air

bubbles are negatively charged in electrolyte solutions. However, the presence of polyvalent cations can reverse their charge depending on the concentration of salt and the desired pH range to work with. Bubble charge modulation could be used in situations where bubble-mineral particle attachment is difficult due to homo-charge. By reversing bubble charge, improvements may be observed as now not only hydrophobic interactions will promote the attachment but also electrostatic interactions. Therefore, it is important the complete understanding of the slurry composition and how that composition could affect nanobubbles' behavior in complex systems.

2.5.4. Effects of frothers on bubble zeta potential

Surfactants are also extensively used to stabilize bubbles, and depending on their nature, nanobubble zeta potential might alter. Zhang et al. (**142**) showed a nanobubble zeta potential drop from pH 3 to 12 by using a non-ionic surfactant such as methyl isobutyl carbinol (MIBC at 4.9 x 10^{-4} M). The same authors discussed that it can be applied to other non-ionic surfactants. However, Elmahdy et al. (**150**) concluded that non-ionic frothers such as MIBC or heptanol, at concentrations of the industrial relevant range (< 20 ppm), do not alter the general trend or isoelectric point (IEP) of air bubbles. Yoon and Yordan (**151**) showed that IEP of microbubbles shifted to higher pH values when generated using polyoxyethylene methyl ether (non-ionic) solutions which was attributed to the high oxygen to carbon ratio in the molecule. When an anionic surfactant such as sodium oleate ($C_{18}H_{33}NaO_2$ at 1.6 x 10^{-4} M) was used, nanobubble zeta potential shifted even further to more negative values (**142**). The same result was observed by Calgaroto et al. (**82**) with the anionic surfactant SDS (10^{-4} M). The sharp drop in zeta potential upon raising anionic surfactant concentrations results from the adsorption of specific ions on the bubble surface (**121**). Those discrepancies call for further investigations, especially regarding the presence of common frothers such as MIBC

The study of the influence of chemical additives in froth flotation circuits is not limited to changes in bubble properties such as size and charge. Ang et al. (**152**) described the detachment of galena (PbS) particles (-75 +20 μm) from bubble surfaces as a function of the frother dosages and types, during the merging of two bubbles. This could alter important steps during the fine bubble-assisted flotation of fine particles, such as particle aggregation as well as flotation rates due to changes in

bubble-bubble interactions (**153**). More details about these processes are provided in the following section.

2.6. Fine bubble assisted flotation

Flotation cells designed to generate small bubbles and conventional bubbles were suggested as a solution to improve mineral recoveries over 35 years ago when Ahmed and Jameson (**49**) studied the collision process of fine particles (< 50 μm) with fine bubbles (< 100 μm). Several authors have recently suggested improvements in flotation performance using a similar technique. Examples are provided in Table 1. Benefits of performing assisted flotation with fine bubbles include selective separation (**84**), lower collector consumption (**84, 88**), and fine particle aggregation (**154**). Despite reported benefits and the use of fine bubble generators in real operations (**155**), most studies refer to laboratory and pilot plant scales (**Table 1**). Descriptions of bubble size distributions in flotation systems are also scarce (**83**) or not provided likely due to measurement limitations. Those may refer to low resolution and accuracy in a representative volume of slurry, and the distinction between fine bubbles and fine mineral particles.

In **Table 1**, a few different methods for generating fine bubbles are cited, but the list of techniques is extensive and includes mechanical stirring, variable pressure (dissolved air, jets, and vacuum), porous medium, ultrasound, and electrolysis as reviewed by Wang et al. (**48**). Several types of flotation cells and columns to treat fine mineral particles can be consulted in a recent review by Hassanzadeh et al. (**156**). However, the effect of distinct fine bubble generation techniques for the same ore regarding shear conditions (e.g., hydrodynamics cavitation vs. dissolved air flotation) is rarely discussed. Ross et al. (**12**) have hypothesized that high shear methods could assist with passivation layer and slimes removal and improve mineral liberation. Others have suggested that fine bubbles generated by hydrodynamic cavitation could desorb (**159**) or prevent the adsorption of reagents on mineral surfaces (**110**). Those “side effects” of flotation with fine bubbles should be further investigated, especially in systems with slurry recirculation (**160**).

Table 1: Selected reported flotation improvements in the literature by fine bubble assisted flotation in the last five years

Material and conditions	Flotation reagents	Fine bubble generation	Bubble sizes	Flotation improvement	Additional comments	Reference
Phosphate ore (P = 10.8% and Fe = 16.4%) d_{80}^{*} = 38 µm pH 9.5 Denver cell (1 L)	Collector Flo-Y-S (700 g/t) Depressant starch (400 g/t)	Hydrodynamic cavitation	distribution peak (volume frequency) ~170 nm (Malvern Mastersizer 2000)	P from 16.15% to 17.62% and Fe from 6.28% to 4.25% by single and dual bubble	Proved selectivity and reduction of collector consumption	(84)
Microcrystalline magnesite ($MgCO_3$ ~ 95%) d_{85}^{*} = 25 µm pH 10 Denver cell (3 L)	Collector NaOl** (120 mg/L) Frother pine oil	Electrolysis	76 µm (High-speed camera 20 MP Canon EOS 70 D)	Mass recovery from ~70% to ~80% by single and dual bubble, respectively	Electrolysis bubbles promoted particle aggregation	(154)
Quartz (SiO_2 = 100%) d_{80}^{*} = 38 µm Agitair LA-500 cell (1.7 L) 3 min flotation time	Collector Flotigam EDA (10 g/t)	Air-in water micro-dispersion generator (Turboflot service Company)	<50 µm	Mass recovery from ~19% to ~34% by single and dual bubble, respectively	Differences in mass recovery reduce at high collector dosages	(157)
Sulphide ore d_{99}^{*} = 44 µm Pneumo-mechanical cell (3L) At 3 min flotation time	Collector SBX*** (0.2 g/kg) Depressant Na_2O_3Si (0.3 g/kg) Frother Aeroflot (0.03 g/kg)	Air-in water micro-dispersion generator (Turboflot service Company)	<50 µm	Cu recovery by ~32%, Pb recovery by ~40%, Zn recovery by ~25%, and Fe recovery by ~11%	Metallurgical recovery improvements even at low bubble dosages (0.1 L/kg)	(158)

The main reason for mass and metallurgical recovery improvements observed in **Table 1** is believed to be a two-stage process (**Figure 10**.a), which has been a topic in recent reviews (**48, 117**). Research has suggested that fine bubbles can act as bridges that enhance particle-particle interaction to form aggregates (**56, 161, 162**). With small bubbles adsorbed and/or nucleated on the surface (see Section **2.4.** Fine bubbles in froth flotation) (**Figure 10**.a), the approach of two

particles causes the bubbles to coalesce and generate an attractive capillary force, as shown in **Figure 10**.b (**163, 164, 165**).

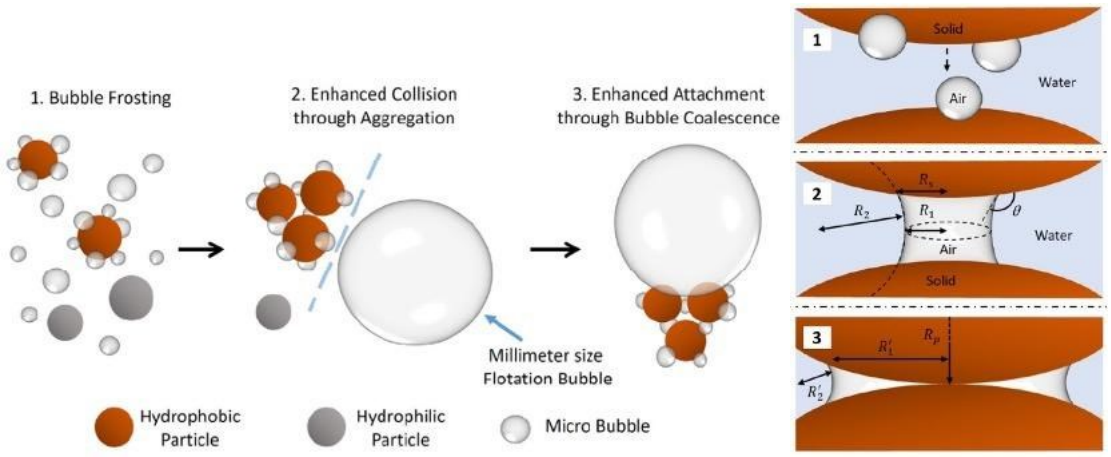

*Figure 10: Schematic representation of processes occurring during fine bubble assisted flotation (a) detailing aggregation of fine bubble-frosted mineral particles via capillary bridging (b). From (**166**).*

The calculation of capillary force (F_{Cap}), illustrated in **Figure 10**.b.2, consists of the Laplace pressure force (F_P) and the surface tension force (F_{ST}) with F_P defined as (**167**)

$$F_P \approx \pi R_S^2 . 2\gamma_w \left(\frac{1}{R_1} + \frac{1}{R_2}\right) \quad (16)$$

where R_S is the radius of the air-solid contact area assuming a flat surface, γ_w is the air-water surface tension, and is the curvature of the air-water interface. In **Figure 10**.b.2, the contact angle (θ) is high enough to generate a curvature concave into the capillary, R_2 is negative, and the curvature is positive, thus generating an attractive Laplace pressure force. On the other hand, F_{ST} is always attractive calculated as (**167**)

$$F_{ST} \approx 2\pi R_s . \gamma_W \sin(\pi - \theta) \quad (17)$$

For a given volume of capillary, as the two particles approach closer, R_S increases. As a result, the overall capillary force increases. When the two particles are in contact as shown in **Figure 10**.b.3, the capillary force reaches the maximum. Assuming R_1' >> R_2', the capillary force can be estimated as (**167**)

$$F_{Cap} \approx 2\pi\gamma_W R_P \quad (18)$$

where the force only depends on the radius of the particles (R_P). Such a capillary force is strong enough to hold two spherical silica particles of about 2 mm against the gravitational force. In reality, the capillary force is often much smaller due to the lower air-solid contact area from surface roughness. Despite that, the surface fine bubbles can hydrodynamically enhance and stabilize the accumulation of particles, forming bubble-particle aggregates.

Experimental investigations into the fine-bubble-assisted agglomeration phenomenon were confirmed using image analysis (**168 – 170**). However, a further demonstration of the effect of fine bubbles to selectively aggregate particles of different physicochemical surface properties is still required. This is extremely relevant to mineral flotation as particle morphology (shape and roughness) has been proved to influence particle aggregation in the absence of fine bubbles (**171**). Additionally, the size of collector chains might control the ability of fine mineral particles to form aggregates. Overall, the longer the hydrophobic chain of the collector, the bigger the aggregate. For instance, size improvement using oleate as a collector resulted in a higher probability of collision between dolomite particles (d_{50} = 14 μm) and bubbles due to particle aggregation in a micro-flotation set-up (**172**). This process was independent of the interaction mechanism between the collector active group and mineral surfaces (**172**).

With an increased apparent size, mineral aggregates have a higher efficiency of collision with conventional size bubbles **(Equations 6-8)**. The presence of frosted fine bubbles on mineral surfaces appears to also enhance the interaction of aggregates with coarser bubbles that could easily float (**Figure 10**.a). In this last stage, discussions of the fundamental mechanism of this interaction are ongoing as recently pointed out in Zhang et al.'s review (**117**).

Although small bubbles can easily collide **(Equations 6-8)** and attach onto mineral particles, their low volume cannot provide sufficient buoyancy force to lift the aggregates up. At this point, large flotation bubbles of millimeter sizes come into play to complete the flotation process. The role of small bubbles in the attachment process between particle aggregates and large flotation bubbles is explained by fine bubbles helping the aggregates adhere to large flotation bubbles (**Figure 10**.a) by reducing the induction time, thereby enhancing attachment probability (**97, 165, 169**). As

previously explained (see **Section 2.3.** Flotation mechanism), the induction time is determined by the thinning of the liquid film trapped between particles and bubbles (**173 – 175**).

For a millimeter size bubble colliding with a flat particle surface (i.e., the bubble is much smaller than the particle), typically, it takes a few seconds for the thin liquid film to reach its critical rupture thickness (**176, 177**). The time is reported to be slightly shorter (hundreds of milliseconds) if the particle is spherical (**178**). When a surface microbubble (~10 μm) larger than the typical film thickness (~1 μm) is present on the particle surface, the situation switches from large bubble-particle attachment to large bubble-surface fine bubble coalescence. This faster attachment was recently reported by Li et al. (**166**) comparing the sliding velocity of a millimetre bubble on clean glass (contact angle 10°), hydrophobized glass (contact angle 45°), and fine bubble-frosted glass surfaces (**Figure 11**). In a hydrophilic glass, no attachment was observed during the 120 ms recording, while bubble attachment happened under 100 ms on the hydrophobized glass. On a fine bubble-frosted surface, bubble attachment occurred approximately five times faster at 20 ms. If the coalescence time is significantly shorter than the reported bubble-particle attachment time (a few milliseconds), mineral flotation can be enhanced.

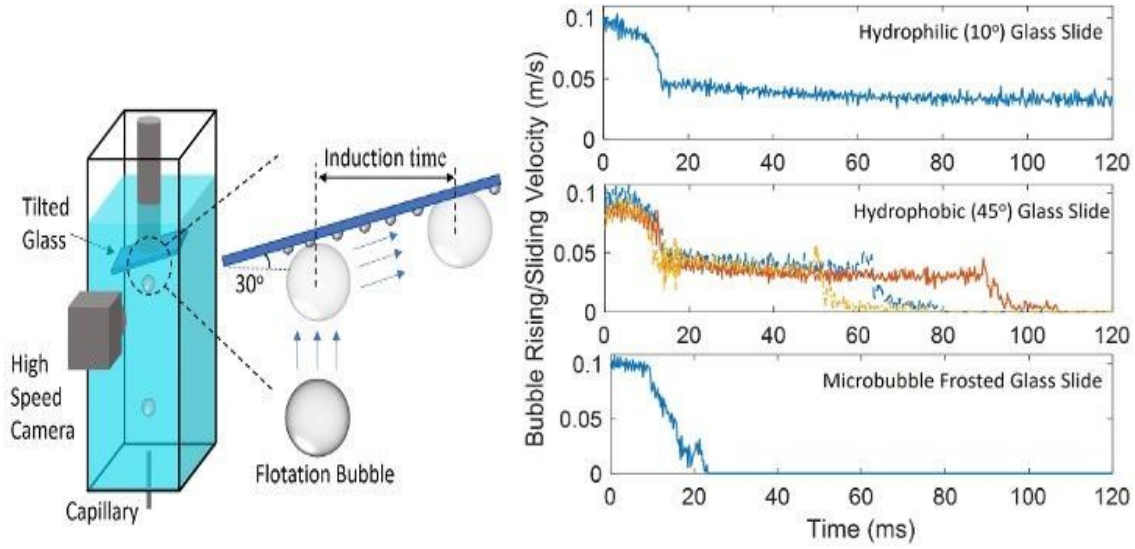

*Figure 11: Designed bubble sliding experiment setup (a) to observe the induction time differences of the attachment of a millimeter bubble on a clean glass surface, hydrophobized glass surface, and a fine bubble-frosted glass surface (b). Extracted from (**166**).*

Extensive research has been done on bubble coalescence (**179 – 184**). These works revealed the complex effect of hydrodynamics, surface deformation, and surface forces on bubble-bubble interaction (**Figure 12**.a). For instance, the dynamic evolution of the thin liquid film trapped between two millimeter-size bubbles was directly observed using the Scheludko cell (**183**), while the time dependent forces between micrometer-size bubbles could be measured by AFM (**179, 184**). However, the experimental collision speeds were limited to below 0.1 mm/s. A new experimental method called Dynamic Force Apparatus (DFA) (**180**), which allowed higher collision speeds to mimic industrial operation conditions, was applied to achieve the simultaneous measurements of interference fringes and interaction forces at bubble speeds on the order of 1 mm/s. The interference fringes provided the asymmetric variation of the thin film thickness with time (**179**). In this experiment, the coalescence time between a micrometer surface bubble (30 - 700 μm) and a large bubble (1.2 mm) was shown to be size-dependent (**185**). In other words, shorter coalescence times were observed for surface bubbles < 100 μm. This reinforces the faster attachment of large flotation bubbles on bubble-frosted mineral surfaces and adds the importance of fine bubbles to this process. However, those studies have a very fundamental basis and usually use hydrophobized glass surfaces (**166, 185**). To this date, it appears that no study of bubble-bubble interaction included the use of minerals as the solid substrate.

Overall, when two bubbles approach, a thin liquid film forms between them and starts to drain. These processes culminate in the deformation of the large bubble due to hydrodynamic pressure, disjoining pressure, and capillary forces (**Figure 12**.a) (**179**). As the drainage process evolves, several other factors influence bubble-bubble coalescence, including viscous forces and the bubble-liquid surface tension (**Figure 12**.a). Another important factor that reduces the drainage velocity is the presence of reagents (immobile surface) as can be seen in **Figure 12**.d and **Figure 12**.e. Differences in the shear-stress at the solid-liquid interface due to the presence of surface bubbles have also been discussed by Bremond et al. (**105**). Surface forces (disjoining pressure) between both bubbles such as Van der Waals (VDW) forces and the electric double-layer (EDL) forces also play a role in the coalescence process (**Figure 12**.b). However, for dynamic systems, the EDL forces are often neglected (**180**) and the VDW forces are the major contribution, resulting in both bubbles attraction.

The presence of a surface fine bubble generates an excess of pressure inside the trapped liquid film that adds to the disjoining pressure (**Figure 12**.c and **Figure 12**.e). The smaller the surface bubble, the higher the Laplace pressure which explains the faster film drainage with smaller bubbles (**179**) compared to the case without surface bubbles (**Figure 12**.b and **Figure 12**.d). All these assumptions are part of the Stokes-Reynolds-Young-Laplace (SRYL) model (**179**) and its agreement with the experimental results provided by Liu et al. (**185**) validates it. A detailed mathematical description can be consulted elsewhere (**179, 186**).

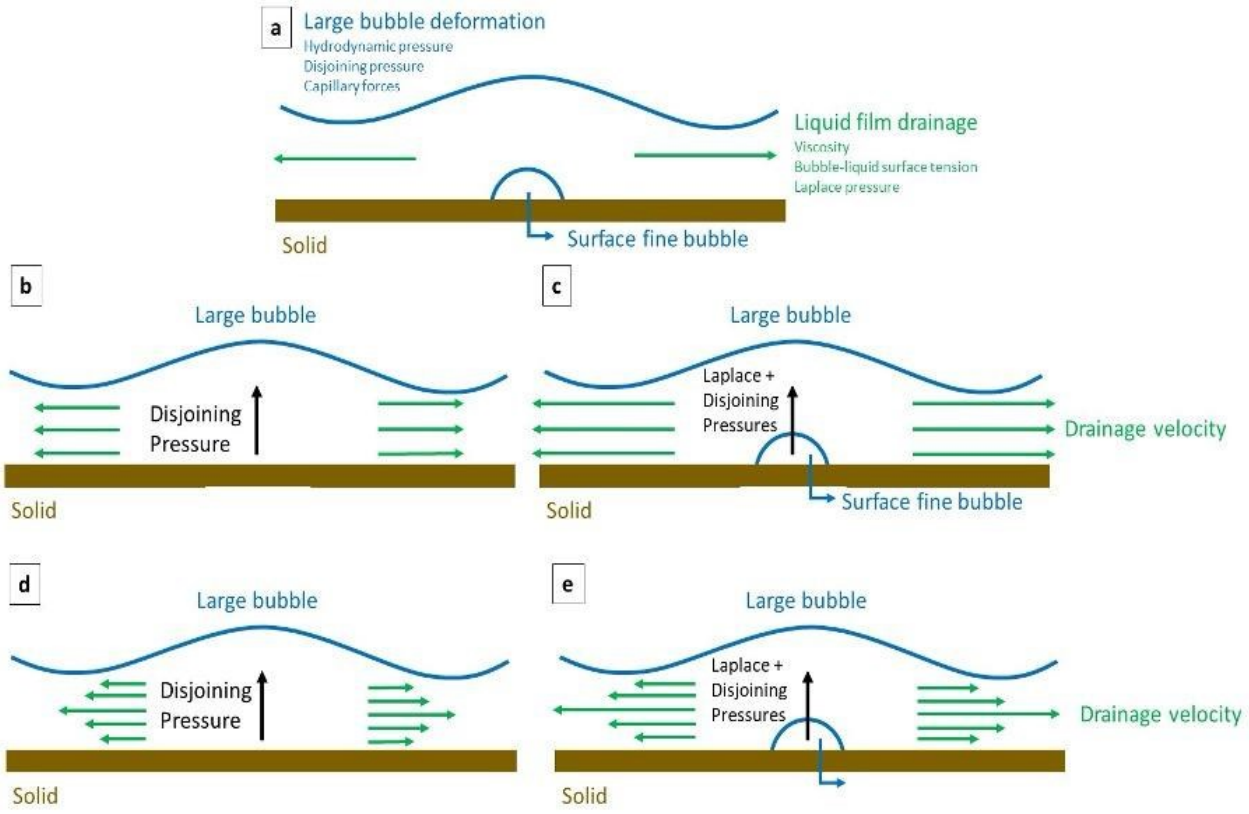

*Figure 12: Schematic process of liquid drainage when a large air bubble approaches a solid surface without (b) and with (c) a surface fine bubble, highlighting the main forces involved (a). Note that the situations (d) and (e) refers to change in drainage velocity in case of immobile surfaces. Compiled from **(179, 186)**.*

2.7. Introduction to flotation gasses for producing conventional and fine bubbles

Regardless of gas type, the role of fine bubbles in enhancing flotation kinetics, especially for fine minerals, has been a great part of mineral processing studies in recent decades. Fine bubbles can bridge water and hydrophobic minerals which has been demonstrated by some studies. Zhang and coworkers used a tapping mode AFM imaging to discover the thin nano-layer gas phase of about 5 – 80 nm produced at the interphase between a surface that is hydrophobic and water surface (**187**). Using sum frequency vibrational spectroscopy (SFVS) and to support the AFM studies, another study was able to demonstrate that the presence of water exclusion zone at the hydrophobic silica surface (due to no hydrogen bonds) facilitates bubble attachment upon contact resulting to film thinning and rupture (**188**). This means that fine bubbles promote its interaction with a hydrophobic surface via van der Waals forces, thereby acting as a bridge for improved bubble attachment and flotation recovery. Thus, formation of a bubble-particle attachment in the flotation process is when there is thin liquid film rupture at the surface of the hydrophobic mineral and a three-phase contact line begins to form and develop (**16**). In terms of producing fine bubbles, carbon dioxide readily dissolves and generates finer bubbles than other gases used in mineral processing such nitrogen gas, oxygen and in most cases, air (**9 – 11**).

Aside from improved solubility and ability to produce finer bubbles, there are other reasons why carbon dioxide is being considered as a better alternative to conventional gases (like air and nitrogen) used in mineral processing. Due to different species of CO_2 gas present when dissolved in water, they can interact with divalent cations in ore suspensions and reduce their negative impacts (**189**). At the same time, CO_2 can be permanently stored in mineral form as carbonates, a strategy to mitigate GHG emissions.[17] Divalent cations usually present in process waters promote the slime-coating of valuable minerals and negatively impacts their recovery, for example, the presence of Ca^{2+} in solution reduces phosphate concentrate (**18, 189**). Divalent cations (Ca^{2+} and Mg^{2+}) are reported to have a detrimental effect on the separation and rheology of ultramafic nickel ores under ordinary conditions (i.e. with air as a flotation gas) (**190 – 192**). Therefore, addressing the issue of high slurry viscosity and slime-coating of valuable minerals contributed by these divalent cations can be achieved when CO_2 is introduced as an alternative gas, specifically in the flotation system. Application of CO_2 to achieve these benefits requires fundamental understanding of CO_2 properties and interactions with mineral surfaces.

2.7.1. CO_2 unique characteristics as a flotation gas

As repeatedly mentioned, one of the distinguishing properties of CO_2 compared to other gasses applied in flotation systems is its enhanced solubility (**9 – 11**). **Table 2** shows the solubility of different gasses dissolved in 100 mg of water at 20 °C and 1 atm total pressure of the solution (**193**). It is evident that the solubility of carbon dioxide is higher than other gasses like nitrogen used in mineral processing. Certain interactions contribute to higher solubility of CO_2 compared to other gasses used in flotation systems. Carbon dioxide has a partial polarization due to its oxygen atom with partial negative charge and readily reacts more with water molecules which also possess partial charge (**194**).

*Table 2: Solubility of gasses (g) dissolved in 100 g of water at 1 atm and 293 K. Modified from (**193**).*

Gas	**Solubility**
Carbon dioxide	0.0169
Nitrogen	0.0019
Oxygen	0.0043

The solubility of CO_2 gas in water is about 20 times greater than that of air in water, and the amount of dissolved CO_2 depend on the conditions of the system (**9**). For example, the solubility of CO_2 gas and the production of CO_2 bubbles for froth flotation would depend on the type of bubble generation system, concentration, types of reagents, pH, pressure, temperature etc., (**Table 1**). To maintain the use of dissolved CO_2, certain conditions promoting its solubility in water should be employed and the other unfavorable conditions should be avoided. For instance, increasing the temperature of a system with dissolved gasses increases the mobility of the molecules and thus, forces the gas molecules to escape instead of remaining in the solution (**10**). This decreases the solubility of CO_2 in water. In a chemical equilibrium state, increasing the concentration of carbonic acid will also cause an increase in CO_2 gas (**194**). Whereas, increasing the pressure of CO_2 gas will increase CO_2 solubility and produce more carbonic acid which is an interpretation of Henry's law on partial pressure and solubility of gasses (**194**). CO_2 has high partial pressure which increases its solubility in water.[19] Having higher gas solubility enhances the production of finer bubbles

required for processing fine mineral particles (**10, 11**). The equation that expresses the solubility of CO_2 in water is given by **Equation 19** (**194**).

$$CO_{2\,(g)} + H_2O \rightarrow H_2CO_{3\,(aq)} \quad (19)$$

At any given condition, there are different species of CO_2 which are in equilibrium with each other. Carbonic acid is initially formed as a result of the interaction between CO_2 and water, which then creates room for more CO_2 to dissolve as defined by Le Chatelier's principle (**194**). At neutral pH, carbonic acid is deprotonated and is in further equilibrium with bicarbonate which is also in equilibrium with carbonate at higher pH (**Figure 13**) (**23, 194**). Thus, the ability of CO_2 to form different species is another distinguishing feature from other flotation gases. The complete equilibrium is given as (**Equations 20 - 22**) (**194**)

$$CO_{2\,(g)} + H_2O \rightarrow H_2CO_{3\,(aq)} \quad (20)$$

$$H_2CO_3 \rightarrow HCO_3^- + H^+ \quad (21)$$

$$HCO_3^- \rightarrow CO_3^{2-} + H^+ \quad (22)$$

As already mentioned, temperature changes have a huge effect on the solubility of any gas (**195**), and this has been demonstrated in a recent study (**10**). They identified an optimum saturation temperature of 4 – 7 °C which caused more CO_2 saturation in the deionized water and rapid increase in flotation recoveries to over 85% in 10 s. As the temperature increased to more than 30 °C, the recovery largely reduced to less than 60% in 120 s. CO_2 gas has high entropy and by increasing the temperature, its equilibrium is shifted towards the free CO_2 (**196**). Thus, to consider its carbonation application, optimum parameters values like the temperature need to be understood.

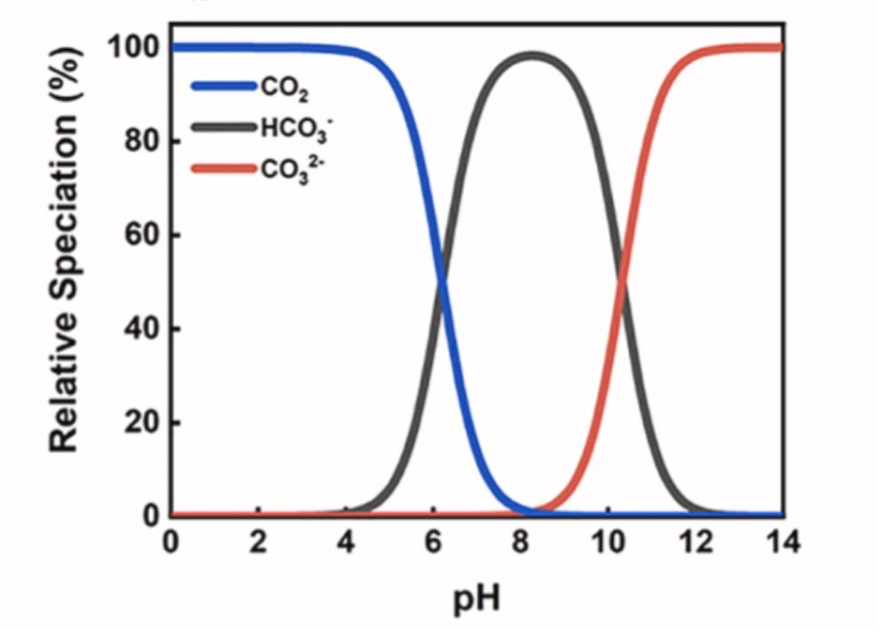

*Figure 13: Species of CO_2 in water at different pH values. Extracted from (**23**).*

It was also shown that CO_2 gas phase has a long life which can be attributed to the fact that CO_2 average density is close to the atmospheric pressure (**187**). Through different experimental procedures (IR, optical images, and AFM) with the same conditions, they demonstrated that stable nanoscale gas bubbles are present at hydrophobic interfaces of methylated silica spheres and water. The CO_2 bubbles had a large radius of curvature R (approximately 4 μm), which is a condition required to maintain a stable bubble (**197**) and are not under high pressure. This is because highly curved bubbles with a small radius of curvature of between 10 nm and 100 nm have high LaPlace pressure resulting in a shorter lifetime (1 to 100 μs) or faster collapse (**198**).

2.7.2. Differentiating CO_2 from other gasses using surface studies or interactions with mineral surfaces

Bubble attachment studies can be used to differentiate CO_2 and other gases. Bubble attachment time in CO_2 saturated solutions is shorter when compared to other gasses, in N_2 saturated solution for example (**16**). A gas bubble having a shorter attachment time (usually less than 20 ms) with a mineral particle or surface indicates that there is strong affinity between them which translates to

good flotation recovery and vice versa for bubble attachment time of 20 ms and above (**199**). Attachment studies revealed that the bubble attachment time in CO_2 saturated solution with pyrite particles is about 5 ms, while an attachment time of 30 ms was recorded for N_2 saturated solution (**16**). Surface area and bubble attachment measurements on coal surfaces indicated that carbon dioxide exhibits a high adsorption potential and thus, higher surface areas than nitrogen and air (**17**). The attachment time for these CO_2 bubbles was found to be about five times shorter than that of air and nitrogen, which translates to the ability of CO_2 bubbles to further improve film rupture and formation of three-phase contact line. This re-emphasizes the strong affinity of carbon dioxide on hydrophobic mineral surfaces.

In another study, saturating the solution with CO_2 prior to nitrogen flotation, produced fine bubbles which nucleated on the hydrophobic surface of pyrite that has been treated ultrasonically, thereby enhancing attachment of the pyrite particle-N_2 bubble, promoting pyrite particle-particle aggregation, and generally improving flotation recoveries (**10**). The bubble attachment time was less than 10 ms for over 80% successful attachment. Similarly, Snoswell and coworkers performed experiments to demonstrate the formation or nucleation of CO_2 nanobubbles at the relatively hydrophobic fresh pyrite surface as soon as the CO_2 saturated solution encounters the pyrite surface (**11**). This resulted in short bubble attachment time and more attractive behaviour between the particles. In comparison to the nitrogen-saturated coal surface which exhibited poor bubbles nucleation, CO_2-treated coal surface showed an enhanced bubbles nucleation and growth (**17**). As demonstrated by Vaziri Hassas and coworkers, CO_2 bubbles have also shown to possess higher elasticity because the bubbles showed elongation behaviour after collision and attachment with the mineral particles (**16**). An explanation given was that part of kinetic energy is utilized in surface deformation for the so-called elastic CO_2 bubbles, thereby reducing the probability of the bubbles to bounce back after collision.

Surface charge experiments have indicated that CO_2 bubbles have negative zeta potential which explains their attachments to hydrophobic mineral surfaces and their ability to improve hydrophobicity on some oxidized mineral surfaces (**24**). Contact angle measurement with a goniometer on coal surfaces revealed a higher contact angle of more than 45° for CO_2 bubbles, while that of nitrogen and air were below 40° (**17**). When the contact angle of different gases was simulated on pyrite surface using Molecular Dynamic Simulations, it was observed that CO_2

bubbles exhibited approximately 180° and N_2 bubbles formed a hemispherical shape with an angle of 90° (**16**). This means that CO_2 bubbles are more hydrophobic and would enhance hydrophobic interactions with valuable minerals. Measuring CO_2 and N_2 bubble sizes generated by the same method revealed that the CO_2 bubbles were < 20 μm up to 1 mm, while that of N_2 bubbles were larger (more than 1 mm). Finer bubbles are necessary to enhance fine mineral recovery by increasing their attachment, aggregation, and floatability. Hence, application of carbon dioxide as a flotation gas would be beneficial in processing low-grade ores that require fine grinding to liberate fine valuable minerals.

Therefore, enhanced solubility of CO_2 is important to phenomena such as hydrophobicity of mineral surfaces. As already indicated, CO_2 dissolves readily in water and can form fine bubbles more than most gasses (**10, 11**). Fine bubbles enhance flotation kinetics by promoting aggregation of fine mineral particles (**7, 8**), and by depositing on the surface of mineral particles which increases mineral hydrophobicity. Gaseous CO_2 shown as a rotational fine structure from the infrared spectrum measurements in an attenuated total internal reflection (ATR) setup, are present at the interface of hydrophobic particles like the methylated silica spheres dispersed in aqueous 10^{-4} M solution at pH 5.6 (**187**), forming tiny submicron bubbles at the surface and enhancing aggregation of the silica particles (**200**). As summarized in a previous study, the formation of fine bubbles on the surface of hydrophobic particles enhances the interaction between the mineral particles, which also increases the aggregation kinetics as the CO_2 concentration increases (**201**). As CO_2 is continuously adsorbed on hydrophobic surfaces or sites, nucleation, and diffusion of CO_2 nanobubbles bubbles follows immediately at those sites, and they continue to grow and spread on these hydrophobic surfaces thereby enhancing their aggregation (**97, 195, 202**).

Understanding these unique properties of CO_2 and their interactions with mineral surfaces explained in these two sections (**2.7.1.** CO2 unique characteristics as a flotation gas **and 2.7.2.** Differentiating CO2 from other gasses using surface studies or interactions with mineral surfaces) are important in establishing their application in mineral processing or mining operations. These properties are summarized as: increased solubility leading to fine bubbles generation, ability to form different species and act as a buffer, long life, and enhancing mineral hydrophobicity, attachment, and aggregation.

2.8. Application of CO_2 in the mining industry

CO_2 has been applied in some mining related or research settings for different purposes including in flotation systems for the processing of minerals and treatment of wastewater. It has also been applied in many other ways such as in tailings management or its storage in geological units as a carbon capture strategy. These applications of CO_2 are explored in this section.

2.8.1. The use of CO_2 in mineral processing and in wastewater treatment

The use of CO_2 as a flotation gas has been reported in some literature for the recovery of different minerals. Researchers have identified many ways in which CO_2 can be beneficial which include acting as a pH modifier (**20, 21**), functioning as a depressant (**18, 19**), or simply being used as a flotation gas (**15, 16**). **Table 3** summarized some applications of CO_2 in flotation systems. In an experiment to investigate CO_2 attachment at pyrite surfaces in the absence of a collector (the effect of CO_2 on the flotation of pyrite), it was reported that the formation of CO_2 nanobubbles at the surface of the pyrite improved the flotation recovery of pyrite (**16**). However, flotation was impacted at alkaline pH values even after sonication treatment due to stabilization of hydroxide species on the pyrite mineral surface which reduced the hydrophobicity of pyrite and the ability of the CO_2 bubbles to attach to them. Poor flotation recoveries at high pH values when carbon dioxide is used remains an area to be addressed in mineral processing. Another study reported improved coal recovery by floating with CO_2 than with air or nitrogen gas (**17**). They revealed that CO_2 indicated a high adsorption potential by having larger surface areas on coal surfaces than air and nitrogen as was observed from surface area measurements. Bubble attachment time also revealed a much less time of 20 ms for CO_2, as well as development of bubbles and nucleation on CO_2-saturated coal surface. These observations indicated increased film rupture in CO_2-assisted flotation necessary for improved recovery which was also observed in the previous study of pyrite flotation experiments.

The use of CO_2 in coal flotation provides an advantage of processing of oxidized and finely ground coal particles (**17**). They demonstrated that even without addition of a collector and a filtration

stage, subjecting coal particles to CO_2 conditioning and flotation yielded a far better recovery plus a reduced ash content than air-assisted coal flotation.

CO_2 can also act as a pH modifier. Klein and Pawlik defined a pH modifier as a dissolved inorganic ion that has the capability of acting as either a dispersant or a coagulant (**203**). They explained that for coagulation to occur, it means that zeta potential is zero at a certain pH called isoelectric point. Whereas dispersion or electrostatic repulsion occurs by increasing or decreasing the zeta potential from point zero. Thus, it is important to understand what the intended use of CO_2 is at any given time and in any given system. In a two-stage flotation process of siliceous carbonate phosphate ore for example, CO_2 was used as pH modifier to concentrate apatite, specifically to float calcite/dolomite followed by apatite flotation with other additives (**18**). In this case, CO_2 was used as an apatite depressant.

Table 3: CO_2 application in mineral processing and wastewater treatment.

Material	Function	Flotation pH	Findings	Reference
Waste activated sludge (WAS)	flotation gas	6.7 to 7.1	CO_2 flotation was better than air flotation at low gas dissolution/ conditioning pressure. Dewatering was improved by increasing the concentration of the WAS by 7 - 10 times. Average diameter size of the CO_2 bubbles is between 150 - 250 micron.	(**9, 207**)
Siliceous carbonate phosphate ore	pH modifier	-	Initial stage flotation of calcite/dolomite, then apatite flotation with corn starch as depressant and a combination of fatty acid soaps and sulphosuccinate as collectors.	(**20**)
Carbonate phosphate ore	pH regulator	-	Direct apatite flotation with corn starch as depressant and sulphosuccinate as collector.	(**21**)
Carbonaceous uranium-phosphate ore	depressant	8 approx.	The first stage flotation, CO_2, was used in a mixture with coconut soap to collect calcite and depress apatite. The next stage involved apatite flotation with sulphosucinnate as	(**18,19**)

			the collector and cornstarch as depressant.	
Carbonaceous uranium-phosphate ore	flotation gas	8.5	Bench scale calcite flotation with coconut fatty acid as a depressant and CO_2 was injected through the bubble generation system to concentrate apatite.	(**15**)
Pyrite minerals	flotation gas	3	CO_2 functioned as a collector when bubbled and led to the formation of CO_2 nanobubbles at the surface of the pyrite improved the flotation recovery of pyrite. As the pH (6 and 10) increased, the flotation recovery of pyrite reduced.	(**10, 16, 24**)
Coal	flotation gas	5	There was shorter attachment time, bubbles development and nucleation on CO_2-saturated coal surface, resulting in improved coal flotation as compared to air and nitrogen.	(**17**)
Sphalerite	Pre-condition/pre-saturation via HIC	6	Increased CO_2 solubility and fine CO_2 bubbles which resulted to enhanced aggregation and flotation kinetics	(**22**)
Ultramafic nickel ores	For pre-condition/pre-saturation	10.1	Enhanced nickel recovery and grade while suppressing the gangue mineral recovery. CO_2 was simultaneously captured as magnesium and calcium carbonates.	(**23**)

In the first step of realizing carbon storage and improving nickel recovery from ultramafic ores, Wani and coworkers have been able to demonstrate that conditioning of the flotation pulp with CO_2 prior to air flotation suppressed recovery of the gangue MgO material, thus reducing viscosity and yield stress, improved nickel grade and recovery, and captured CO_2 in the form of $MgCO_3$ and $CaCO_3$ (**23**). The study has therefore provided a strong background for the potential use of CO_2 in mineral processing operations and specifically, its potential use as a flotation gas in processing ultramafic ores. Another important information obtained from this study is that pre-conditioning with CO_2 at pH 10.1 should also make flotation at pH 10.1 possible, which is the optimal flotation

pH for nickel recovery (**204**). Thus, a combination of pre-conditioning with CO_2 and its use as a flotation gas can improve the overall process of nickel recovery and increase storage of CO_2 in the form of $MgCO_3$ and $CaCO_3$. This promising method will contribute to mitigating climate change effects caused by carbon emissions from mining and mineral processing operations. It will also provide a new idea for mining companies to capture emitted CO_2 from their processes.

Interestingly, the use of CO_2 for both precondition and as bubbles has been attempted to float pyrite samples in a different study (**24**). They found out that the fresh pyrite samples were recovered at both acidic and alkaline conditions even when the froth stability was negatively impacted at pH 10. They argued that the reason for pyrite recovery at pH 10 (with poor froth phase) can be linked to the nucleation and growth of CO_2 fine bubbles on pyrite surfaces which increased the hydrophobicity of pyrite particles and promoted bubble-particle attachment. Thus, investigations at different pH values exhibited different flotation behaviours when CO_2 was used to float some sulphide minerals. CO_2 flotation of pyrite at pH 3, pH 6, and pH 10 revealed that the repulsive interaction between pyrite particle and pyrite surface increased as the pH increases (**16**). A similar result was confirmed by Ozun et al. (**10**) where at high pH values, the CO_2 flotation of pyrite is impacted due reappearance of oxidized mineral surface even after sonication treatment. The sonication of the pyrite was only able to maintain a hydrophobic surface at a low pH (pH 3) regardless of the treatment time. Longer sonication time above 60 mins even impacted recovery negatively at this pH. It was observed in their study that there was strong buffering capacity of CO_2 saturation at pH 4, meaning that a huge amount of basic solutions is required to attain higher pH values. The implication is that at basic pH values, CO_2 flotation can be affected. This supports a previous study, where they reported that the resulting effect of increasing pH is high oxidation of the pyrite surface, thereby increasing the hydrophilicity (or reducing the hydrophobicity) of the pyrite surface (**205**).

In a study carried out by Tabor and coworkers, they summarized that at below pH 6 or an acidic pH, CO_2 nanobubbles are more stable, while the carbonic acid (H_2CO_3) and bicarbonate (HCO_3^-) species dominate at higher pH values (**206**). Thus, more studies are needed to understand the behaviour of CO_2 at alkaline conditions as some sulphide minerals are floated better at pH above 6. Poor froth stability and decreased flotation recoveries for CO_2-assisted flotation at pH 10 has been a common issue for researchers and more studies are required to fill this gap. However, CO_2

flotation at pH 10.1 remains to be explored for ultramafic ores and this thesis is aimed at investigating that.

Although CO_2 already produces smaller sized bubbles than other flotation gases, certain methods can be used to enhance the production of CO_2 fine bubbles or other gasses bubbles which have been discussed in **Section 2.6.** Fine bubble assisted flotation **and Table 1**. Studies have employed high intensity conditioning (HIC) through hydrodynamic cavitation to produce smaller air bubbles (**22, 84**). Through hydrodynamic cavitation, HIC can produce small size bubbles when a gas dissolves in water. Since the poor solubility of air in water under ambient conditions does not improve flotation of fine particles by hydrodynamic cavitation, the higher solubility of CO_2 makes it more suitable for saturation prior to HIC providing a better hydrodynamic cavitation. In essence, the CO_2 option will produce more smaller bubbles thereby promoting fine particle aggregation. In their experiment, they showed that saturation of the slurry with CO_2 addresses the limitation of use of air as a saturation gas. Therefore, an increased solubility of CO_2 resulted in a more efficient aggregation and enhanced flotation of fine sphalerite. A smaller bubble size, and higher collected gas volume was also observed for CO_2.

2.8.2 Application of CO_2 in tailings management or for decarbonization purposes.

Studies have explored ways to remove carbon dioxide from the atmosphere, process or make them less harmful. For example, a laboratory-scale study used ultrasonic bathing and excitation reaction with a flotation cell to promote the dissociation of CO_2 gas into a harmless form ($C + O_2$) using copper catalyst, as well as demonstrating the ability of monoethanolamine to absorb CO_2 gas when excited (**208**). In the mineral processing and mining industries, CCUS technologies are rapidly progressing. For instance, direct carbonation of many fly ash or coal tailings in coal power plants is now considered as studies have shown it is feasible, due to the high CO_2 adsorption capabilities of these materials (**209**). The studies showed that the fly ash contains oxides of calcium and magnesium which are able to fix CO_2 forming calcium and magnesium carbonates respectively as shown in equation 5 and 6 respectively (**194, 210, 211**). This provides a stable mineral carbonation process. Hence, the consideration for the direct carbonation of geological formation due to presence of oxides calcium and magnesium in silicate minerals distributed worldwide.

$$Ca^{2+} + CO_3^{2-} \rightarrow CaCO_3 \quad (23)$$

$$Mg^{2+} + CO_3^{2-} \rightarrow MgCO_3 \quad (24)$$

A big advantage of mineral carbon storage in a chemical process like this is that they are thermodynamically stable and they possess the ability to bring about carbon neutrality (**196**). This is because there are abundant oxides of calcium and magnesium in silicate minerals that easily react and bind to CO_2 under ambient conditions like those found in ultramafic nickel deposits (serpentine, $Mg_3Si_2O_5(OH)_4$) in the earth's mantle (**212**). The thermodynamic stability also minimizes the risk of accidental release of CO_2 because this carbonation reaction is not easily reversed, and the CO_2 is not kept in free phase. The GHG emission contribution from mining operations can be completely addressed if these deposits with oxides of calcium and magnesium are optimized for absorbing and storing carbon. Similarly in the oil industry, a decarbonization approach referred as CO_2 enhance oil recovery is being used to simultaneously store carbon and recover oil (**213**), due to similar composition found in those oil deposits. To fix CO_2 released from burning one ton or carbon will require 3.3 of MgO (equivalent to 4.7 t of CaO). Thus, Lackner and coworkers summarized several considerations for mineral carbonation (**196**). They include: (a) direct carbonation of ground mineral samples in a gas-solid reaction process; (b) carbonation of oxides/ hydroxides of calcium and magnesium; (c) carbonation of $Mg(OH)_2$ in a non-aqueous environment under high pressure; (d) carbonation of $Mg(OH)_2$ in a aqueous environment at low temperatures; and (e) Using high temperatures to directly inject CO_2 into underground reservoirs that contain calcium bearing minerals. One of these considerations can be employed when designing carbonation strategies for tailings or waste rocks.

Interestingly, ultramafic nickel ores contain oxides of magnesium which makes them suitable for carbon storage opportunities. By using CO_2 as a flotation gas in processing ultramafic nickel ores, such opportunities can be explored simultaneously with flotation benefits. Ultramafic nickel ores and how CO_2 flotation can be used to enhance nickel recovery are discussed in the following section.

2.9. The complexity of nickel bearing minerals and the role of CO_2 bubbles.

Nickel containing ores such as ultramafic nickel ores are distributed at several locations worldwide. Due to the high content of serpentine (> 50 wt.%) and low content of pentlandite (< 5 wt.%) (**214**), found in the Thompson Nickel Belt located in the Manitoba province of Canada (**6, 215, 216**), extraction of nickel from this ore and other ultramafic ores poses a difficult task. Although it possesses the alkalinity property needed to store CO_2, serpentine ($Mg_3Si_2O_5(OH)_4$) is an unwanted phyllosilicate mineral in this ore which negatively influences processing of ultramafic nickel ores and recovery of nickel (**190**). Serpentine comprises of an octahedral brucite ($Mg(OH)_2$) sheet ($Mg(OH)_2$) and a tetrahedral silica (SiO_2) sheet in a 1:1 arrangement and are joined by van der Waals forces (**214**). There are three polymorphs of serpentine in the form of fibrous chrysotile, corrugated antigorite, and platy lizardite (**23**). Due to these different polymorphs, they can form long/tiny fiber networks that increase slurry viscosity, a fiber-bubble aggregate to be collected in the concentrate, or contribute to yield stress issues (**191, 217, 218**). Thus, besides the problem of ultramafic ore being a low-grade ore source for nickel, there is an issue of slime coating of the valuable pentlandite mineral by serpentine due to fine grinding required to release the valuable mineral, which increases the production of serpentine slimes (**23**). Under the normal flotation pH (alkaline conditions) for sulphide minerals, serpentine's surface is positively charged due to the presence of the magnesium cations (Mg^{2+}) (**14**), which further increases slime-coating of valuable minerals.

Slime coating of the pentlandite mineral can be contributed by both Mg^{2+} from the serpentine mineral, and Ca^{2+} from recycled process water where lime is used as pH modifier (**23**). Slime coating of valuable minerals by slimes has been a repeated occurrence in the industry over the years. As such, several works using different methods have been carried out to mitigate the slime effect. Yu et al. (**219**) reviewed and summarized some of the methods used to reduce slime coating of valuable minerals in froth flotation. They broadly classified them into chemical and physical means. Chemical methods include the use of dispersant and clay binder, while physical methods include high intensity conditioning (HIC), desliming before flotation, ultrasonic treatment, and addition of another mineral. They emphasized more on HIC because it was found to enhance flotation not just by reducing slime coating, but also by facilitating the diffusion of soluble collectors and particle collision with oily collectors. Thereby, concluding that the physical methods

are more effective. CO_2 will produce finer bubbles than other gases when combined with HIC because of higher solubility of CO_2 gas. Some other techniques to improve flotation of ultramafic nickel ore have also been reported. Uddin et al. (**220**) reported the use of sulphuric acid and mechanical treatment to improve MgO-pentlandite separation and nickel recovery. However, high costs of acids and new equipment to withstand acid attack becomes a problem. They also reported that some of the nickel is lost to solution. In an experiment performed by Yang and coworkers, they used vinylimidazole polystyrene nanoparticles as a collector to selectively adsorb onto pentlandite surfaces, by binding nickel ions to imidazole groups, thereby improving flotation of ultramafic nickel ores (**216**). A major issue reported by the author is the high dosage requirement of this collector making it very expensive. Other pre-treatment methods like microwave heating have been reported to reduce ore yield stress and slurry viscosity of ultramafic suspensions, thereby converting serpentine to olivine (a non-problematic mineral in ultramafic nickel ore processing) (**190, 214**). However, these methods even though they helped in treating serpentine, they have not been fully demonstrated to effectively improve flotation of pentlandite. The success from the use of Na_2CO_3 as both a dispersant and pH modifier as reported by Gibson et al. (**145**), highlighted the potential use of CO_2 as a flotation gas.

In addition, addressing the issue of poor flotation kinetics of low-grade ores like the ultramafic nickel ores have also been demonstrated by other studies and they include the reduction of bubble sizes by dissolved air flotation (**221**), electroflotation (**222**), oscillatory air supply (**223**) and hydrodynamic cavitation (**224**), the increase of apparent size of particles by flocculation and hydrophobic aggregation (**225, 226**), and the intensification of particle collisions via turbulent flotation (**62**). As has been clearly demonstrated in the preceding sections, the use of fine bubbles can be applied as a desliming strategy to improve fine mineral flotation. Studies have shown that the addition of fine bubbles promotes improvements in fine mineral flotation recovery by enhancing fine particle aggregation (**7, 8**), but the "dispersing or desliming" ability of these fine bubbles is not fully investigated. In a high shear environment, Ross et al. (**12**) indicated that bubbling the system with fine air bubbles at high shear and dissipation rates could enhance the removal of oxidized layers and slimes from the minerals' surfaces, thereby improving the flotation kinetics. Due to the higher solubility of CO_2 gas and its ability to produce fine bubbles than other gases used in mineral processing (**9 – 11**), it provides a better alternative to processing ultramafic nickel ores. CO_2 bubbles will assist in desliming pentlandite surface by precipitating magnesium

cations as mineral carbonates as well as increasing the aggregation, hydrophobicity, and floatability of pentlandite minerals

As pointed out by Chipakwe et al. (**89**), use of fine bubbles in combination with flotation reagents can further help to float valuable minerals. Complex ores such as ultramafic nickel ores therefore require special treatments with modifiers to target serpentine, rendering them more hydrophilic and facilitating improved recovery of nickel minerals. A special serpentine depressant called sodium tripolyphosphate (STPP) is explored further in the next section.

2.10. STPP reagent and its role in addressing the complexity of nickel bearing minerals.

STPP ($Na_5P_3O_{10}$) possess the ability to adsorb on serpentine's surface and trigger the dissolution of magnesium cations, thereby changing the charge from positive to a negative charge to reduce its slime coating on valuable sulphide minerals (**14**). Sodium tripolyphosphate, STPP also known as triphosphate (V) pentasodium, is an inorganic compound with wide applications such as in ceramics production, component of both household and industrial cleaning substance, as well as present in many food substances of animals and humans (**14, 227 – 238**). It has also been used to enhance anti-corrosive performance of waterborne epoxy coatings (**228**). From its name, STPP is a sodium containing compound with three phosphate groups with five sodium (**Figure 14**).

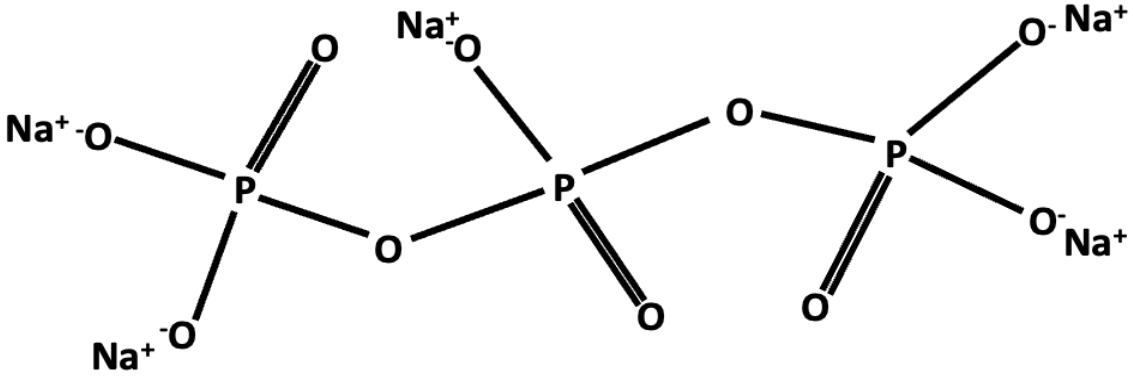

*Figure 14: Structure of Sodium Tripolyphosphate. Drawn from (**14, 235**).*

It is an amorphous linear polyphosphate molecule and due its Na_2PO_4 at each end of the molecular structure, it dissolves quickly in water (**14, 227, 231**). Early studies pointed out the complexing

abilities of phosphates towards magnesium and calcium cations (**236**), and a more recent study by Chen and co-workers demonstrated the ability of a trisodium phosphate (Na_3PO_4) to complex magnesium cations which subsequently improved the flotation of pyrite (**238**). STPP is one of such phosphate compounds that has also been employed to chelate these divalent cations in many mineral processing applications. **Table 4** below summarizes some applications of STPP in mineral processing where it has mostly been used as a depressant in the flotation of Ca-bearing minerals.

Table 4: Application of STPP in mineral processing

Mineral or non-mineral system	Function	Reference
Pyrite-serpentine	serpentine depressant	(**14**)
Yttria-stabilized zirconia suspension	dispersant	(**230**)
Skim milk powder (SMP)	dispersant	(**232**)
Magnesite-calcite	calcite depressant or inhibitor	(**233**)
Scheelite-calcite	calcite depressant or inhibitor	(**234**)
Magnesite-dolomite	depressant	(**235**)

STPP can interact and form complexes with or chelate calcium ions (**232**) and magnesium ions (**14**), thereby reversing the surface charge on the divalent cations bearing gangue minerals. By promoting surface charge reversal of the gangue minerals, their electrostatic interactions with valuable minerals are decreased and the floatability of the valuable minerals is enhanced. According to Li and coworkers, STPP has an enhanced efficiency to depress serpentine than other known serpentine depressants like sodium hexametaphosphate (SHMP) due to the increased capability of the ring phosphate groups to chelate magnesium ions on serpentine surfaces (**14**). They also highlighted that STPP are not easily decomposable and in their results, they demonstrated that STPP depresses more serpentine than other serpentine depressants like SHMP and citric acid (CA) under similar conditions, thereby achieving better flotation benefits. Interestingly, the improved flotation recovery and faster flotation rate obtained in the study was achieved at lower STPP concentration (25 mg/L) when compared to the other depressants' concentrations (CA-40 mg/L and SHMP-60 mg/L) (**14**). Upon interaction with STPP, the magnesium cations present on the surface of serpentine minerals can be chelated with the oxygen

anion present in STPP, thereby leading to the formation of a P-O-Mg type of bonding (**14**). This implies that when STPP is adsorbed onto serpentine surfaces, it reduces the interaction between serpentine and pentlandite minerals, and subsequently increases the amount of free pentlandite that reports to the froth.

2.11. Summary and next steps

The recovery of fine particles by froth flotation poses complex challenges. A lot of work has been done in the last two decades, especially in the last five years as highlighted in **Section 2.1.** Introduction to mineral processing and froth flotation **to 2.2.** Principles of froth flotation. The use of fine bubbles is one of the factors that could help boost mineral recoveries but some of its mechanisms of action are still unknown. For that reason, this literature review attempted to "bridge" fundamental research about fine bubbles with some aspects that could influence froth flotation while, in parallel, identified potential future research.

A description of the main forces present during the interaction of a falling particle and a rising bubbles is provided in **Section 2.3.** Flotation mechanism followed by a discussion about the characteristics of mineral particles and bubbles that affect the collision and attachment sub-processes. Overall, the probability of collision increases when bubble size decreases. The attachment probability is also higher for smaller bubbles due to a faster establishment of a wetting perimeter. However, research focusing on particle-bubble collision and attachment in the presence of reagents (e.g., frothers and collectors) is still necessary since bubble surface mobility may become an essential factor when bubble size decreases.

As bubble characteristics are considered key in this literature review, the process of formation of bulk and surface bubbles is outlined in Section **2.4.** Fine bubbles in froth flotation considering the classic nucleation theory. The presence of pre-gas cavities and particles assist with bubble cavitation by decreasing the energy barrier and demand for dissolved gas. In terms of froth flotation, the goal is to generate surface fine bubbles on target fine mineral surfaces that could promote their aggregation, increasing the chances of collision with larger bubbles. The presence of surface fine bubbles also promotes a faster rupture of the thin liquid film with a conventional bubble due to bubble-bubble coalescence as has been recently proven (see **Section 2.4.2.** On the stability of

surface and bulk nanobubbles). The smaller the surface bubble, the faster is the attachment to a larger bubble. Factors that alter the bubble properties with special attention to different frothers and electrolyte species were discussed in **Section 2.5.** Chemical factors affecting bubble properties. Fine bubble assisted flotation was then introduced into the subsequent section (**Section 2.6.** Fine bubble assisted flotation) demonstrating all the flotation benefits achieved by employing fine bubbles. In that context, the literature review then explored the use of CO_2 as a flotation gas because of its many unique properties including acting as a pH modifier, enhanced hydrophobicity, increased solubility and the ability to produce finer bubbles (**sections 2.7.** Introduction to flotation gasses for producing conventional and fine bubbles to **2.9.** The complexity of nickel bearing minerals and the role of CO2 bubbles.).

However, using the fine bubble assisted approach regardless of the gas type, performance issues with selectivity in real ores may be a reality as penalties in concentrate grades were observed due to higher overall mass recovery. One of the reasons could be the poor understanding of surface bubble nucleation and/or bulk bubble adsorption on mineral particles. For instance, it is completely unclear if surface nucleation is a function of surface hydrophobicity only or also surface roughness. Questions such as "What would rule fine bubble selectivity in a more complex environment?" still remain, hindering the development of more efficient flotation systems. Some additional topics to be addressed are listed below but are not limited to them:

1. The effect of different physicochemical properties of mineral surfaces on selective aggregation using fine bubbles is still required.
2. It would also be beneficial to explore the stability of the froth phase in a CO_2-assisted flotation system (especially with respect to different frothers), as this will further enhance recovery of valuable minerals.
3. While fundamental stability studies seem to focus on justifying their existence, for froth flotation, to know how stable they are under different conditions (e.g., shear and reagents) would be relevant.
4. Investigating the effect of fine bubbles characteristics (type, composition and generation strategy) on the slime coating removal on valuable mineral's surface.
5. It may also be beneficial to study functionalization of bubbles to increase their selectivity for valuable minerals.

Many of these fundamental studies are still required to properly understand fine bubble or CO_2 assisted flotation. By understanding these fundamentals, it will increase their wide acceptance in the mining industry and the subsequent commercialization of these technologies. Despite all challenges and research gaps, fine bubbles assisted flotation is undoubtedly a crucial technology in the context of froth flotation of fine and low-grade ores. Because of its ability to produce finer bubbles than other gasses, CO_2 assisted flotation even presents an added advantage in terms of improving hydrophobicity and recovering more valuable minerals. It has been used for pre-saturation (on in the conditioning stage) as well as a flotation gas for a variety of ores. In a pentlandite-serpentine mineral system, CO_2 gas has never been used as a flotation gas but has only been used to condition the mineral suspension and has shown to enhance pentlandite recovery. This opens the possibility to further explore the use of CO_2 gas in improving recovery in serpentine-pentlandite mineral systems or in ultramafic nickel ores. Thus, a combination of pre-conditioning with CO_2 and its use as a flotation gas can improve the overall process of nickel recovery and increase storage of CO_2 in the form of $MgCO_3$ and $CaCO_3$. It was also established that using STPP as a serpentine depressant would go a long way and further increase the flotation recoveries of pentlandite (**Section 2.10.** STPP reagent and its role in addressing the complexity of nickel bearing minerals.). Since this modifier has never been tested for a serpentine-pentlandite mineral system or in ultramafic nickel ores, it serves as a novel reagent to be employed in this study.

Therefore, it would be interesting to explore the use of STPP in a pentlandite-serpentine system as a serpentine depressant, and the use of CO_2 as a flotation gas. The following experimental study highlights the valuable mineral recovery and gangue mineral suppressive capabilities of both CO_2 and STPP by performing zeta potential measurements, flotation tests, and XPS analyses. The methodology and results are presented in the subsequent sections.

3. Materials and Methods

3.1. Materials

3.1.1. Ore samples

The mineral samples used in this research were obtained as separate minerals from various companies (**Table 5**). Pentlandite was obtained from the Vale Voisey's bay operations, and the serpentine samples were supplied by FPX Nickel from their Baptiste deposit in British Columbia, Canada. Brucite samples were obtained from Fengcheng City Hequi Brucite Mining CO., Ltd., while silica samples were purchased from US Silica. Further size reduction of the samples (pentlandite and serpentine) involved crushing and pulverizing using a bb 200 jaw crusher and a dm 200-disc mill. Further classification was necessary to produce mineral samples in the range required for specific tests. The milled samples were then classified using the Ro-Tap method to obtain -38 μm samples used for flotation tests and XPS measurements. The particle size chosen for flotation tests was because they partly fall within the optimum size range of 20 to 300 μm for flotation (**33 – 36**). This was also to mimic similar size ranges studied by Senior and co-workers, where they demonstrated that pentlandite samples of -2 μm had poor floatability (< 40%), that of - 10 μm had flotation recoveries of < 60%, and pentlandite sample sizes ranging from 15 to 80 μm were nearly recovered (**58**). Since the chosen feed size of -38 μm is not optimal, flotation recoveries under normal conditions (air flotation) should be impacted, and it would make sense to test the effects of STPP and CO_2 with this particular feed size.

The -38 μm powdered mineral samples were further reduced with mortar and pestle to obtain less than 2 μm particle sizes required for zeta potential measurements. To remove possible surface oxidation of the pentlandite samples, the samples were washed in 0.1 m hydrochloric acid (HCl) solution for about 6 h, rinsed with deionized (DI) water, freeze-dried for 48 h, and was stored in a -80 ˚C freezer prior to experiments. Mineralogical characterization of samples was performed by X-ray diffraction (XRD) with a Bruker D8 Discover diffraction system at 2theta range of 5 and 80 degrees, 0.05 step size and 3 degrees/min scan speed (**239**). The obtained data was evaluated using the DIFFRAC.EVA software to identify the mineralogical phases, peaks and plot of the XRD patterns which are presented in **Section 4**.

Table 5: Composition of the mineral samples

Samples	Chemical Formula	XRD Composition	Company
Serpentine	$Mg_3Si_2O_5(OH)_4$	Chrysotile, antigorite and lizardite	FPX Nickel
Pentlandite	$(Fe,Ni)_9S_8$	Pentlandite and pyrrhotite	Vale
Silica	SiO_2	Quartz	US Silica
Brucite	$Mg(OH)_2$	Brucite	Fengcheng City Hequi Brucite Mining Co. Ltd

3.1.2. Reagents

Flotation reagents (**Table 6**) including methyl isobutyl carbinol (MIBC) and potassium amyl xanthate (PAX) were supplied by Flottec. Reagent-grade hydrochloric acid (HCl) was supplied by ACP Chemicals, while sodium hydroxide (NaOH) was obtained from Fisher Scientific. Both were used as pH modifiers for all experiments performed in this work. Analytical grade Sodium tripolyphosphate (STPP) of ≥ 98.0% purity was purchased from Fisher Scientific and was used as serpentine depressant in this work. Research grade carbon dioxide cylinder from PRAXAIR was supplied by Linde Canada Inc.

Table 6: Composition of the flotation reagents

Reagent	Chemical formula	% purity by weight	Function	Brand
Methyl isobutyl carbinol (MIBC)	$C_6H_{14}O$	≥ 98.5%	Frother	Flottec
Potassium amyl xanthate (PAX)	$C_6H_{11}KOS_2$	> 90%	Collector	Flottec
Hydrochloric acid	HCl	30 – 50%	pH modifier	ACP Chemicals
Sodium hydroxide	NaOH	2%	pH modifier	Fisher Scientific
STPP	$Na_5P_3O_{10}$	≥ 98.0%	Depressant	Fisher Scientific
Carbon dioxide gas	$CO_{2(g)}$	99.998%	Flotation gas and depressant	PRAXAIR

3.2. Experimental Procedure

3.2.1. Zeta potential measurements

Zeta potential measurements were performed using the Malvern Zetasizer Nano Particle characterization system (**240**). The device uses micro-electrophoresis, which means that the electrophoretic mobility is determined by performing an electrophoresis experiment on colloidal samples and measuring the velocity of the samples using Laser Doppler Velocimetry. The device measures the zeta potential by obtaining the electrophoretic mobility which is then converted to zeta potential by applying the Henry's equation as shown in **Equation 25**.

$$U_e = 2\zeta\frac{f(Ka)}{3} \tag{25}$$

where,
ζ = zeta potential
U_e = electrophoretic mobility
Ɛ = dielectric constant
η = viscosity
f(Ka) = Henry's function.

When the Henry function f(ka) = 1.5, it is referred to as the Smoluchowski approximation or limit which is appropriate for measuring zeta potential of aqueous media with moderate electrolyte concentrations. By performing zeta potential measurements, it allows us to predict the interaction of different gangue minerals with the valuable mineral, thus, being able to determine those gangue minerals that can slime coat the valuable mineral at different pH values.

3.2.1.1. General conditions for the zeta potential measurements

To perform the zeta potential measurements for any of the experimental types, 40 mg of each mineral samples (serpentine, pentlandite, silica, and brucite) was added into a 100 mL beaker containing 40 mL KCl solution in the presence or absence of serpentine depressants. The pH of the individual mineral suspension was adjusted to pH 10.1 with NaOH (or HCl when necessary) and stirred for 30 mins using a magnetic stirrer. The suspension was then allowed to settle for 10 mins, the supernatant collected and sonicated using Fisherbrand CPX5800 Ultrasonic Bath to remove any bubbles before zeta potential measurements. All experiment types were performed in

triplicates. Specific conditions for each experiment type are explained below and summarized in **Table 7**.

3.2.1.2. Baseline experiments

For the baseline case, no reagent for serpentine depression was used. 40 mg of mineral samples were simply added into a 100 mL beaker containing 40 mL KCl solution only. The pH of the suspension was adjusted to pH 10.1 with NaOH (or HCl when necessary) and stirred for 30 mins using a magnetic stirrer. The suspension was then allowed to settle for 10 mins and the supernatant was collected for zeta potential measurements. Prior to measurements, the collected supernatant was sonicated using Fisherbrand CPX5800 Ultrasonic Bath to remove any bubbles.

3.2.1.3. STPP effect

For the STPP case, different concentrations of STPP ranging between 5 mg/L to 100 mg/L were investigated to determine the optimum concentration for serpentine depression. Actual STPP concentrations that were investigated include: 5 mg/L, 10 mg/L, 15 mg/L, 20 mg/L, 25 mg/L, 35 mg/L, 50 mg/L, 80 mg/L, 100 mg/L. The optimum concentration of 50 mg/L STPP was then applied to other minerals (pentlandite, silica, brucite) to investigate their responses. All other conditions are the same as highlighted in the general conditions and in **Table 7**.

3.2.1.4. CO_2 effect

In the CO_2 case, CO_2 gas was continuously bubbled for about 5 mins while stirring and adjusting the pH to 10.1 with NaOH. Thereafter, the suspension was stirred further for another 25 mins and allowed to settle for 10 mins prior to measurements. Every other condition is the same as highlighted in the general conditions and in **Table 7**.

Table 7: Experimental conditions for zeta potential measurements

Experiment types	Reagent (Depressant)	Amount of mineral	Volume	Electrolyte concentration	pH
Baseline case	None	40 mg	40 mL	10 mM KCl	10.1
STPP case	STPP	40 mg	40 mL	10 mM KCl	10.1
CO_2 case	CO_2	40 mg	40 mL	10 mM KCl	10.1

3.2.2. Microflotation tests

Microflotation experiments were performed in a 120 ml column with a collection chamber and a tube opening fitted at the upper part of the column to allow collection of the froth (**Figure 15**). A frit was constructed at the lower part of the column which allowed bubbles to be produced when flotation gas was introduced at the lower tube opening.

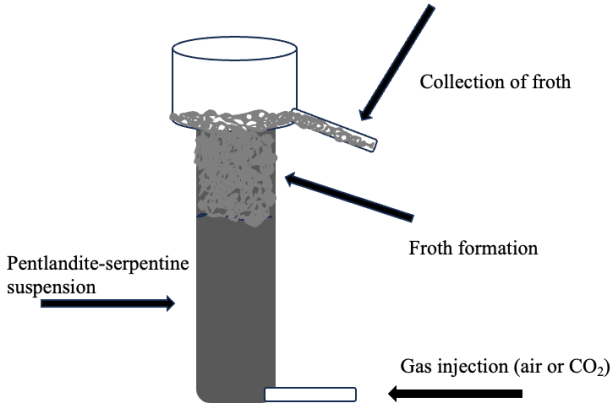

Figure 15: Setup of the microflotation experiment.

All experiments were performed with a 1.5:1 mass ratio of serpentine and pentlandite in 10 mM KCl solution as background electrolyte at pH 10.1. Since the samples are obtained individually, the ratio of 1.5:1 was chosen to imitate the concentrations of serpentine and pentlandite in a real ultramafic nickel ore (**204**). Another reason is to maintain similar conditions used in a previous study (**23**), so as to provide direct comparisons while adjusting to a novel reagent (in this case, STPP), feed size and flotation gas in the serpentine-pentlandite mixture. Thirdly, is to keep the elemental concentrations above detection limits. The choice of pH 10.1 was based on the industrial flotation pH of ultramafic nickel ores (**204**). They confirmed from their metallurgical tests that flotation at pH 10.1 reduces the positive charge of serpentine, thereby reducing the serpentine-pentlandite electrostatic attraction and has remained the optimal pH in the industrial flotation circuits.

A feed particle size of -38 μm was used in the flotation tests and the rationale for the choice has been explained in **Section 3.1.1**. NaOH and HCl were used as pH modifiers, while methyl isobutyl carbinol and potassium amyl xanthate were used as frother and collector respectively. High mass recoveries using smaller bubbles for flotation in the presence of MIBC frother were readily

associated with better recovery of – 38 μm fractions (**89**). It has been repeatedly pointed out by several studies that frothers help to reduce and stabilize bubbles, especially MIBC and hence the reason MIBC frother was chosen for this thesis (**135, 138, 142**). PAX belongs to the xanthate family of collectors which adsorbs preferentially on sulphide minerals and helps to improve their recovery (**35**). The experiments are performed in triplicates to increase accuracy. The different flotation experimental types with varying conditions used in this thesis are presented in the **Table 8** below.

Table 8: Four conditions used in the flotation test.

Experiment type	Gas	Depressant	Description
Baseline	Air	none	Serpentine and pentlandite mixture in air flotation.
Air + STPP	Air	STPP	Serpentine, pentlandite and 50 mg/L of STPP in air flotation.
Air + CO_2	Air	CO_2	Serpentine, pentlandite and 5 mins of CO_2 conditioning prior to air flotation.
CO_2 only	CO_2	CO_2	Serpentine, pentlandite and 5 mins of CO_2 conditioning prior to CO_2 flotation.

3.2.2.1. Experimental procedure for the baseline case

Five g of the mineral suspension at 1.5:1 ratio of serpentine and pentlandite respectively, were prepared in a beaker containing 45 mL KCl solution (10 mM) as background electrolyte. 20 mL of the solution was then used to rinse the beaker after transfer and make up to 65 mL total volume. Prior to flotation cell transfer, 75 ul of PAX collector was added in the beaker, pH was adjusted 10.1 with NaOH or HCl solution and the suspension was conditioned for about 4 mins. Thereafter, the suspension was transferred to the microflotation cell and the flowrate at was maintained between 0.2 L/min and 0.4 L/min. This was followed by the addition of one drop of MIBC frother and 1 min conditioning time before the flow rate was increased to 0.6 L/min, and time started. The flotation gas employed in the baseline experiments is air. The froth was collected, and the froth collection time was recorded accordingly. The process was repeated and a maximum of four

concentrates were collected for each experiment. The experiments were performed in triplicates. The concentrate obtained from the flotation experiments was dried overnight at 60 ℃, and the dried samples were weighed, and analyzed using inductively coupled plasma optical emission spectrometry (ICP-OES).

3.2.2.2. Experimental procedure for air + STPP

The experimental procedure follows the same steps in the baseline case except that there is addition of STPP as serpentine depressant in this case. The addition of STPP occurs during the same time as the addition of 75 ul PAX collector. Every other condition and steps remain the same as the baseline case.

3.2.2.3. Experimental procedure for air + CO_2 and CO_2 only

Just like the air + STPP and baseline cases, the experimental procedure follows the same steps but with some parameter changes. In the case of air + CO_2**,** CO_2 was employed as a serpentine depressant with air as the flotation gas. While for CO_2 only case, CO_2 was used for both conditioning (*i.e.,* as a serpentine depressant) and as a flotation gas.

3.2.3. Inductively Coupled Plasma Optical Emission Spectrometry (ICP-OES)

To determine the recovery and grade of the nickel-bearing pentlandite and quantify the Mg-bearing gangue mineral (serpentine), the overnight dried samples from the flotation tests were subjected to ICP-OES analysis. The instrument is Thermo iCAP 6300 Duo (N. America) inductively coupled plasma-optical emission spectrometer manufactured by Thermo Fisher Corp. Registration No. 441506, SOLAAR House, 19 Mercers Row, Cambridge, CB5 8BZ, United Kingdom, 2012 (**241, 242**). ICP-OES uses an analytical method used to determine dissolved metals like nickel and magnesium in aqueous solutions 2012 (**241, 242, 243**). To perform ICP-OES analysis, about 0.1g of the dried mineral samples were digested overnight in 5 mL of trace metal grade concentrated HNO_3 and diluted to 25 mL with milliQ water (EPA 3051a modified; EPA 6010d modified). The results are presented appropriately.

3.2.4. X-ray Photoelectron Spectroscopy (XPS) tests

XPS is an analytical method used to identify any alterations in the chemical compositions of sample surfaces, such as mineral powder (**14, 237, 244**). Thus, the XPS test were performed on serpentine minerals to demonstrate how the chelating group present in the reagents would react with the ions on the surface of serpentine. In this study, XPS tests are performed on both pretreated and non-treated mineral samples (**Table 9**), following similar experimental procedure in a previous study (**14**).

To get the samples ready for XPS analysis, 1 g of mineral was added to a 40 mL deionized water in the presence or absence of a depressant, the pH adjusted to 10.1 with NaOH or HCl solution and the suspension was continuously stirred for 5 min. For the STPP case, 50 mg/L of STPP depressant was used. In the CO_2 case, the suspensions were continuously bubbled with CO_2 gas as a depressant for 5 mins while stirring and the pH was maintained at pH 10.1 with NaOH or HCl solution. The baseline case did not employ the use of any depressant. After 5 mins stirring or conditioning, the suspension was filtered, the mineral samples were dried below 40 °C in a vacuum oven, and the dried mineral samples were vacuum preserved prior to XPS analysis.

Table 9: Experimental conditions for XPS tests

	Baseline	**STPP Case**	**CO_2 case**
Mineral sample	1 g	1 g	1 g
Reagent	none	50 mg/L STPP	5 mins of CO_2 conditioning
pH	10.1	10.1	10.1
DI water	40 mL	40 mL	40 mL

Room-temperature XPS experiments of the serpentine samples in the absence and presence were performed using Kratos Axis (Ultra) spectrometer (**245**) with monochromatized Al Kα (hυ = 1486.71 eV). The spectrometer was calibrated by the binding energy (84.0 eV) of Au 4f7/2 with reference to Fermi level. The pressure of the analysis chamber during experiments is better than 5×10-10 Torr. A hemispherical electron-energy analyzer working at the pass energy of 20 eV was used to collect core-level spectra while survey spectrum within a range of binding energies from 0 to 1100 eV was collected at analyzer pass energy of 160 eV. Charge effects were corrected by using C 1s peak at 284.8 eV.

A Shirley background was applied to subtract the inelastic background of core-level peaks. Non-linear optimization using the Marquardt Algorithm (CasaXPS) was used to determine the peak model parameters such as peak positions, widths and peak intensities. The model peak to describe XPS core-level lines for curve fitting was a product of Gaussian and Lorentzian functions. CasaXPS was used for component analysis to fit the spectra of C 1s with peaks related to different chemical bonds.

Compositions were calculated from the survey spectra using the major elemental peaks and sensitivity factors provided by the database (Appendix 1 and 2). Baseline values are duplicate values of s1 and s2 from Appendix 1, STPP case values are duplicate values of s4 and s5 from Appendix 1, while CO_2 case values are duplicates of s8 and s9 from Appendix 2. These duplicate values of the different experiments were then compiled in **Table 11** for Mg 2s peaks. Average composition values of the Mg 2s peaks (**Table 11**) were then used to produce plots for raw area (**Figure 30**), atomic and mass concentrations (**Figure 31**).

4. Results and Discussion

4.1. X-ray Diffraction (XRD)

The mineral samples were subjected to XRD, and the pattern revealed the three polymorphs of serpentine namely: chrysotile, antigorite and lizardite (**Figure 16a**). Chrysotile and antigorite are monoclinic in their crystal lattice while lizardite exhibits a hexagonal crystal lattice. Peaks at 12°, 19.8°, 24.3°, 35.4°, and 60.1°corresponds to chrysotile, peaks at 12.1°, 24.7°, and 35.6° corresponds to antigorite, while lizardite peaks at 12.2°, 24.5°, 35.8°, 42°, 50.9°, and 59.9°. For the pentlandite sample, patterns of pentlandite and pyrrhotite with cubic and orthorhombic crystal lattice respectively, are shown in (**Figure 16b**). Pentlandite peaked at 15.3°, 39.1°, 29.4°, 30.8°, 46.9°, 51.4°, 72.1°, and 75.6°, while the peaks at 29.9°, 33.8°, 43.7° and 53° corresponds to pyrrhotite. Sharp peaks at 20.8° and 26.6° were detected for quartz in the silica sample (**Figure 17a**), while peaks for brucite occur at 18.6°, 38°, and 50.8° (**Figure 17b**). Both silica and brucite samples have hexagonal crystal lattices.

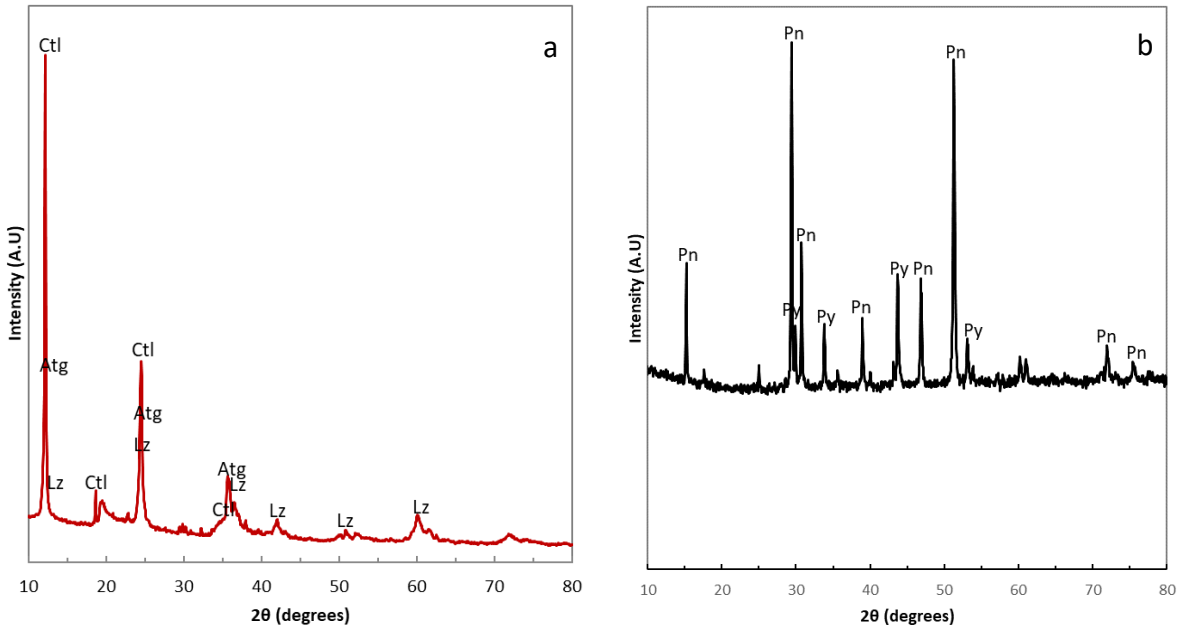

Figure 16: XRD pattern for mineral samples (a) Serpentine and (b) Pentlandite. Ctl = chrysotile, Atg = antigorite, Lz = lizardite, Pn = pentlandite, Py = pyrrhotite

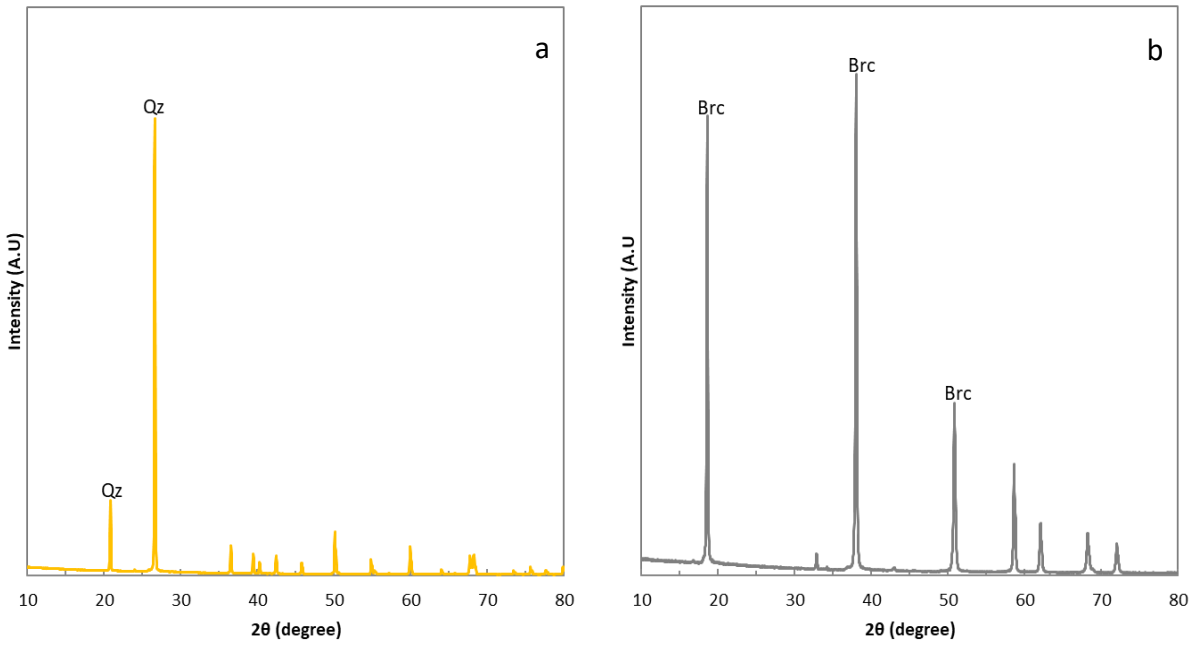

Figure 17: XRD pattern for mineral samples (a) Silica and (b) Brucite. Qz = quartz, Brc = brucite

4.2. Zeta potential

4.2.1. Mineral sizes used in zeta potential measurements

Table 10 which shows the mean particle sizes of the mineral samples used for zeta potential measurements, were also determined with the Malvern Zetasizer (**240**) and it revealed that the pentlandite samples were 881 nm and serpentine samples were 1799 nm, while that of brucite and silica samples were 700 nm and 1048 nm respectively.

Table 10: Mean particle sizes of mineral samples used in the zeta potential experiments.

Mineral	Mean Particle Size (nm)
Serpentine	1799
Pentlandite	881
Brucite	700
Silica	1048

4.2.2. Zeta potential measurements under normal conditions (baseline experiments)

These mineral samples of different sizes below 2 microns were subjected to zeta potential measurements using conditions stated **Table 7** and described in **Section 3.2.1.2**. As seen from **Figure 18a & Figure 18b**, the zeta potential for serpentine showed a positive charge while that of pentlandite exhibited negative charge at pH 10.1. Studies have also shown that serpentine maintains a positive zeta potential over a wide pH range without or little treatment (**246, 247**). Brucite showed a slightly positive charge while silica samples exhibited the most negative charge at the same pH 10.1(**Figure 18a**). The positive brucite plane and the negative silica plane creates a negative interaction energy which means that serpentine exhibits attractive forces which results in an agglomerated microstructure and hence, the reason why serpentine has a positive zeta potential value (**246, 247**).

In the aqueous solution, the hydroxyl group of the brucite plane dissolves easily and leaves behind magnesium cations on the surface of serpentine, thereby creating a positive charge and determining the serpentine's surface charge (**247**). The positively charged serpentine surface contributed by the magnesium cations attracts the negatively charged pentlandite surface which would impact pentlandite's recovery in flotation systems. It indicates that there would be a heterogeneous agglomeration between pentlandite and serpentine meaning that serpentine will slime coat pentlandite particles through its brucite plane resulting in negative total interaction energy for brucite with pentlandite *i.e.,* attractive force or electrostatic attraction (**23, 246, 247**). Due to this electrostatic attraction between serpentine and pentlandite minerals, more serpentine is expected to report to the froth phase together with any pentlandite mineral that eventually attaches to the gas bubbles in the flotation system. In addition, the action of magnesium cations by forming magnesium monohydroxide complexes (**Equation 26**) on the surface of pentlandite renders it hydrophilic and makes it unable to float (**23**).

$$\mathrm{Mg}^{2+} + OH^{-} \rightarrow \mathrm{Mg}(OH)^{+} \quad (26)$$

Moreover, the action of the magnesium monohydroxide also prevents pentlandite from interacting properly with the PAX collector, which in turn impacts its recovery (**23, 248, 249**). That implies that only fewer free pentlandite minerals are available because the pentlandite minerals are either

being attached to serpentine or they are being rendered hydrophilic, thereby reducing the recovery of pentlandite as well as diluting the nickel grade.

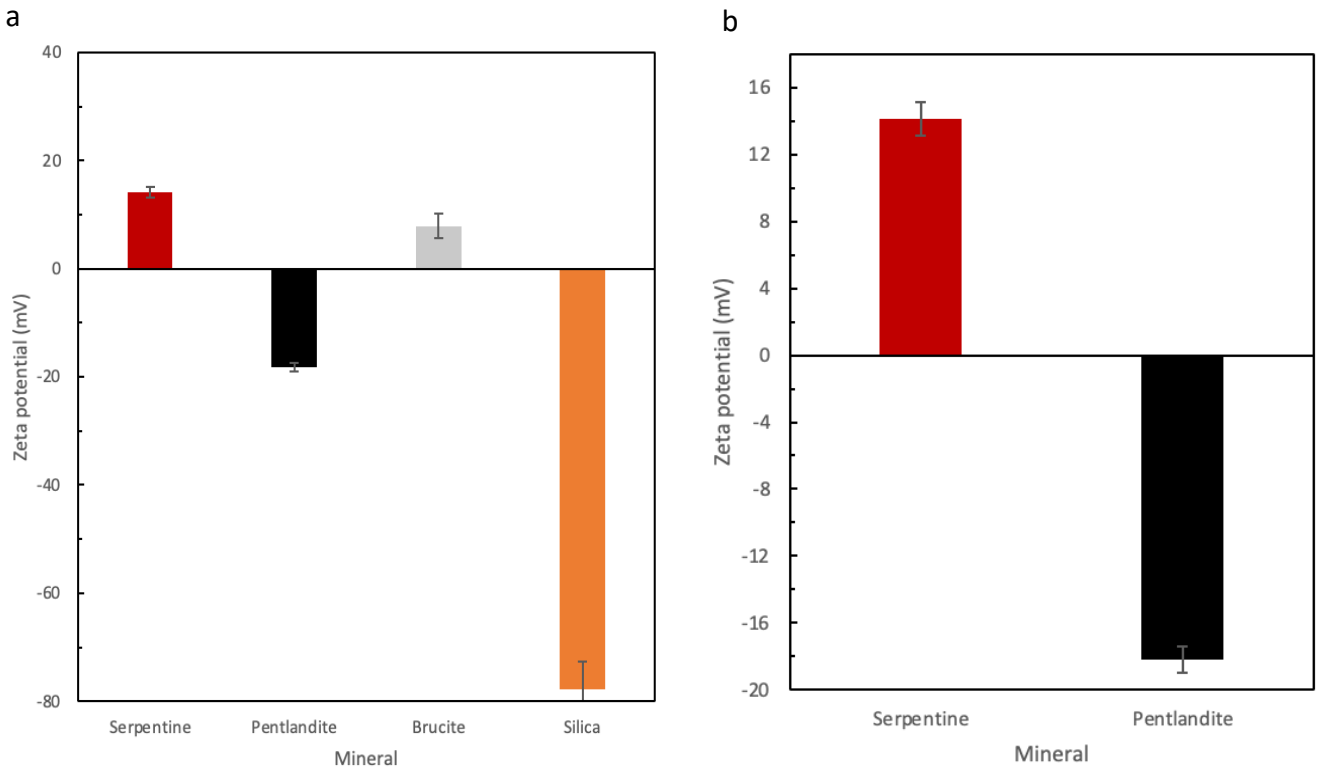

Figure 18: Zeta potential measurements of mineral suspensions (a) serpentine, pentlandite, brucite and silica (b) serpentine and pentlandite only.

40 mg of mineral sample was added into a 100 mL beaker containing 40 mL of KCl solution in the absence of serpentine depressants at pH 10.1, stirred for 30 mins and allowed to settle for 10 mins prior to zeta potential measurements. The values are average of triplicates ± SD (standard deviation). More details in ***Table 7*** *and described in* ***Section 3.2.1.2.***

4.2.3. Effect of STPP on zeta potential measurements (STPP experiments)

Upon introduction of STPP following experimental conditions in **Table 7 and Section 3.2.1.3**, the zeta potential of serpentine decreased to about 1 mV at 5 mg/L of STPP (**Figure 19**). Further increase in STPP's concentration resulted to a charge reversal of serpentine from a positive zeta potential to a negative zeta potential of -21 mV at 10 mg/L which clearly continued to change until above a concentration of 50 mg/L at which no significant difference in the zeta potential was further observed. At 50 mg/l, the zeta potential attained an optimum value of -54 mV and even

when the STPP concentration was doubled to 100 mg/L, only a minor difference of -2 mV was observed. At this optimum concentration (50 mg/L) of STPP for serpentine's charge reversal, zeta potential of brucite also reversed from a slightly positive potential of 8 mV to highly negative potential of -51 mV (**Figure 20**). The zeta potential magnitude of pentlandite changed from -18 mV to -53 mV, while that of silica remains unaffected at -77 mV (**Figure 20**). STPP was able to complex Mg^{2+} on the surface of serpentine through its phosphate groups (**Equation 27**), forming a P-O-Mg bond and enhancing the positive charge reversal on serpentine's surface (**14**).

$$3Mg^{2+} + 2PO_4^{3-} \rightarrow Mg_3(PO_4)_2 \quad (27)$$

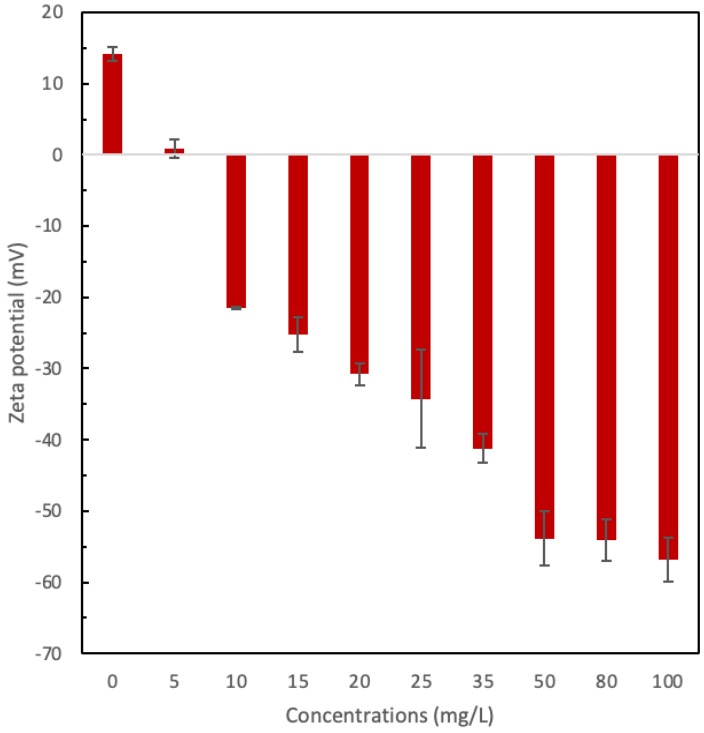

Figure 19: Zeta potential measurements of serpentine suspensions at different concentrations of STPP. 40 mg of mineral sample was added into a 100 mL beaker containing 40 mL of KCl solution in the presence of serpentine depressant (STPP) at pH 10.1, stirred for 30 mins and allowed to settle for 10 mins prior to zeta potential measurements. The values are average of triplicates ± SD. More details in ***Table 7*** *and described in* ***Section 3.2.1.3.***

By reversing the charge of serpentine from a positive to a negative zeta potential, STPP should depress serpentine and prevent slime coating of pentlandite in flotation tests. It also indicates that the attractive interaction or heterogeneous agglomeration between serpentine through its brucite plane and pentlandite samples are reversed or prevented. This implies a positive total interaction between serpentine and pentlandite *i.e.,* a repulsive force (**23, 246, 247**). The more negative zeta potential behaviour of pentlandite samples after STPP introduction also indicates an enhanced floatability and recovery of the nickel mineral. The implication is that freer pentlandite should be reported to the froth, thereby increasing both recovery and grade. To test this hypothesis and provide further proof of concept, the optimum STPP's concentration (50 mg/L) was employed in the flotation tests and XPS analysis.

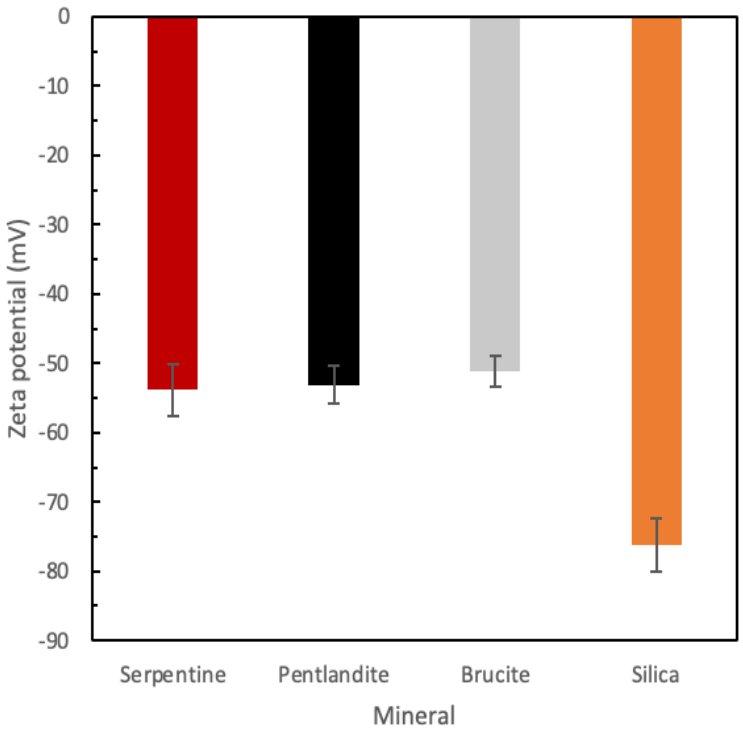

Figure 20 Zeta potential measurements of different mineral suspensions in the presence of STPP.

40 mg of mineral sample was added into a 100 mL beaker containing 40 mL of KCl solution in the presence of serpentine depressant (STPP) at pH 10.1, stirred for 30 mins and allowed to settle for 10 mins prior to zeta potential measurements. The values are average of triplicates ± SD. More details in ***Table 7*** *and described in* ***Section 3.2.1.3.***

4.2.4. Effect of CO_2 gas on zeta potential measurements (CO_2 experiments)

Additionally, the effect of CO_2 gas after 5 mins conditioning was also investigated with regards to experimental conditions in **Table 7** and **Section 3.2.1.4**, and the results revealed a zeta potential value of -30 mV, - 34 mV, -23 mV, -50 mV for serpentine, pentlandite, brucite, and silica respectively (**Figure 21**). By also reversing the charge of serpentine from a positive to a negative zeta potential, CO_2 facilitated serpentine depression and should prevent slime coating of pentlandite by serpentine in flotation tests. It is also an indication that the negative total energy interaction or heterogeneous agglomeration between serpentine through its brucite plane and pentlandite samples are reversed or prevented. Thus, implying a positive total interaction energy between serpentine and pentlandite i.e., a repulsive force. Therefore, a few minutes conditioning of the mineral suspension with CO_2 gas reverses the charge on serpentine's surface, thereby limiting slime coating on pentlandite's surface and enhancing overall pentlandite recovery plus grade. It can therefore be inferred that the detrimental effects (slime coating effect) caused by the presence of magnesium cations can be addressed by conditioning the mineral suspension with CO_2, which converts the magnesium cations into mineral carbonates (**Equation 24**), and remove any metal-monohydroxide complexes on the surface of pentlandite (**23**). Hence, the use of CO_2 as both a conditioning reagent for serpentine suppression and its use as a flotation gas is also explored.

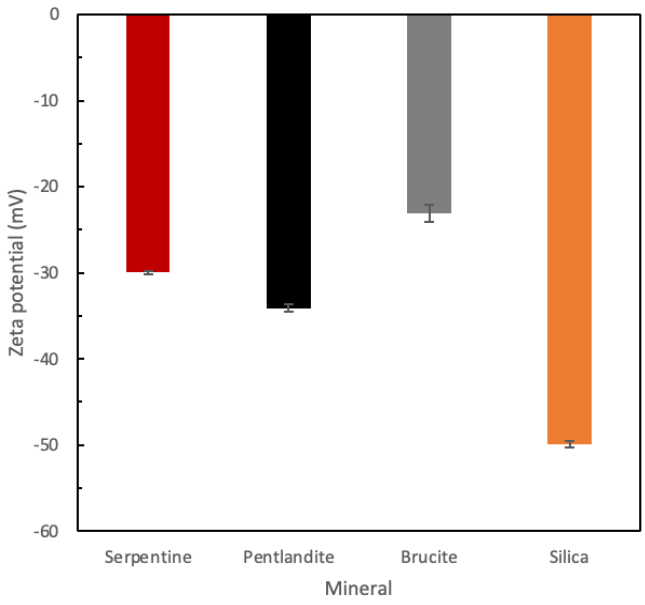

Figure 21: Zeta potential measurements of different mineral suspensions after conditioning with CO_2 gas.

40 mg of mineral sample was added into a 100 mL beaker containing 40 mL of KCl solution which was then conditioned with CO_2 gas for 5 mins at pH 10.1, stirred for 30 mins and allowed to settle for 10 mins prior to zeta potential measurements. The values are average of triplicates ± SD. More details in ***Table 7*** *and described in* ***Section 3.2.1.4.***

4.3. Flotation tests

4.3.1. Flotation response of serpentine-pentlandite suspensions under normal conditions (baseline case)

The flotation response of pentlandite and serpentine were monitored by following the recovery of nickel (Ni) and magnesium (Mg) respectively from the collected concentrate using experimental conditions explained in **Section 3.2.2.1** and **Table 8**. ICP-OES analysis of the dried samples from flotation tests revealed that after 460 seconds, a maximum nickel recovery of 68% as well as a magnesium maximum recovery of 77% was achieved for the baseline case (**Figure 22**).

This result therefore confirms a heterogeneous agglomeration between pentlandite and serpentine meaning that serpentine slime coats pentlandite particles through its brucite plane resulting in negative total interaction energy for brucite with pentlandite i.e., attractive force (**23, 247**). The attractive force resulted in a significant and even higher amount of serpentine that reported to the froth and was collected as concentrate. Through this attractive force, freer pentlandite were reduced and most pentlandite samples reported to the froth together with serpentine particles via the heterogeneous agglomeration. This indicates that the positively charged serpentine has a strong slime coating effect on pentlandite, impacting its recovery and grade (**Figure 28**), thereby validating the results from zeta potential measurements in Section 4.2.2.

The results from the baseline case also indicate that there is a poor collision probability and attachment efficiency for the air bubble-mineral interaction (**8, 199, 202**) which produced low pentlandite flotation recoveries.

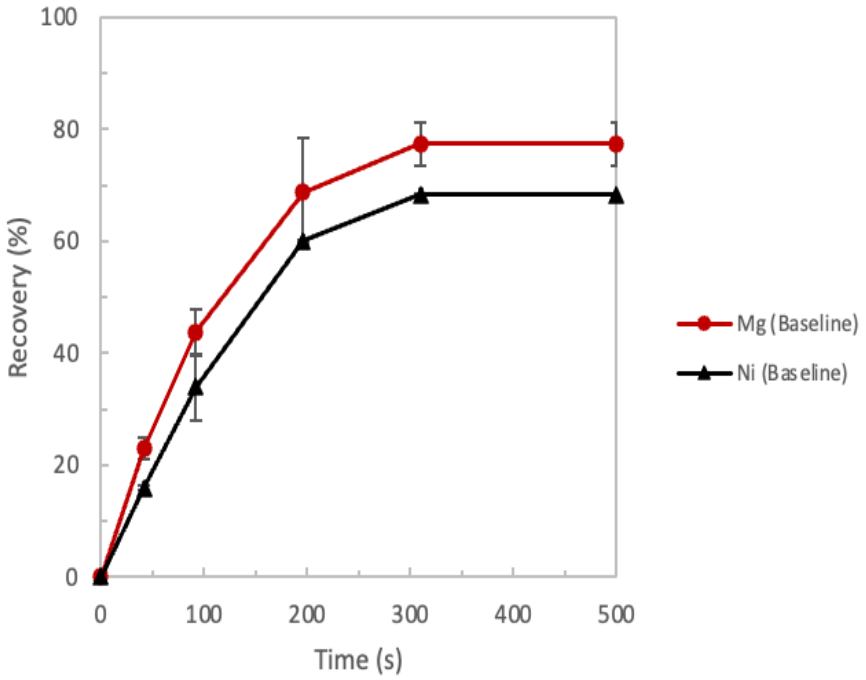

Figure 22: Cumulative nickel and magnesium recoveries vs flotation time for the baseline case (ie., air flotation with no depressant).

5 g of mineral suspension at 1.5:1 ratio of serpentine and pentlandite in 65 mL KCl solution (10 mM) at pH 10.1. NaOH and HCl were used as pH modifiers, while MIBC and PAX were used as frother and collector respectively. A feed particle size of –38 µm was used in the flotation tests. The values are average of triplicates ± SD. More details are provided in ***Section 3.2.2.1*** *and* ***Table 8.***

High collision probability as well as increased attachment efficiency between air bubbles and mineral particles are required to improve flotation recovery. In this case in particular, the slime coating effect of serpentine plays a significant role in reducing the recovery of pentlandite by either rendering them more hydrophilic or preventing them from attaching to the air bubbles. To prevent or reduce the effect of serpentine on pentlandite's surface, serpentine depressants are planned in the subsequent experiments. In the next section (**4.3.2**) in particular, STPP is used to selectively interact with serpentine's surface to reduce their heterogeneous agglomeration with pentlandite.

4.3.2. Flotation response of serpentine-pentlandite suspensions using STPP as serpentine depressant (Air + STPP experiment)

Upon the introduction of STPP using experimental conditions explained in **Section 3.2.2.2** and **Table 8**, the slime coating effect on pentlandite's surface was reduced and the overall nickel recovery increased to 83% from baseline of 68% while magnesium recovery decreased to 72% from 77% in the baseline case, thereby reducing the amount of serpentine in the concentrate (**Figure 23**). The result demonstrates that as attractive forces (and thus, the heterogeneous agglomeration) between the serpentine and pentlandite were being reversed, free pentlandite minerals are released and are able to attach to the air bubbles. The resulting effect is that more pentlandite were reported to the froth phase and are collected in the concentrate compared to the baseline case. Once there is free pentlandite in the suspensions, they are able to attach to the air bubbles through hydrophobic interactions.

In a previous study by Li and co-workers, they demonstrated the ability of STPP to reverse surface charge of serpentine and subsequently increased the floatability of pyrite (**14**), which correlates to the results in this study. This means that the phosphate groups in STPP were able to interact with magnesium cations (which contributes to slime coating) (**231, 232**), and facilitate the charge reversal of serpentine (**14**), thereby reducing the heterogeneous agglomeration between serpentine and pentlandite. By doing so, freer pentlandite particles are released in the suspension and are able to attach to the air bubbles which subsequently report to the froth phase and are collected. At the same, the amount of serpentine reporting to the froth is reduced because their charge has been reversed and their electrostatic attractions with pentlandite particles has been reduced by their interaction with STPP.

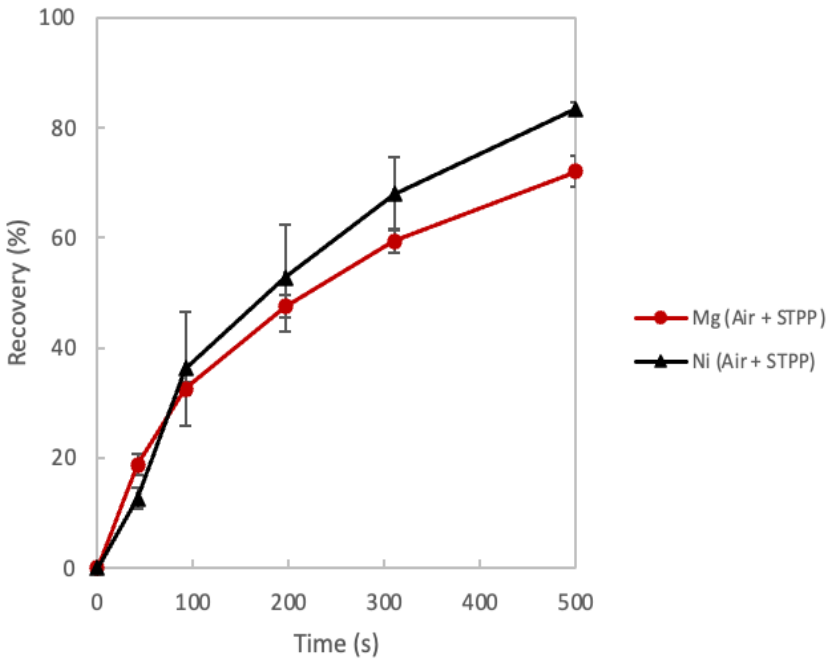

Figure 23: Cumulative nickel and magnesium recoveries vs flotation time for Air + STPP case (ie., air flotation with STPP as the depressant).

5 g of mineral suspension at 1.5:1 ratio of serpentine and pentlandite in 65 mL KCl solution (10 mM) at pH 10.1. NaOH and HCl were used as pH modifiers, while MIBC and PAX were used as frother and collector respectively. A feed particle size of –38 µm was used in the flotation tests. The values are average of triplicates ± SD. More details are provided in ***Section 3.2.2.2*** *and* ***Table 8.***

4.3.3. Flotation response of serpentine-pentlandite suspensions using CO_2 as a serpentine depressant (Air + CO_2 experiments)

Owing to the ability of CO_2 to interact with divalent cations such as magnesium cations present in serpentine, CO_2 bubbles are also used to express their serpentine suppressing capabilities and simultaneously improve pentlandite recovery. CO_2 is solely used as a depressant in this case during the conditioning stage before being subjected to air flotation (**Section 3.2.2.3** and **Table 8)**. Similar metal recovery trend as the STPP case was also observed when mineral suspension was conditioned with CO_2 prior to air flotation, yielding 78% and 73% for nickel and magnesium respectively (**Figure 24**). This also demonstrates that as attractive forces (and thus, the heterogeneous agglomeration) between the serpentine and pentlandite were being reversed, free pentlandite minerals are released and are able to attach to the air bubbles. The resulting effect is

that more pentlandite were reported to the froth phase and are collected in the concentrate compared to the baseline case. The freed pentlandite particles are able to attach to the air bubbles through hydrophobic interactions.

As reported by Wani et al. (**23**), conditioning the mineral suspension with CO_2 converts magnesium cation (Mg^{2+}) into its carbonated form as $MgCO_3$ (**Equation 24**), thereby reducing the slime coating effect of Mg^{2+} on pentlandite. This in turn, enhanced the flotation recovery of pentlandite and generally recovered more pentlandite than serpentine which is opposite of what was observed in the baseline case.

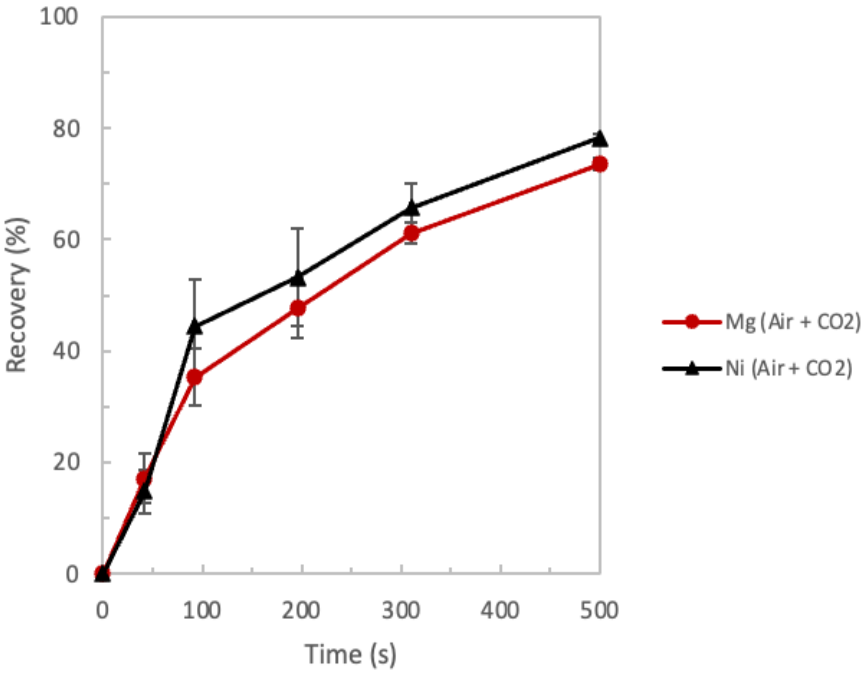

Figure 24: Cumulative nickel and magnesium recoveries vs flotation time for Air + CO_2 case (ie., air flotation with CO_2 as a depressant).

5 g of mineral suspension at 1.5:1 ratio of serpentine and pentlandite in 65 mL KCl solution (10 mM) at pH 10.1. NaOH and HCl were used as pH modifiers, while MIBC and PAX were used as frother and collector respectively. A feed particle size of –38 µm was used in the flotation tests. The values are average of triplicates ± SD. More details are provided in ***Section 3.2.2.3*** *and* ***Table 8.***

4.3.4. Flotation response of serpentine-pentlandite suspensions using CO_2 as both a serpentine depressant and as a flotation gas (CO_2 only experiments)

By following experimental conditions explained in **Section 3.2.2.1** and **Table 8,** nickel recovery of 88% was observed when CO_2 was used as both a reagent and a flotation gas which is 20% more than the baseline case, while the magnesium recovery was reduced to 74% in CO_2 only case from 77% observed in the baseline case (**Figure 25**). Just like Air + STPP and Air + CO_2 cases, the flotation recovery demonstrates that as attractive forces (and thus, the heterogeneous agglomeration) between the serpentine and pentlandite were being reversed upon CO_2 conditioning, free pentlandite minerals are released and are able to attach to the CO_2 bubbles.

Thus, it is important to point out that not only that CO_2 conditioning converts magnesium cation (Mg^{2+}) into its carbonated form as $MgCO_3$ (**23**), its subsequent use as a flotation gas in this case produced the necessary fine bubbles required to facilitate hydrophobic interactions (**24, 54, 199, 222**) with pentlandite, thereby enhancing its recovery. The resulting effect is that more pentlandite were reported to the froth phase and are collected in the concentrate compared to the baseline case. Once there is free pentlandite in the suspension, they are able to effectively collide and attach to the CO_2 bubbles through hydrophobic interactions. CO_2 bubbles are more hydrophobic than air bubbles as demonstrated by Miller and Misra (**17**), and thus, were able to facilitate more attachment to the pentlandite minerals in this study. Being more hydrophobic indicates a faster induction time between CO_2 bubbles and the pentlandite particles once they are in contact (24, **199, 222,**). This resulted in the highest nickel recovery experienced in this case. This re-emphasizes the recovery importance of CO_2 gas in flotation systems.

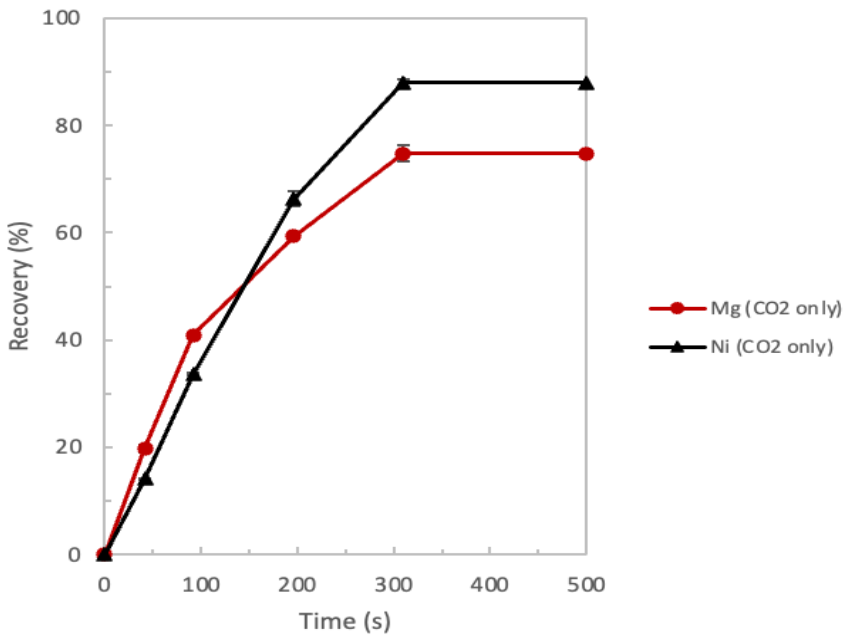

Figure 25: Cumulative nickel and magnesium recoveries vs flotation time for CO_2 only case (ie., CO_2 gas for both flotation and as a depressant).

5 g of mineral suspension at 1.5:1 ratio of serpentine and pentlandite in 65 mL KCl solution (10 mM) at pH 10.1. NaOH and HCl were used as pH modifiers, while MIBC and PAX were used as frother and collector respectively. A feed particle size of –38 µm was used in the flotation tests. The values are average of triplicates ± SD. More details are provided in ***Section 3.2.2.3*** *and* ***Table 8.***

4.3.5. Comparison of the various reagent- and gas- dependent flotation experiments (All cases comparison).

To properly compare the responses of the different cases or methods (reagents and gasses) used in the flotation experiments, the flotation recoveries of pentlandite and serpentine expressed by following the release of nickel and magnesium respectively for the different experiments are combined in single graphs. **Figure 26** shows the cumulative nickel contained in the concentrates for all the experimental types and it clearly shows that the CO_2 only case attained the highest nickel recovery followed by the Air + STPP case and closely by the Air + CO_2 case. Leading up to the first 50 s, a similar flotation rate was observed for all the cases until about 100 s where the flotation rate for the Air + CO_2 case experienced the highest rate. As the flotation time increased, both the flotation recovery and rates for the CO_2 only case became increasingly better than other cases. This

shows that CO_2 bubbles are better at enhancing the recovery of pentlandite than air bubbles or in the presence of STPP reagent.

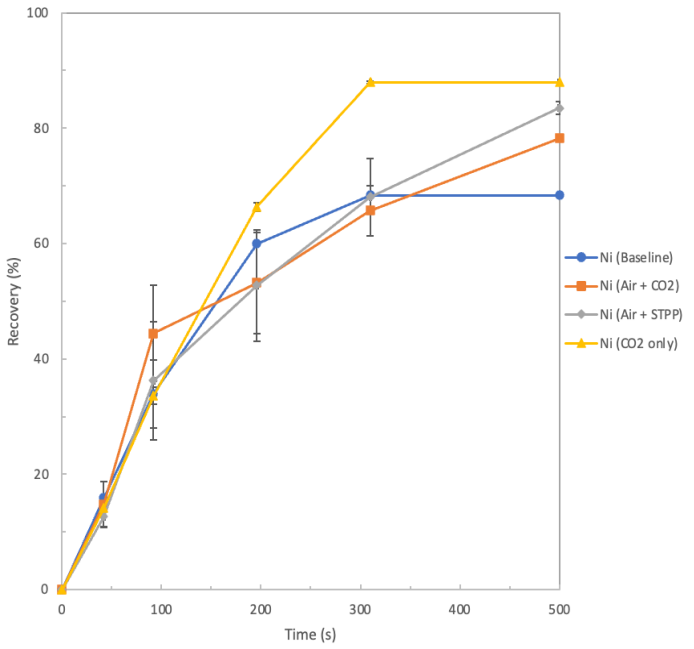

Figure 26: Cumulative nickel recovery vs flotation time for baseline case (air flotation with no depressant), Air + CO_2 (air flotation with CO_2 as a depressant), Air + STPP (air flotation with STPP as the depressant), CO_2 only (CO_2 gas for both flotation and as a depressant).

Enhanced pentlandite recovery implies that the CO_2 bubbles acted by either enhancing dispersion of slimes on pentlandite's surface (**24, 203**) or by facilitating the aggregation of pentlandite particles (**7, 8**), thereby increasing their hydrophobicity and floatability. It is not clear which is the leading mechanism or if both occur simultaneously at the same rate. However, it has been demonstrated in previous studies that by continuously bubbling the flotation system with CO_2, they nucleate and grow simultaneously on hydrophobic mineral surfaces, thereby enhancing interactions between neighboring hydrophobic valuable minerals making them to aggregate and to float (**97, 195, 201, 202**). Since the effect of introducing CO_2 gas is more pronounced towards improving pentlandite recovery rather than depressing serpentine, it can be concluded that facilitating pentlandites' aggregation through hydrophobic interactions is the leading mechanism (**Figure 32**) for the improved recovery observed in the CO_2-assisted flotation cases.

Serpentine recovery was also monitored by following the cumulative release of magnesium in the ICP-OES analysis. The results clearly show that the case of Air + STPP was the most effective in depressing serpentine. STPP decreased magnesium recovery from 77% to 72%, a difference of 5% which is the highest reduction observed among all treated cases (**Figure 27**). This validates the results observed in the zeta potential measurements where the introduction of STPP was more effective in reversing the surface charge on serpentine (**Figure 20**) than CO_2 conditioned suspension (**Figure 21**). STPP acts by chelating and complexing the magnesium cations on serpentine surfaces through its phosphate group (**Equation 27**) (**236, 238**), limiting serpentine's electrostatic attraction with pentlandite and rendering serpentine particles more hydrophilic (14). Because some serpentine particles are no longer heterogeneously agglomerated with pentlandite particles, they are no longer recovered together when air bubbles attach to pentlandite through hydrophobic interactions.

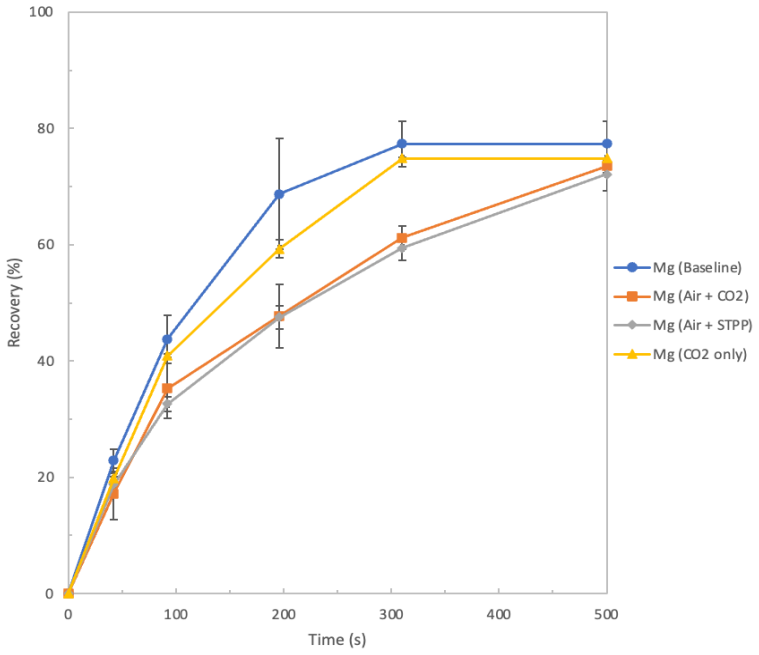

Figure 27: Cumulative magnesium recovery vs flotation time for baseline case (air flotation with no depressant), Air + CO_2 (air flotation with CO_2 as a depressant), Air + STPP (air flotation with STPP as the depressant), CO_2 only (CO_2 gas for both flotation and as a depressant).

Furthermore, introduction of the reagents (STPP and CO_2) in the treated cases increased the nickel grade from below 10% in the baseline case to about 15% in both STPP and CO_2 cases **(Figure 28)**. The poor recovery of nickel in the baseline case is an indication of the high slime coating effect of the serpentine minerals on pentlandite, resulting in both minerals to report to the froth phase, and thereby diluting the nickel grade. Thus, the use of STPP as depressant and the use of CO_2 as both a depressant and a flotation gas, did not only enhance the recovery of nickel, but they also helped to improve the overall nickel grade in the concentrate. This implies that the electrostatic interactions between serpentine particles and pentlandite minerals were reduced upon introduction of either STPP or CO_2 gas resulting in a lesser amount of serpentine particles to report to the froth phase. Therefore, nickel grade was improved as compared to the baseline case (**Figure 28**).

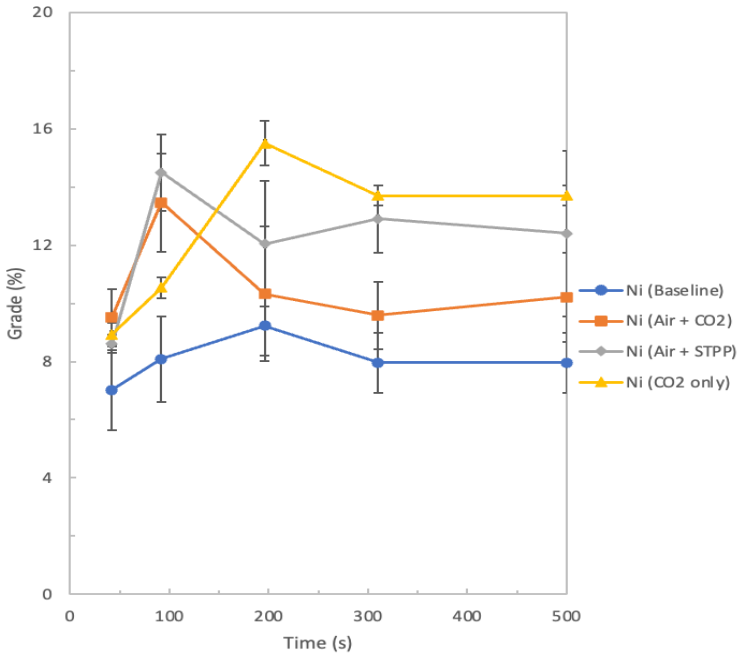

Figure 28: Cumulative nickel grade vs flotation time for baseline case (air flotation with no depressant), Air + CO_2 (air flotation with CO_2 as a depressant), Air + STPP (air flotation with STPP as the depressant), CO_2 only (CO_2 gas for both flotation and as a depressant).

However, as was observed during the flotation tests, the froth phase of the experiments performed with only CO_2 gas were not stable for a long time which impacted overall recovery performance. This agrees with a previous study on pyrite flotation where CO_2 flotation was also impacted at pH 10 due poor stability of the froth phase (**24**). At lower pH conditions, they showed that the froth was stable and that the use of CO_2 gas improved pyrite recovery. Increasing the pH in a CO_2-

assisted flotation consumes a lot of NaOH as was observed in the experiments, increases the ionic strength of the solution and has an impact on the froth stability (**24**). Even though the stability of the froth phase was impacted in both studies at pH 10, improved valuable mineral recovery was observed in both cases and can be attributed to the ability of CO_2 to form fine bubbles on the surfaces of hydrophobic minerals increasing their aggregation (**11, 24, 201**). The problem of poor froth stability opens up another area for further research, especially with respect to frother types as it was observed that both studies employed the use of MIBC. Other frothers can be explored under similar conditions used in this study to establish which frother type can help to form a more stable froth phase in CO_2-assisted flotation.

The plot of cumulative mass pull against time shows a fast flotation kinetics as more than half of the mass for all cases were recovered (**Figure 29**). The mass recovery was however, faster in the CO_2 and baseline cases. This indicates that overall flotation recovery in CO_2 only was fast and if the froth was more stable, it would have resulted in an increased pentlandite recovery. The cumulative mass pull is also an indication that STPP was more geared towards reducing the effect of serpentine and rendering them more hydrophilic, rather than enhancing more pentlandite recovery. Therefore, it would be interesting to explore STPP reagent and CO_2 gas in a single flotation experiment of ultramafic nickel ores to investigate their combined effect on serpentine depression and pentlandite recovery.

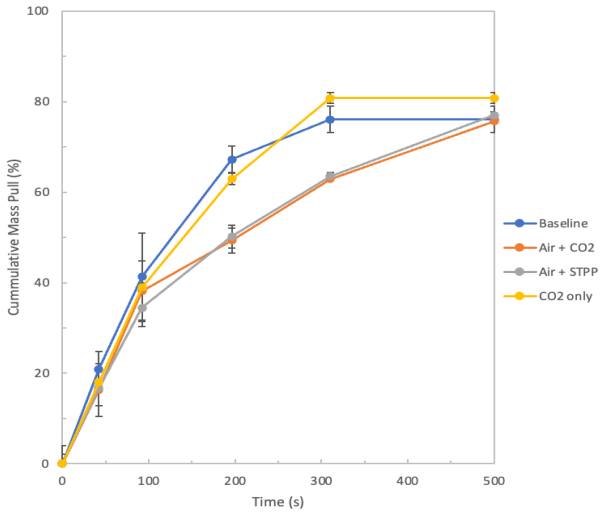

Figure 29: Cumulative mass pull vs time for baseline case (air flotation with no depressant), Air + CO_2 (air flotation with CO_2 as a depressant), Air + STPP (air flotation with STPP as the depressant), CO_2 only (CO_2 gas for both flotation and as a depressant).

4.4. XPS analysis

XPS analysis was performed to investigate how the chemical composition on serpentine's surface reacts upon treatment with the reagents used in this thesis. Both zeta potential measurements and flotation tests were validated by performing XPS analyses and the results as shown in **Table 11** revealed a significant decrease of the Mg 2s peak area from 13533.15 cps.eV in the baseline case to 7207.25 cps.eV in the STPP treated serpentine (**Figure 30**), which is in agreement with study done by Li and coworkers (**14**). This means that the phosphate groups in STPP effectively removed magnesium cations on serpentine surfaces to form soluble complexes (**14**). Same experiment was repeated for CO_2-conditioned serpentine suspension and the Mg 2s peak area reads 12426.1 cps.eV **(Figure 30 and Table 11**). Thus, magnesium ions on serpentine surfaces are complexed by STPP and CO_2, which is in line with results obtained from ICP-OES analysis for metal release. However, STPP demonstrated a much stronger suppression ability by complexing about half of the Mg^{2+}. As previously mentioned, the phosphate groups in STPP easily chelate Mg^{2+} present on serpentine's surface, facilitating its suppression in mixed mineral systems.

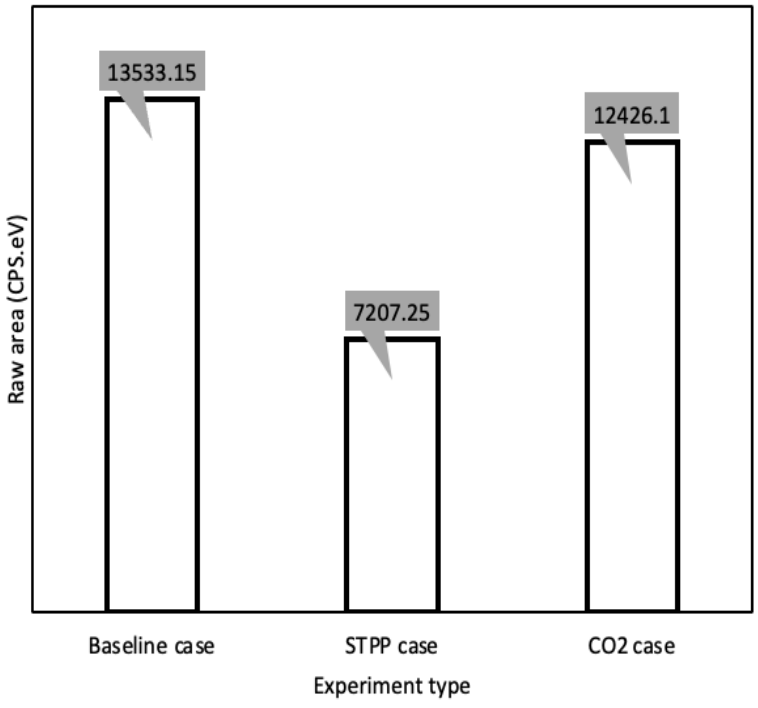

Figure 30: Peak raw area of Mg 2s of the serpentine before and after treatment with STPP and CO_2.

Table 11: Chemical composition of serpentine's surface before and after treating with STPP and CO_2. The values are the average of duplicates ± SD.

Case	Raw Area (cps.eV)	Atomic conc (%)	Mass Conc (%)
Baseline	13533.15	13.30	18.06
STPP	7207.25	10.12	13.98
CO_2	12426.10	11.17	15.73

In fact, the composition of atomic and mass concentration further demonstrated that the initial concentration of metal ions present in the baseline case were reduced because of the complexation reaction that took place upon the introduction of the reagents in the treated cases (**Figure 31 and Table 11**). Therefore, chelating of Mg^{2+} by phosphate group leads to the formation of Mg-O-P chemical bonding as demonstrated through high resolution scans performed in previous studies (**14, 233, 250**). These trends validate the serpentine suppression observed in flotation tests and zeta potential measurements for STPP and CO_2 cases.

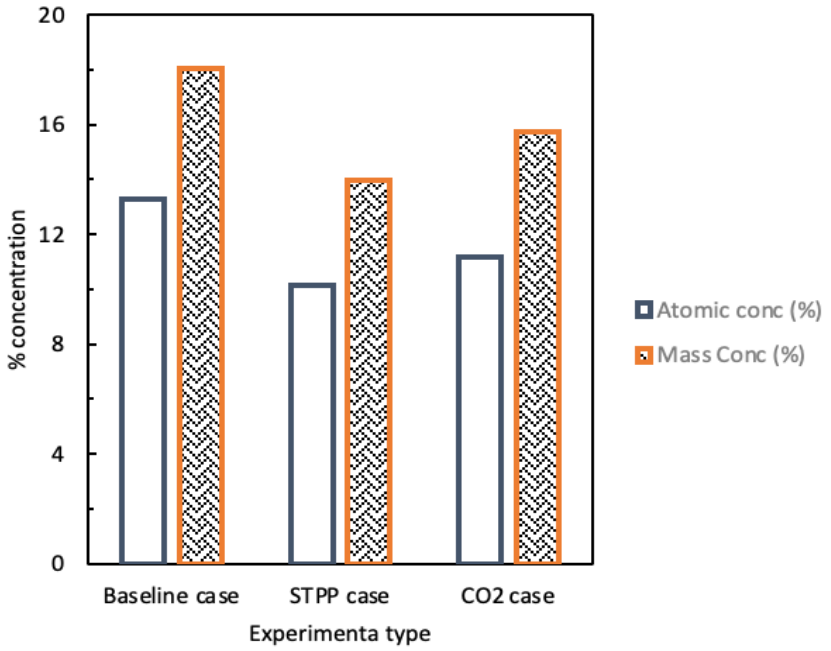

Figure 31: Peak concentrations of Mg 2s of serpentine before and after treatment with STPP and CO_2.

4.5. Further discussion

By using CO_2 as either a flotation gas or as a conditioning reagent for gangue mineral depression, improvements in the valuable mineral recovery was achieved which supports similar previous studies presented in (**Table 3**). However, when CO_2 was used as both a flotation gas and as a conditioning reagent, higher pentlandite recoveries were observed. This validates that CO_2 bubbles are more effective in colliding and attaching to pentlandite particles. Because CO_2 gas produces smaller bubbles than air, they are able to increase their probability of collision with fine pentlandite particles and therefore, increasing the flotation rates. As has been demonstrated by various collision studies, the probability of collision between air bubbles and fine particles is small (**47**, **52**, **57, 59, 62**), which in turn slows the rate of flotation (**52, 54**).

Thus, by introducing CO_2 bubbles which are generally smaller than air bubbles, collision probability and flotation rates were enhanced which is demonstrated by increased recovery of pentlandite minerals through the release of nickel confirmed in the ICP-MS analysis. Increased flotation rates achieved when CO_2 bubbles were introduced also confirms that liquid film thinning and rupture, establishment of a wetting perimeter and a three-phase contact line were faster than the case with air bubbles. Therefore, induction time is faster for CO_2 bubbles than other gas bubbles used in mineral flotation, and this phenomenon has been confirmed by earlier studies where CO_2 bubbles induction time was faster than N_2 bubbles (**16, 24, 64**). Additionally, faster induction time relates to higher hydrophobic interaction which is the underlying interaction for bubble-particle attachment (**24, 54**). CO_2 bubbles are more hydrophobic and can enhance hydrophobic interactions with mineral surfaces resulting in faster induction time and high flotation recoveries. Also, bubbling the mineral suspension with CO_2 at pH 10.1 precipitates Mg^{2+} because of the dominant CO_3^{2-} specie (**Equation 24**), and therefore carbonation of the mineral suspension will produce $MgCO_3$ and SiO_2 (**Equation 28**) (**23**).

$$Mg_3Si_2O_5(OH)_4 + 3CO_2 \rightarrow 3MgCO_3 + 2SiO_2 + 2H_2O \quad (28)$$

In terms of both recovery and suppressive capability and in a more similar study to this thesis work, Wani and co-workers demonstrated that by conditioning a nickel ore with CO_2 gas prior to air flotation, improvement in the recovery of pentlandite from 83% to 93 % was observed and serpentine recovery was decreased by about 10% (**23**) Although it seems that overall recovery

observed by Wani and co-workers was higher than that observed in this work, a possible explanation could be related to the different feed sizes used in both experiments. They employed a feed size of -75 um while a feed size of - 38 um was used in this work. Particle size plays an important role in the recovery of valuable minerals (**37**).

As particle size decreases, it becomes increasingly difficult to recover valuable minerals (**58, 59**), and would require strategies or new technologies to enhance recovery. And as already stated, poor flotation recoveries of fine particles are related to their low collision probability with air bubbles (**47, 58, 59, 62**), and their low kinetic energy to bring about effective attachment to the bubble surface. The use of CO_2 as a flotation gas is one of such initiatives and has already been demonstrated in this work. CO_2 facilitated higher flotation recoveries due to higher solubility and the ability to produce smaller bubbles necessary for attachment to fine particles used in this work. Hence, confirming that particle-bubble attachment (EA) is higher for smaller bubbles due to a faster establishment of a wetting perimeter (**64**). Through enhanced hydrophobic interactions of CO_2 bubbles, there was high collision probability and high attachment efficiency of CO_2 bubbles with pentlandite particles which resulted in the aggregation of mineral particles remains one of the underlying mechanisms why the highest flotation recoveries were achieved for the CO_2 only case (**Figure 32)** .

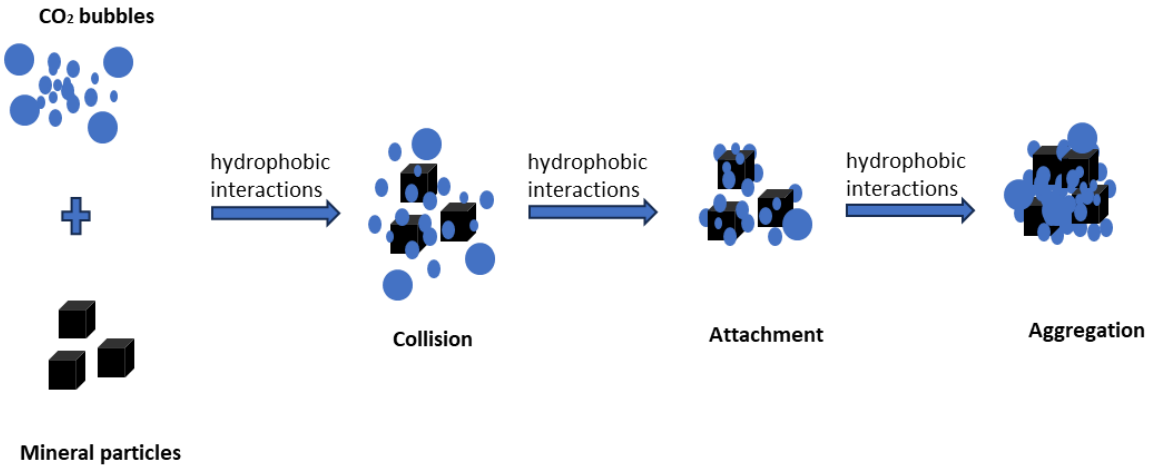

Figure 32: Schematic representation of fine mineral aggregation due to enhanced hydrophobic interactions with CO_2 bubbles.

Even though pentlandite recovery was enhanced and serpentine depression initiated, high recoveries of the gangue serpentine were still observed in the treated cases, and this is an indication that bubble attachment to the mineral particles was not selective. This is due to the electrostatic force (because of electric double layer superposition) that is generated when a bubble comes close to a particle, which can establish attachment between a bubble and a particle of opposite charge (or a hydrophilic particle) (**71**) and explains why gangue minerals report to the froth and decrease the concentrate grade.

As already proposed in **Section 2.11**, The effect of different physicochemical properties of mineral surfaces on selective aggregation using fine bubbles is still required to demonstrate preferential attachment to valuable minerals. An opposite approach to this issue will be a study that investigates the functionalizing of bubbles to increase their selectivity for pentlandite or any other mineral. Note that the mechanism of action during froth flotation is mostly by hydrophobic forces but can also be influenced by electrostatic force as already highlighted. Also note that traditionally, anionic collectors like xanthate have been used to separate pentlandite from ultramafic ores. While at alkaline pH both the bubble and xanthate coated mineral are negatively charged, the mechanism of recovery is solely due to hydrophobic interaction. However, if the bubble is functionalized to be positively charged or a cationic collector is used this will lead to attractive electrostatic interaction between the mineral of interest and gas bubble. The addition of electrostatic forces in addition to the hydrophobic interactions should yield more efficient mineral recovery and should reduce the amount of serpentine that reports to the froth. Thus, selectivity in the flotation recoveries of fine mineral particles using fine bubbles in the presence of flotation reagents requires further investigations.

In addition, certain strategies and parameters can be employed to optimize the process. For example, size of the gas bubbles was not considered (measured) in this study, and it has been repeatedly shown that the use of smaller or fine bubbles enhance flotation kinetics of fine particles. By confirming the actual bubble sizes in flotation columns through real time bubble size measurements, it would be easier to adjust to the desired bubble sizes during flotation test. It is important to reiterate that fine bubbles enhance flotation of fine particles by promoting their aggregation as well as increasing probability of bubble-particle collision (**251**). Hence, it is proposed to plan a dual bubble system (very fine or ultra-fine and larger bubble) (**7, 8, 85**) for further studies, where the ultra-fine bubbles will be utilized to promote collision and aggregation

while the larger bubbles will assist to float the particles to the top due to insufficient buoyancy of fine bubbles. Due to higher solubility of CO_2 as repeatedly highlighted in this thesis, it tends to produce finer bubbles and would be a great fit for dual bubble flotation of very fine particles, thereby improving the overall flotation performance.

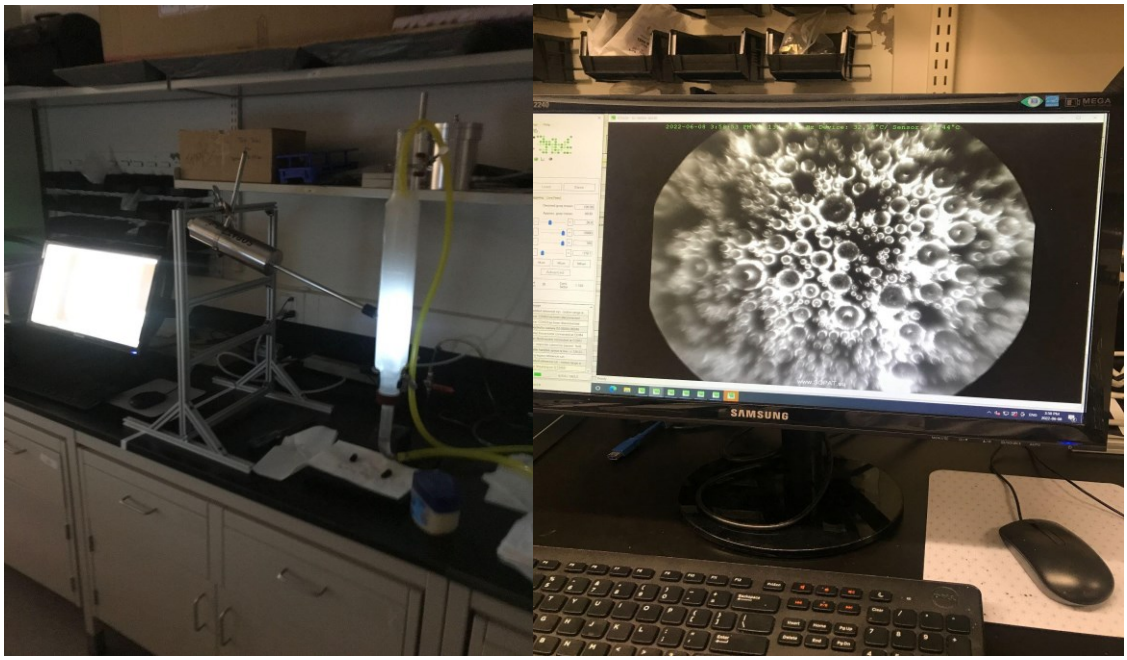

Figure 33: (a) Positioning of the SOPAT device in a small flotation column, and (b) bubbles sticking on the SOPAT probe during a test run.

However, fine bubble generation as well as their usage presents another challenge of real time and actual measurement of these fine bubbles during the flotation process. To address this challenge, Eriez CavTube for generating fine bubbles and SOPAT (Smart Online Particle Analysis Technology) probe for in-situ bubble size measurements were originally planned for the microflotation tests in a column set up. SOPAT provides quantitative data on real bubble images from the flotation process and can provide real-time size data of bubbles measuring down to 500 nm. This will not only guarantee unbiased results, but it is also necessary for scaling up laboratory tests.

An initial test run of the SOPAT device revealed that bubbles were sticking in front of the lens and camera making it difficult to visualize moving bubbles (**Figure 33),** implying that the surface of the probe is hydrophobic and has a high contact angle. To address this issue, a highly hydrophilic and transparent adapter ($\theta < 20°$) was planned. Unfortunately, the experimental design of incorporating a SOPAT probe to a column flotation setup coupled with an Eriez CavTube requires additional modifications from the manufacturer specific for measuring gas bubbles and were not readily available during the completion of this thesis. New programming specifically designed to measure and differentiate fine bubbles from fine particles are required from the company to further this research area. The SOPAT probe used for the test run were not originally designed for bubbles measurement and thus, the reason why the bubbles were not dimensioned. This remains an important research area that needs to be explored further to highlight its benefits and potential to address some issues related to complex flotation systems.

Furthermore, STPP effect was also effective in improving the recovery of pentlandite. In the baseline zeta potential measurement, it is shown that serpentine was positively charged due to the residual magnesium cations contributed by its brucite plane, and thus, slime coated the negatively charged pentlandite through electrostatic force which was evident in the flotation test as well. By introducing STPP, the negative phosphate groups in STPP chelated the magnesium cations on serpentine's surface through the generation of P-O-Mg bonds which is agrees with a previous study (**14**), thereby decomposing Mg^{2+} from the bulk serpentine (**Figure 34**). These actions resulted in a negatively charged serpentine's surface, meaning that the hetero-coagulation between pentlandite and fine serpentine was reversed because a new electrostatic repulsion now exists between them (**Figure 34**). Therefore, the pentlandite particles have renewed surfaces to better adsorb to PAX collectors and attach to air bubbles, facilitating overall improved pentlandite recovery. At the same time, the recovery of serpentine particles was also reduced.

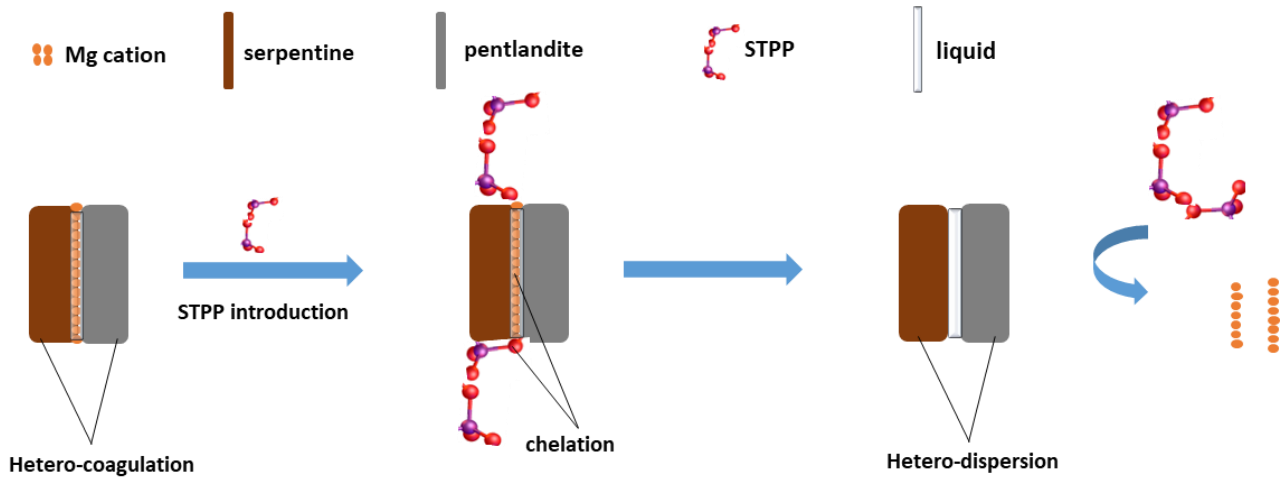

Figure 34: Schematic representation of the role of STPP in serpentine-pentlandite system.

Even though STPP had the most significant impact on depressing serpentine as evident in zeta potential measurements, XPS analyses and flotation tests, the use of CO_2 as a flotation gas showed the most significant improvement in pentlandite recovery. This presents the potential combination of both reagents for processing of ultramafic nickel ores, where STPP acts as a depressant and CO_2 will be used as a flotation gas.

5. Conclusion and recommendation

The use of STPP and CO_2 gas help to improve flotation processes in many ways as demonstrated in the study. Conditioning and floating the mineral suspension with CO_2 converted the monohydroxide complexes to magnesium carbonate, resulting in improved pentlandite recovery because $MgCO_3$ is negatively charged and is not known to slime coat pentlandite. This improved the recovery of pentlandite by 20% and depressed serpentine by 3%, thereby improving the cumulative nickel grade. In the experiment where CO_2 was used only in the conditioning stage (Air + CO_2 case), pentlandite recovery was improved by 10% and serpentine depression by 4%. It provides a proof of concept that CO_2 can be permanently stored in the form of $MgCO_3$ and can facilitate gangue mineral suppression in a flotation system. CO_2 gas bubbles enhanced pentlandite recovery through improving their hydrophobicity, aggregation, and floatability. Through the complexation of Mg^{2+} on serpentine's surface by the phosphate group in STPP, heterogenous agglomeration was limited, thereby reversing the electrostatic attraction between serpentine and pentlandite to electrostatic repulsion. This resulted in serpentine suppression by 5% (the highest among all cases) and subsequent improved pentlandite recovery. In general, a good agreement between zeta potential measurements, micro-flotation tests and XPS analyses was established for all cases.

One of the implications of the study is that it provides a background to further explore the use of CO_2 as a flotation gas in flotation circuits or studies. That means that researchers can leverage information from this study to advance CO_2 flotation studies where CO_2 is specifically used as a flotation gas. It also provides a proof of concept that CO_2 can be utilized in mineral processing operations serving both to improve recovery of valuable minerals and to simultaneously store carbon as mineral carbonates, thereby introducing a strong decarbonization strategy. Companies can obtain carbon credits through this approach and can integrate CO_2 flotation as a part of the CCUS technology. This study will open opportunities to explore the use of CO_2 to recover other sulphide and non-sulphide minerals. Due to understanding of how CO_2 bubbles interact, it can serve as an opportunity to explore their use with other reagents. Since this is the first time STPP is used in serpentine-pentlandite mineral mixture and having realized flotation benefits, it will open an opportunity for further studies in this direction. By removing divalent cations from process waters in the mineral processing operations, it will reduce water viscosity and decrease the need

for water treatment. In addition to that, it greatly reduces the need draw process water from fresh water sources which further strengthens sustainability. More studies are however required to further demonstrate the importance of the use of CO_2 and STPP for processing sulphide minerals, especially ultramafic nickel ores.

Therefore, the following are recommended for future studies and are discussed below.

- It is recommended to explore the combined use of CO_2 gas and STPP in a single experiment to float ultramafic nickel ores or serpentine-pentlandite mixture for further studies. By STPP being the most effective serpentine depressant and by CO_2 bubbles demonstrating the most effective in improving pentlandite recovery, combining both reagents in a single experiment will even yield more flotation benefits. Thus, to further enhance pentlandite recovery and serpentine depression flotation of ultramafic nickel ores, it is proposed to simultaneously use STPP and CO_2 as depressant and flotation gas respectively.

- It is suggested to explore methods that generate, and measure CO_2 fine bubbles as already described in the previous section (**Section 4.5 and Figure 33**), which are needed to further enhance the recovery of valuable minerals. Introducing real time or in-situ bubble size measurement should also explore dual bubble flotation (as highlighted in **Section 4.5**).

- Investigating the effect of fine bubbles characteristics (type, composition and generation strategy) on the slime coating removal on pentlandite ((Fe,Ni)9S8) surface requires comprehensive studies. The study here should explore in greater detail, the cleaning or dispersive abilities of fine bubbles to increase their selectivity for pentlandite. Functionalizing the bubbles to improve their selectivity (as highlighted in the previous section) is also another approach that can be used to enhance bubbles selectivity to pentlandite and should be considered in future studies. Selectivity in flotation of fine particles (-38 um) using fine bubbles and reagents like MIBC is also not just an issue experienced in this study but has been identified in a previous study (**89**) and should be investigated in further studies. Generation of the fine bubbles can be compared with high intensity conditioning (HIC) due to high shear force which overcomes the adhesion forces (**252**), to aid the surface cleaning abilities of fine bubbles in desliming the valuable

pentlandite. Surface and bulk fine bubbles should both be studied as they may have different roles. Impact of fine bubbles composition is another aspect that should be carefully investigated, air and CO_2. The use of CO_2 bubbles remains of special interest because of their pH buffering capacity and their ability to form carbonate minerals with the divalent cations at alkaline pH. The experiments should also involve in-situ measurements of bubble size distribution with SOPAT probe to address the issue of identifying nanometer-range fine bubbles in real time desliming.

- Generally, the use of technologies that fixes emitted and atmospheric carbon dioxide are important to addressing the GHG emissions. But more important, are technologies that simultaneously utilize CO_2 for commercial or industrial purposes and capture or store them permanently. This is what a CO_2 assisted mineral flotation provides and has been demonstrated in this study to some extent. A similar process is already being demonstrated in the oil and gas industry called the CO_2 Enhanced Oil Recovery (EOR) (**213**). Experimental studies to improve bitumen recovery in a CO_2-assisted paraffinic froth treatment has been conducted (**253**) in oil sands extraction. By capturing and utilizing carbon dioxide from its operations, the mining industry can reduce its carbon intensity and GHG emissions. Information from this study provides understanding of CO_2 use as a flotation gas for authors that want to perform experiments in this direction, provide alternative methods of processing ultramafic nickel ores, and introduce an alternative way of carbon storage.

- Finally, more investigations are required to determine the optimal stability of CO_2 froth at alkaline pH. Due to the high amounts of the pH modifier required to maintain pH at 10.1, it resulted in high ionic strength which can impact froth stability. This has been a major issue with the use of CO_2. It is proposed that a variety of frothers be investigated as only methyl isobutyl carbinol (MIBC) frother was used in this study which is also the case in another study (**24**). Even though froth stability of the CO_2 flotation system was impacted, flotation recovery was achieved and can be attributed to the formation of CO_2 fine bubbles on the mineral surfaces which attained equilibrium and promoted bubble-particle

attachment. However, stable froth conditions are necessary for optimal flotation recoveries and more studies are required in this direction.

Bibliography

(1) G.M. Mudd, Global trends and environmental issues in nickel mining: Sulfides versus laterites, Ore Geol. Rev. 38 (2010) 9–26. https://doi.org/https://doi.org/10.1016/j.oregeorev.2010.05.003.

(2) N. Rötzer, M. Schmidt, Decreasing metal ore grades-Is the fear of resource depletion justified?, Resources. 7 (2018) 1–14. https://doi.org/10.3390/resources7040088.

(3) M. Ericsson, J. Drielsma, D. Humphreys, P. Storm, P. Weihed, Why current assessments of 'future efforts' are no basis for establishing policies on material use - a response to research on ore grades, Miner. Econ. 32 (2019) 111–121. https://doi.org/10.1007/s13563-019-00175-6.

(4) S.M. Jowitt, G.M. Mudd, J.F.H. Thompson, Future availability of non-renewable metal resources and the influence of environmental, social, and governance conflicts on metal production, Commun. Earth Environ. 13 (2020) 1–9. https://doi.org/10.1038/s43247-020-0011-0.

(5) J. Spooren, K. Binnemans, J. Björkmalm, K. Breemersch, Y. Dams, K. Folens, M. Gonzalez-Moya, L. Horckmans, K. Komnitsas, W. Kurylak, M. Lopez, J. Makinen, S. Onisei, K. Oorts, A. Peys, G. Pietek, Y. Pontikes, R. Snellings, M. Tripiana, J. Varia, K. Willquist, L. Yurramendi, P. Kinnunen, Near-zero-waste processing of low-grade, complex primary ores and secondary raw materials in Europe: technology development trends, Resour. Conserv. Recycl. 160 (2020) 104919. https://doi.org/https://doi.org/10.1016/j.resconrec.2020.104919.

(6) M. Xu, K. Scholey, S. Marcuson, Vale-Cytec-University research consortium on processing low grade ultramafic nickel ore. In Proceedings of the 50th Conference of Metallurgists (2011) 2-5.

(7) M. Fan, D. Tao, R. Honaker, Z. Luo, Nanobubble generation and its applications in froth flotation (part IV): Mechanical cells and specially designed column flotation of coal, Min. Sci. Technol. 20 (2010) 641–671. https://doi.org/10.1016/S1674-5264(09)60259-3.

(8) Y. Tao, J. Liu, S. Yu, D, Tao, Picobubble enhanced fine coal flotation, Separation Sci. and Technol. 41(16) (2006) 3597-3607

(9) M. El-Zahar, M. Salih, K. Fujisaki, Basic study of bubble formation in dissolved CO_2 gas flotation of waste activated sludge, In Proceedings of FILTECH EUROPA International conference and Exhibition. 1 (2001) 413-420.

(10) S. Ozun, B. V. Hassas, J. D. Miller, Collectorless flotation of oxidized pyrite, Colloids and Surfaces A: Physicochemical and Eng. Aspects. 561 (2019) 349-356.

(11) D.R. Snoswell, J. Yang, J. Duan, D. Fornasiero, J. Ralston, Dissolved gas, very small bubbles, and interparticle interactions. In Innovations in Natural Resource Processing-Proceedings of the Jan D. Miller Symposium (2005), Society for Mining, Metallurgy, and Exploration Inc (SME) (2005).

(12) V. Ross, A. Singh, K. Pillay, Improved flotation of PGM tailings with a high-shear hydrodynamic cavitation device. Minerals Engineering. Jun 15;137 (2019) 133-9.

(13) C.R. Edwards, W.B. Kipkie, G.E. Agar, The effect of slime coatings of the serpentine minerals, chrysotile and lizardite, on pentlandite flotation, Int. Journal of Miner. Processing. May 1;7(1) (1980) 33-42.

(14) B. Li, G. Zhang, D. Liu, J. Chen, Selective alteration mechanisms of sodium tripolyphosphate towards serpentine: Implications for flotation of pyrite from serpentine, Journal of Molecular Liquids. Dec 15;368 (2022) 120687.

(15) A.S. Freitas, E. Matiolo, R.T. Rodrigues, Flotation of calcite from apatite of a uranium-carbonate phosphate ore using carbon dioxide, Miner. Eng. 173 (2021) 107240.

(16) B. Vaziri Hassas, J. Jin, L.X. Dang, X. Wang, J.D. Miller, Attachment, coalescence, and spreading of carbon dioxide nanobubbles at pyrite surfaces, Langmuir. 34(47) (2018) 14317-14327.

(17) J. D. Miller, M. Misra, Carbon dioxide flotation of fine coal, Coal Preparation. 2(1) (1985) 69-73.

(18) E. Matiolo, L.M. Gonzaga, A.L. Guedes, An alternative flotation process for apatite concentration of the Santa Quitéria (Brazil) carbonaceous uranium-phosphate ore, Zangh, P.; Miller, J.; Wingate, E. (2016) 81-89.

(19) V.P. Mehrotra, K.N. Sivaramakrishnan, Beneficiation of high carbonate phosphate rock. US Patent 4.568.454. (1986).

(20) L.A. Takata, N.T. Shimabukuro, Processo para a obtenção de concentrados de apatita. BR N. PI 0504210-0. Depósito: 29 set. 2005, Concessão: 14 fev. (2006).

(21) S.E. Rezende, J.S. Martins, L.A. Takata, E. Matiolo, Processo para obtenção de concentrados de apatita por flotação. Brazilian Patent, 0902233-3. (2011).

(22) S.U.N. Wei, M.J. DENG, Y.H. HU, Fine particle aggregating and flotation behavior induced by high intensity conditioning of a CO_2 saturation slurry, Mining Sci. and Technol. (China). (2009) 19(4), 483-488.

(23) O.B. Wani, S. Khan, M. Shoaib, H. Zeng, E.R. Bobicki, Decarbonization of Mineral Processing Operations: Realizing the Potential of Carbon Capture and Utilization in the Processing of Ultramafic Nickel Ores, Chem. Eng. J. (2022) 134203.

(24) B.V. Hassas, J.D. Miller, The effect of carbon dioxide and nitrogen on pyrite surface properties and flotation response. Miner. Eng. (2019) 144, 106048.

(25) J. Grotzinger, T.H. Jordan, Understanding Earth, 7th ed., W. H> Freeman and Company. (2014).

(26) K. Panchuk, Physical Geology, 1st ed., University of Saskatchewan. (2019).

(27) M.A. McCrae, Early stage copper projects have grades one-third below operating mines, Mining[DOT]Com. (2018). https://www.mining.com/copper-supply-deficit-worse-think/ (accessed December 8, 2021).

(28) G. Calvo, G. Mudd, A. Valero, A. Valero, Decreasing ore grades in global metallic mining: A theoretical issue or a global reality, Resources. 5 (2016) 36. https://doi.org/10.3390/resources5040036.

(29) G.M. Mudd, Assessing the availability of global metals and minerals for the sustainable century: From aluminium to zirconium, Sustain. 13 (2021). https://doi.org/10.3390/su131910855.

(30) S.A. Hamid, P. Alfonso, H. Anticoi, E. Guasch, J. Oliva, M. Dosbaba, ... M. Chugunova, Quantitative mineralogical comparison between HPGR and ball mill products of a Sn-Ta ore, Minerals. 8(4) (2018) 151.

(31) R.P. King, C.L. Schneider, Mineral liberation and the batch comminution equation. Miner. Eng. 11(12) (1998) 1143-1160.

(32) N.O. Lotter, L.J. Kormos, J. Oliveira, D. Fragomeni, E. Whiteman, Modern process mineralogy: two case studies, Miner. Eng. 24(7) (2011) 638-650.

(33) G.J. Jameson, A.V. Nguyen, S. Ata, The flotation of fine and coarse particles. Froth Flotation: A Century of Innovation. Jan 1 (2007) 339-72.

(34) T. Leistner, U.A. Peuker, M. Rudolph, How gangue particle size can affect the recovery of ultrafine and fine particles during froth flotation, Miner. Eng. 109 (2017) 1–9. https://doi.org/10.1016/j.mineng.2017.02.005.

(35) A.V. Nguyen, Flotation. University of Newcastle, New South Wales, Australia (c) 2007 Elsevier Ltd.

(36) B.A. Wills, J.A. Finch, Froth Flotation, in: Wills' Miner. Process. Technol., 8th ed., Butterworth-Heinemann, Oxford, 2016: pp. 265–380.

(37) B.A. Wills, J.A. Finch, Introduction, in: Wills' Miner. Process. Technol., 8th ed., Butterworth-Heinemann, Oxford, 2016: pp. 1–27. https://doi.org/10.1016/b978-0-08-097053-0.00001-7.

(38) E.G. Kelly, D.J. Spottiswood, Introduction to mineral processing, Wiley- Interscience, New York, 1982.

(39) J. Mouat, The development of the flotation process: technological change and the genesis of modern mining, 1898-1911, Aust. Econ. Hist. Rev. 36 (1996) 3–31. https://doi.org/10.1111/aehr.361001.

(40) J. Nesset, The History of Flotation (Blowing Bubbles for Profit), (2021) 1–74.

(41) R.R. Klimpel, Froth Flotation, in: R.A. Meyers (Ed.), Encycl. Phys. Sci. Technol., Third Edit, (2003) 219–234.

(42) T.T. Chau, A review of techniques for measurement of contact angles and their applicability on mineral surfaces, Miner. Eng. 22 (2009) 213–219. https://doi.org/10.1016/j.mineng.2008.07.009.

(43) D.R. Nagaraj, S.A. Ravishankar, Flotation reagents—A critical overview from an industry perspective. Froth flotation: A century of innovation. (2007) 375-424.

(44) D.R. Nagaraj, R.S. Farinato, Evolution of flotation chemistry and chemicals: A century of innovations and the lingering challenges, Miner. Eng. 96–97 (2016) 2–14. https://doi.org/10.1016/j.mineng.2016.06.019.

(45) R. Honaker, B.C. Paul, K. Ho, A comparison study of column flotation technologies for cleaning Illinois coal, Carbondale, 1994.

(46) R.H. Yoon, G.H. Luttrell, The effect of bubble size on fine coal flotation, Coal Prep. 2 (1986) 179–192. https://doi.org/10.1080/07349348508905163.

(47) D. Tao, Role of Bubble Size in Flotation of Coarse and Fine Particles - A Review, Sep. Sci. Technol. 39 (2005) 741–760. https://doi.org/10.1081/ss-120028444.

(48) D. Wang, Q. Liu, Hydrodynamics of froth flotation and its effects on fine and ultrafine mineral particle flotation: A literature review, Miner. Eng. 173 (2021) 107220. https://doi.org/10.1016/j.mineng.2021.107220.

(49) N. Ahmed, G.J. Jameson, The effect of bubble size on the rate of flotation of fine particles, Int. J. Miner. Process. 14 (1985) 195–215.

(50) J. Ralston, Chapter 6: The influence of particle size and contact angle in flotation, in: Colloid Chem. Miner. Process., 1992: pp. 203–224. https://doi.org/10.1016/B978-0-444-88284-4.50011-1.

(51) J. Ralston, S.S. Dukhin, The interaction between particles and bubbles, Colloids Surfaces A Physicochem. Eng. Asp. 151 (1999) 3–14.

(52) Z. Dai, D. Fornasiero, J. Ralston, Particle-bubble collision models - a review, Adv. Colloid Interface Sci. 85 (2000) 231–256.

(53) B. V. Derjaguin, S.S. Dukhin, Theory of Flotation of Small and Medium-size Particles, Prog. Surf. Sci. 43 (1993) 241–266.

(54) D.I. Verrelli, P.T.L. Koh, A. V. Nguyen, Particle–bubble interaction and attachment in flotation, Chem. Eng. Sci. 66 (2011) 5910–5921. https://doi.org/https://doi.org/10.1016/j.ces.2011.08.016.

(55) L. Chen, J. Wu, Z. Sun, Effect of cationic collector on the attachment of glass beads to a stationary bubble, Colloids Surfaces A Physicochem. Eng. Asp. 625 (2021). https://doi.org/10.1016/j.colsurfa.2021.126979.

(56) D. Tao, A. Sobhy, Nanobubble effects on hydrodynamic interactions between particles and bubbles, Powder Technol. 346 (2019) 385–395. https://doi.org/10.1016/j.powtec.2019.02.024.

(57) L. Wang, R.H. Yoon, Hydrophobic forces in thin aqueous films and their role in film thinning, Colloids Surfaces A Physicochem. Eng. Asp. 263 (2005) 267–274. https://doi.org/10.1016/j.colsurfa.2004.12.045.

(58) G.D. Senior, L.K. Shannon, W.J. Trahar, The flotation of pentlandite from pyrrhotite with particular reference to the effects of particle size, Int. J. Miner. Process. 42 (1994) 169–190. https://doi.org/10.1016/0301-7516(94)00031-X.

(59) D. Feng, C. Aldrich, Effect of particle size on flotation performance of complex sulphide ores, Miner. Eng. 12 (1999) 721–731.

(60) A. Sobhy, D. Tao, Nanobubble column flotation of fine coal particles and associated fundamentals, Int. J. Miner. Process. 124 (2013) 109–116. http://dx.doi.org/10.1016/j.minpro.2013.04.016.

(61) Z. Zhang, L. Ren, Y. Zhang, Role of nanobubbles in the flotation of fine rutile particles, Miner. Eng. 172 (2021) 1–8. https://doi.org/10.1016/j.mineng.2021.107140.

(62) T. Miettinen, J. Ralston, D. Fornasiero, The limits of fine particle flotation, Miner. Eng. Apr 1;23(5) (2010) 420-37.

(63) A. V. Nguyen, D.A. An-Vo, T. Tran-Cong, G.M. Evans, A review of stochastic description of the turbulence effect on bubble-particle interactions in flotation, Int. J. Miner. Process. 156 (2016) 75–86. https://doi.org/10.1016/j.minpro.2016.05.002.

(64) D. Hewitt, D. Fornasiero, J. Ralston, Bubble particle attachment efficiency, Miner. Eng. 7 (1994) 657–665.

(65) B. Albijanic, O. Ozdemir, M.A. Hampton, P.T. Nguyen, A. V. Nguyen, D. Bradshaw, Fundamental aspects of bubble particle attachment mechanism in flotation separation.pdf, Miner. Eng. 65 (2014) 187–195. https://doi.org/10.1016/j.mineng.2014.06.008.

(66) B. Albijanic, D.J. Bradshaw, A. V. Nguyen, The relationships between the bubble-particle attachment time, collector dosage and the mineralogy of a copper sulfide ore, Miner. Eng. 36–38 (2012) 309–313. https://doi.org/10.1016/j.mineng.2012.06.007.

(67) A. V. Nguyen, G.M. Evans, Attachment interaction between air bubbles and particles in froth flotation, Exp. Therm. Fluid Sci. 28 (2004) 381–385. https://doi.org/10.1016/j.expthermflusci.2002.12.001.

(68) A. V. Nguyen, G.M. Evans, Movement of fine particles on an air bubble surface studied using high-speed video microscopy, J. Colloid Interface Sci. 273 (2004) 271–277. https://doi.org/10.1016/j.jcis.2003.12.066.

(69) Y. Gao, G.M. Evans, E.J. Wanless, R. Moreno-Atanasio, DEM modelling of particle-bubble capture through extended DLVO theory, Colloids Surfaces A Physicochem. Eng. Asp. 529 (2017) 876–885. https://doi.org/10.1016/j.colsurfa.2017.06.082.

(70) G.S. Dobby, J.A. Finch, Particle Size Dependance in Flotation Derived from a Fundamental Model of the Capture Process, Int. J. Miner. Process. 21 (1987) 241–260.

(71) P. Chu, M. Mirnezami, J.A. Finch, Quantifying particle pick up at a pendant bubble: A study of non-hydrophobic particle-bubble interaction, Miner. Eng. 55 (2014) 162–164. https://doi.org/10.1016/j.mineng.2013.10.009.

(72) S.R. Rao, Surface Chemistry of Froth Flotation, Springer US. (2004). https://doi.org/10.1007/978-1-4757-4302-9.

(73) J. Sygusch, M. Rudolph, A contribution to wettability and wetting characterisation of ultrafine particles with varying shape and degree of hydrophobization, Appl. Surf. Sci. 566 (2021) 150725. https://doi.org/10.1016/j.apsusc.2021.150725.

(74) D.I. Verrelli, W.J. Bruckard, P.T.L. Koh, M.P. Schwarz, B. Follink, Particle shape effects in flotation. Part 1: Microscale experimental observations, Miner. Eng. 58 (2014) 80–89. https://doi.org/10.1016/j.mineng.2014.01.004.

(75) P.T.L. Koh, F.P. Hao, L.K. Smith, T.T. Chau, W.J. Bruckard, The effect of particle shape and hydrophobicity in flotation, Int. J. Miner. Process. 93 (2009) 128–134. https://doi.org/10.1016/j.minpro.2009.07.007.

(76) L. Parkinson, J. Ralston, Dynamic aspects of small bubble and hydrophilic solid encounters, Adv. Colloid Interface Sci. 168 (2011) 198–209. https://doi.org/10.1016/j.cis.2011.08.002.

(77) B. Shahbazi, B. Rezai, S.M. Javad Koleini, Bubble particle collision and attachment probability on fine particles flotation, Chem. Eng. Process. Process Intensif. 49 (2010) 622–627. https://doi.org/10.1016/j.cep.2010.04.009.

(78) S. Mitra, M.M. Hoque, G. Evans, A. V. Nguyen, Direct visualization of bubble-particle interactions in presence of cavitation bubbles in an ultrasonic flotation cell, Miner. Eng. 174 (2021). https://doi.org/10.1016/j.mineng.2021.107258.

(79) T.A. Rickard, The Flotation Process, 1st ed., Dewey Pubishing Co, San Francisco, CA, 1916.

(80) International Organization for Standardization, Fine bubble technology — General principles for usage and measurement of fine bubbles — Part 1: Terminology, ISO 20480-12017. (2017). https://www.iso.org/obp/ui/#iso:std:iso:20480:-1:ed-1:v1:en (accessed December 11, 2021).

(81) C. Li, H. Zhang, A review of bulk nanobubbles and their roles in flotation of fine particles, Powder Technol. 395 (2022) 618–633. https://doi.org/https://doi.org/10.1016/j.powtec.2021.10.004

(82) S. Calgaroto, K.Q. Wilberg, J. Rubio, On the nanobubbles interfacial properties and future applications in flotation, Miner. Eng. 60 (2014) 33–40. https://doi.org/10.1016/j.mineng.2014.02.002.

(83) A. Azevedo, H. Oliveira, J. Rubio, Bulk nanobubbles in the mineral and environmental areas: Updating research and applications, Adv. Colloid Interface Sci. 271 (2019) 101992. https://doi.org/10.1016/j.cis.2019.101992.

(84) Z. Pourkarimi, B. Rezai, M. Noaparast, A. V. Nguyen, S.C. Chelgani, Proving the existence of nanobubbles produced by hydrodynamic cavitation and their significant effects in powder flotation, Adv. Powder Technol. 32 (2021) 1810–1818. https://doi.org/10.1016/j.apt.2021.03.039.

(85) C. Qiao, D. Yang, X. Mao, L. Xie, L. Gong, X. Peng, Q. Peng, T. Wang, H. Zhang, H. Zeng, Recent advances in bubble-based technologies: Underlying interaction mechanisms and applications, Appl. Phys. Rev. 8 (2021) 011315. https://doi.org/10.1063/5.0040331.

(86) E. Matiolo, H.J.B. Couto, M.F. De Lira Teixeira, R.N. De Almeida, A.S. De Freitas, A comparative study of different column sizes for ultrafine apatite flotation, Benef. Phosphates Sustain. Crit. Mater. Smart Process. (2019) 200–209.

(87) D. Tao, S. Yu, X. Zhou, R.Q. Honaker, B.K. Parekh, Picobubble column flotation of fine coal, Int. J. Coal Prep. Util. 28 (2008) 1–14. https://doi.org/10.1080/07349340701640901.

(88) A. Azevedo, R. Etchepare, S. Calgaroto, J. Rubio, Aqueous dispersions of nanobubbles: Generation, properties and features, Miner. Eng. 94 (2016) 29–37. https://doi.org/10.1016/j.mineng.2016.05.001.

(89) V. Chipakwe, A. Sand, S.C. Chelgani, Nanobubble assisted flotation separation of complex Pb – Cu – Zn sulfide ore – Assessment of process readiness, Sep. Sci. Technol. (2021) 1–8. https://doi.org/10.1080/01496395.2021.1981942.

(90) Z.A. Zhou, Z. Xu, J.A. Finch, On the role of cavitation in particle collection during flotation - a critical review, Miner. Eng. 7 (1994) 1073–1084. https://doi.org/10.1016/0892-6875(94)00053-0.

(91) K.J. Vachaparambil, K.E. Einarsrud, Explanation of Bubble Nucleation Mechanisms - A Gradient Theory Approach, J. Electrochem. Soc. 165 (2018) 504–512.

(92) T. Takahashi, T. Miyahara, H. Mochizuki, Fundamental Study of Bubble Formation in Dissolved Air Pressure Flotation, J. Chem. Eng. Japan. 12 (1979) 275–280.

(93) S.F. Jones, G.M. Evans, K.P. Galvin, Bubble nucleation from gas cavities - A review, Adv. Colloid Interface Sci. 80 (1999) 27–50. https://doi.org/10.1016/S0001-8686(98)00074-8.

(94) T.F. Groß, P.F. Pelz, Diffusion-driven nucleation from surface nuclei in hydrodynamic cavitation, J. Fluid Mech. 830 (2017) 138–164. https://doi.org/10.1017/jfm.2017.587.

(95) M. Li, Influence of Venturi Tube Geometry and Particle Properties on the Hydrodynamic Cavitation for Fine Particle Flotation, University of Alberta, 2017.

(96) S.R. German, M.A. Edwards, Q. Chen, H.S. White, Laplace Pressure of Individual H2 Nanobubbles from Pressure-Addition Electrochemistry, Nano Lett. 16 (2016) 6691–6694. https://doi.org/10.1021/acs.nanolett.6b03590.

(97) Z.A. Zhou, Z. Xu, J.A. Finch, J.H. Masliyah, R.S. Chow, On the role of cavitation in particle collection in flotation - A critical review II, Miner. Eng. 22 (2009) 419–433. https://doi.org/10.1016/j.mineng.2008.12.010.

(98) J. Yang, J. Duan, D. Fornasiero, J. Ralston, Kinetics of CO_2 nanobubble formation at the solid/water interface, Phys. Chem. Chem. Phys. 9 (2007) 6327–6332. https://doi.org/10.1039/b709624k.

(99) P.M. Wilt, Nucleation rates and bubble stability in water carbon dioxide solutions, J. Colloid Interface Sci. 112 (1986) 530–538.

(100) Z.-A. Zhou, Gas nucleation and cavitation in flotation, McGill University, 1996.

(101) Z.A. Zhou, R.S. Chow, Z. Xu, J.H. Masliyah, Spontaneous bubble nucleation on bitumen, in: 24th Int. Miner. Process. Congr., 2008: pp. 1–25.

(102) E.M. Gates, The influence of freestream turbulence, freestream nuclei populations and drag reducing polymer on cavitation inception on two axisymetric bodies, California Institute of Technology, 1977.

(103) B.H. Tan, H. An, C.D. Ohl, Stability of surface and bulk nanobubbles, Curr. Opnion Colloid Interface Sci. 53 (2021) 101428.

(104) J. Zou, H. Zhang, Z. Guo, Y. Liu, J. Wei, Y. Huang, X. Zhang, Surface Nanobubbles Nucleate Liquid Boiling, Langmuir. 34 (2018) 14096–14101. https://doi.org/10.1021/acs.langmuir.8b03290.

(105) N. Bremond, M. Arora, C.D. Ohl, D. Lohse, Cavitation on surfaces, J. Phys. Condens. Matter. 17 (2005). https://doi.org/10.1088/0953-8984/17/45/054.

(106) J. Yang, J. Duan, D. Fornasiero, J. Ralston, Very small bubble formation at the solid-water interface, J. Phys. Chem. B. 107 (2003) 6139–6147. https://doi.org/10.1021/jp0224113.

(107) M. Li, A. Bussonnière, B. Xiang, R. Manica, Q. Liu, Effect of solid wettability on three-phase hydrodynamic cavitation, Miner. Eng. 180 (2022) 107455. https://doi.org/10.1016/j.mineng.2022.107455.

(108) W.L. Ryan, E.A. Hemmingsen, Bubble formation in water at smooth hydrophobic surfaces.pdf, J. Colloid Interface Sci. 157 (1993) 312–317.

(109) M. Xu, C. Li, H. Zhang, N. Kupka, U.A. Peuker, M. Rudolph, A contribution to exploring the importance of surface air nucleation in froth flotation – The effects of dissolved air on graphite flotation, Colloids Surfaces A Physicochem. Eng. Asp. 633 (2022) 127866. https://doi.org/10.1016/j.colsurfa.2021.127866.

(110) W. Zhou, J. Niu, W. Xiao, L. Ou, Adsorption of bulk nanobubbles on the chemically surface-modified muscovite minerals, Ultrason. Sonochem. 51 (2019) 31–39. https://doi.org/10.1016/j.ultsonch.2018.10.021.

(111) W. Xiao, Y. Zhao, J. Yang, Y. Ren, W. Yang, X. Huang, L. Zhang, Effect of Sodium Oleate on the Adsorption Morphology and Mechanism of Nanobubbles on the Mica Surface, Langmuir. 35 (2019) 9239–9245. https://doi.org/10.1021/acs.langmuir.9b01384.

(112) X. Deng, B. Lv, G. Cheng, Y. Lu, Mechanism of micro/nano-bubble formation and cavitation effect on bubbles size distribution in flotation, Physicochem. Probl. Miner. Process. 56 (2020) 504–512. https://doi.org/10.37190/PPMP/119883.

(113) C. Li, D. Li, X. Li, M. Xu, H. Zhang, Surface nanobubbles on hydrophobic surface and its implication to flotation, Int. J. Miner. Metall. Mater. (2020). https://doi.org/10.1007/s12613-021-2279-1.

(114) F. Zhang, Y. Xing, L. Sun, M. Liu, X. Gui, Y. Cao, Characteristics of interfacial nanobubbles and their interaction with solid surfaces, Appl. Surf. Sci. 550 (2021). https://doi.org/10.1016/j.apsusc.2021.149258.

(115) S. Nazari, S.Z. Shafaei, B. Shahbazi, S. Chehreh Chelgani, Study relationships between flotation variables and recovery of coarse particles in the absence and presence of nanobubble, Colloids Surfaces A Physicochem. Eng. Asp. 559 (2018) 284–288. https://doi.org/10.1016/j.colsurfa.2018.09.066.

(116) A.J. Jadhav, M. Barigou, Bulk Nanobubbles or Not Nanobubbles : That is the Question, Langmuir. 36 (2020) 1699–1708. https://doi.org/10.1021/acs.langmuir.9b03532.

(117) F. Zhang, L. Sun, H. Yang, X. Gui, H. Schönherr, M. Kappl, Y. Cao, Y. Xing, Recent advances for understanding the role of nanobubbles in particles flotation, Adv. Colloid Interface Sci. 291 (2021) 102403. https://doi.org/10.1016/j.cis.2021.102403.

(118) D. Tao, Recent advances in fundamentals and applications of nanobubble enhanced froth flotation: A review, Miner. Eng. 183 (2022) 107554. https://doi.org/10.1016/j.mineng.2022.107554.

(119) F.E. Fox, K.F. Herzfeld, Gas Bubbles with Organic Skin as Cavitation Nuclei, J. Acoust. Soc. Am. 26 (1954) 984–989. https://doi.org/10.1121/1.1907466.

(120) D.E. Yount, Skins of varying permeability: A stabilization mechanism for gas cavitation nuclei, J. Acoust. Soc. Am. 65 (1979) 1429–1439. https://doi.org/10.1121/1.382930.

(121) N. Nirmalkar, A.W. Pacek, M. Barigou, On the Existence and Stability of Bulk Nanobubbles, Langmuir. 34 (2018) 10964–10973. https://doi.org/10.1021/acs.langmuir.8b01163.

(122) M.P. Brenner, D. Lohse, Dynamic equilibrium mechanism for surface nanobubble stabilization, Phys. Rev. Lett. 101 (2008) 1–4. https://doi.org/10.1103/PhysRevLett.101.214505.

(123) X. Zhang, D.Y.C. Chan, D. Wang, N. Maeda, Stability of interfacial nanobubbles, Langmuir. 29 (2013) 1017–1023. https://doi.org/10.1021/la303837c.

(124) Y. Sun, G. Xie, Y. Peng, W. Xia, J. Sha, Stability theories of nanobubbles at solid–liquid interface: A review, Colloids Surfaces A Physicochem. Eng. Asp. 495 (2016) 176–186. https://doi.org/10.1016/j.colsurfa.2016.01.050.

(125) D. Lohse, X. Zhang, Surface nanobubbles and nanodroplets, Rev. Mod. Phys. 87 (2015) 981–1035. https://doi.org/10.1103/RevModPhys.87.981.

(126) Z. Pourkarimi, B. Rezai, M. Noaparast, Effective parameters on generation of nanobubbles by cavitation method for froth flotation applications, Physicochem. Probl. Miner. Process. 53 (2017) 920–942. https://doi.org/10.5277/ppmp170220.

(127) Y. Pan, I. Gresham, G. Bournival, S. Prescott, S. Ata, Synergistic effects of frothers , collector and salt on bubble stability, Powder Technol. 397 (2022) 117028. https://doi.org/10.1016/j.powtec.2021.117028.

(128) Y.S. Cho, J.S. Laskowski, Effect of flotation frothers on bubble size and foam stability, Int. J. Miner. Process. 64 (2002) 69–80.

(129) J.A. Finch, J.E. Nesset, C. Acuña, Role of frother on bubble production and behaviour in flotation, Miner. Eng. 21 (2008) 949–957. https://doi.org/10.1016/j.mineng.2008.04.006.

(130) W. Kracht, J.A. Finch, Bubble break-up and the role of frother and salt, Int. J. Miner. Process. 92 (2009) 153–161. https://doi.org/10.1016/j.minpro.2009.03.011.

(131) A. Atrafi, M. Pawlik, Surface tension and gas dispersion properties of fatty acid solutions, Miner. Eng. 85 (2016) 138–147. https://doi.org/10.1016/j.mineng.2015.11.006.

(132) P. Chu, K.E. Waters, J.A. Finch, Break-up in formation of small bubbles : Break-up in a confined volume, Colloids Surfaces A Physicochem. Eng. Asp. 503 (2016) 88–93. https://doi.org/10.1016/j.colsurfa.2016.06.037.

(133) K. Batjargal, O. Guven, O. Ozdemir, S.I. Karakashev, N.A. Grozev, F. Boylu, M.S. Çelik, Adsorption Kinetics of Various Frothers on Rising Bubbles of Different Sizes under Flotation Conditions, Minerals. 11 (2021) 304. https://doi.org/10.3390/min11030304.

(134) J. Pyecha, B. Lacouture, S. Sims, G. Hope, A. Stradling, Evaluatio of a Microcel sparger in the Red Dog column flotation cells, Miner. Eng. 19 (2006) 748–757. https://doi.org/10.1016/j.mineng.2005.09.044.

(135) P. Chu, K.E. Waters, J.A. Finch, Break-up in formation of small bubbles: Comparison between low and high frother concentrations, Miner. Eng. 97 (2016) 15–19. https://doi.org/10.1016/j.mineng.2016.06.002.

(136) M.A. Corona-Arroyo, A. López-Valdivieso, J.S. Laskowski, A. Encinas-Oropesa, Effect of frothers and dodecylamine on bubble size and gas holdup in a downflow column, Miner. Eng. 81 (2015) 109–115. https://doi.org/10.1016/j.mineng.2015.07.023.

(137) J.M. Sovechles, K.E. Waters, Effect of Ionic Strength on Bubble Coalescence in Inorganic Salt and Seawater Solutions, AIChE J. 61 (2015) 2489–2496. https://doi.org/10.1002/aic.

(138) J.M. Sovechles, M.R. Lepage, B. Johnson, K.E. Waters, Effect of gas rate and impeller speed on bubble size in frother-electrolyte solutions, Miner. Eng. 99 (2016) 133–141.

(139) J.J. Quinn, W. Kracht, C.O. Gomez, C. Gagnon, J.A. Finch, Comparing the effect of salts and frother (MIBC) on gas dispersion and froth properties, Miner. Eng. 20 (2007) 1296–1302. https://doi.org/10.1016/j.mineng.2007.07.007.

(140) K.C. Corin, S. Tetlow, M.S. Manono, Considering the action of frothers under degrading water quality, Miner. Eng. 181 (2022) 107546. https://doi.org/10.1016/j.mineng.2022.107546.

(141) M. Li, A. Bussonnière, M. Bronson, Z. Xu, Q. Liu, Study of Venturi tube geometry on the hydrodynamic cavitation for the generation of microbubbles, Miner. Eng. 132 (2019) 268–274. https://doi.org/10.1016/j.mineng.2018.11.001.

(142) X. Zhang, Q. shuai Wang, Z. xian Wu, D. ping Tao, An experimental study on size distribution and zeta potential of bulk cavitation nanobubbles, Int. J. Miner. Metall. Mater. 27 (2020) 152–161. https://doi.org/10.1007/s12613-019-1936-0

(143) T.T. Bui, D.C. Nguyen, M. Han, Average size and zeta potential of nanobubbles in different reagent solutions, J. Nanoparticle Res. 21 (2019) 11. https://doi.org/10.1007/s11051-019-4618-y.

(144) F. Ikumapayi, M. Makitalo, B. Johansson, K.H. Rao, Recycling of process water in sulphide flotation - Effect of calcium and sulphate ions on flotation of galena, Miner. Eng. 39 (2012) 77–88. https://doi.org/10.1016/j.mineng.2012.07.016.

(145) R.I. Jeldres, L. Forbes, L.A. Cisternas, Effect of Seawater on Sulfide Ore Flotation : A Review, Miner. Process. Extr. Metall. Rev. 37 (2016) 369–384. https://doi.org/10.1080/08827508.2016.1218871.

(146) L. Wang, C. Li, A Brief Review of Pulp and Froth Rheology in Mineral Flotation, J. Chem. 2020 (2020) 16. https://doi.org/10.1155/2020/3894542.

(147) C.E. Gibson, S. Kelebek, Sensitivity of pentlandite flotation in complex sulfide ores towards pH control by lime versus soda ash: Effect on ore type, Int. J. Miner. Process. 127 (2014) 44–51. https://doi.org/10.1016/j.minpro.2014.01.001.

(148) C. Li, P. Somasundaran, Reversal of Bubble Charge in Multivalent Inorganic Salt Solutions - Effect of Magnesium, J. Colloid Interface Sci. 146 (1991) 215–218.

(149) C. Li, P. Somasundaran, Reversal of Bubble Charge in Multivalent Inorganic Salt Solutions - Effect of Aluminum, J. Colloid Interface Sci. 148 (1992) 587–591.

(150) A.M. Elmahdy, M. Mirnezami, J.A. Finch, Zeta potential of air bubbles in presence of frothers, Int. J. Miner. Process. 89 (2008) 40–43. https://doi.org/10.1016/j.minpro.2008.09.003.

(151) R.H. Yoon, J.L. Yordan, Zeta potential measurements on microbubbles generated using various surfactants, J. Colloid Interface Sci. 113 (1986) 430–438.

(152) Z.J. Ang, G. Bournival, S. Ata, Influence of frothers on the detachment of galena particles from bubbles, Int. J. Miner. Process. 121 (2013) 59–64. https://doi.org/10.1016/j.minpro.2013.02.003

(153) O. Manor, D.Y.C. Chan, Influence of Surfactants on the Force between Two Bubbles, Langmuir. 26 (2010) 655–662. https://doi.org/10.1021/la902243q.

(154) P.K. Tsave, M. Kostoglou, T.D. Karapantsios, N.K. Lazaridis, A Hybrid Device for Enhancing Flotation of Fine Particles by Combining Micro-Bubbles with Conventional Bubbles, Minerals. 11 (2021) 18. https://doi.org/10.3390/min11060561.

(155) T. Krolak, K. Palmer, B. Lacouture, N. Paley, NI 43-101 Technical Report Red Dog Mine Alaska, USA, 2017. https://www.miningdataonline.com/reports/Red Dog Mine_TR12312016.pdf.

(156) A. Hassanzadeh, M. Safari, D.H. Hoang, H. Khoshdast, B. Albijanic, P.B. Kowalczuk, Technological assessments on recent developments in fine and coarse particle flotation systems, Miner. Eng. 18 (2022) 107509. https://doi.org/10.1016/j.mineng.2022.107.509.

(157) S. Farrokhpay, I. Filippova, L. Filippov, A. Picarra, N. Rulyov, D. Fornasiero, Flotation of fine particles in the presence of combined microbubbles and conventional bubbles, Miner. Eng. 155 (2020) 106439. https://doi.org/10.1016/j.mineng.2020.106439.

(158) N. Rulyov, T. Nessipbay, T. Dulatbek, S. Larissa, K. Zhamikhan, Effect of microbubbles as flotation carriers on fine sulphide ore beneficiation, Miner. Process. Extr. Metall. Trans. Inst. Min. Metall. 127 (2018) 133–139. https://doi.org/10.1080/03719553.2017.1351067.

(159) W. Zhou, K. Liu, L. Wang, B. Zhou, J. Niu, L. Ou, The role of bulk micro-bubbles in reagent desorption and potential implication in flotation separation of highly hydrophobized minerals, Ultrason. Sonochem. 64 (2020) 104996. https://doi.org/10.1016/j.ultsonch.2020.104996.

(160) Eriez Flotation Division, Cavitation Tube Sparging Systems, (2022). https://www.eriez.com/Documents/Literature/Brochures/Products/Flotation/CavTube/FGB-103-Eriez-Cavitation-Tube-Sparging-Systems.pdf (accessed February 3, 2022).

(161) Y. Li, F. Wu, W. Xia, Y. Mao, Y. Peng, G. Xie, The bridging action of microbubbles in particle-bubble adhesion, Powder Technol. 375 (2020) 271–274. https://doi.org/10.1016/j.powtec.2020.07.109.

(162) M.A. Hampton, A. V. Nguyen, Systematically altering the hydrophobic nanobubble bridging capillary force from attractive to repulsive, J. Colloid Interface Sci. 333 (2009) 800–806. https://doi.org/10.1016/j.jcis.2009.01.035.

(163) M.A. Hampton, A. V. Nguyen, Nanobubbles and the nanobubble bridging capillary force, Adv. Colloid Interface Sci. 154 (2010) 30–55. https://doi.org/10.1016/j.cis.2010.01.006.

(164) H. Schubert, Nanobubbles, hydrophobic effect, heterocoagulation and hydrodynamics in flotation, Int. J. Miner. Process. 78 (2005) 11–21. https://doi.org/10.1016/j.minpro.2005.07.002.

(165) A. Rahman, K.D. Ahmad, A. Mahmoud, F. Maoming, Nano-microbubble flotation of fine and ultrafine chalcopyrite particles, Int. J. Min. Sci. Technol. 24 (2014) 559–566. https://doi.org/10.1016/j.ijmst.2014.05.021.

(166) M. Li, J. Liu, J. Li, B. Xiang, R. Manica, Q. Liu, Enhancement of selective fine particle flotation by microbubbles generated through hydrodynamic cavitation, Powder Technol. 405 (2022) 117502. https://doi.org/10.1016/j.powtec.2022.117502.

(167) H.-J. Butt, K. Graf, M. Kappl, Physics and Chemistry of Interfaces, Wiley-VCH Verlag, 2003.

(168) S. Calgaroto, A. Azevedo, J. Rubio, Flotation of quartz particles assisted by nanobubbles, Int. J. Miner. Process. 137 (2015) 64–70. https://doi.org/10.1016/j.minpro.2015.02.010.

(169) H. Li, A. Afacan, Q. Liu, Z. Xu, Study interactions between fine particles and micron size bubbles generated by hydrodynamic cavitation, Miner. Eng. 84 (2015) 106–115. https://doi.org/10.1016/j.mineng.2015.09.023.

(170) W. Zhou, H. Chen, L. Ou, Q. Shi, Aggregation of ultra-fine scheelite particles induced by hydrodynamic cavitation, Int. J. Miner. Process. 157 (2016) 236–240. https://doi.org/10.1016/j.minpro.2016.11.003.

(171) T. Uysal, O. Guven, O. Ozdemir, E. Karaagaclioglu, B. Tunç, M.S. Çelik, Contribution of particle morphology on flotation and aggregation of sphalerite particles, Miner. Eng. 165 (2021) 106860. https://doi.org/10.1016/j.mineng.2021.106860.

(172) A.R.S. de Medeiros, C.A.M. Baltar, Importance of collector chain length in flotation of fine particles, Miner. Eng. 122 (2018) 179–184. https://doi.org/10.1016/j.mineng.2018.03.008.

(173) J. Ralston, D. Fornasiero, R. Hayes, Bubble-particle attachment and detachment in flotation, Int. J. Miner. Process. 56 (1999) 133–164. https://doi.org/10.1016/S0301-7516(98)00046-5.

(174) X. Zhang, R. Manica, Y. Tang, P. Tchoukov, Q. Liu, Z. Xu, Probing Boundary Conditions at Hydrophobic Solid-Water Interfaces by Dynamic Film Drainage Measurement, Langmuir. 34 (2018) 12025–12035. https://doi.org/10.1021/acs.langmuir.8b02492.

(175) L. Pan, R.-H. Yoon, Measurement of hydrophobic forces in thin liquid films of water between bubbles and xanthate-treated gold surfaces, Miner. Eng. 98 (2016) 240–250. https://doi.org/10.1016/j.mineng.2016.09.005.

(176) A. Nikolaev, Flotation kinetic model with respect to particle heterogeneity and roughness, Int. J. Miner. Process. 155 (2016) 74–82. https://doi.org/10.1016/j.minpro.2016.08.005.

(177) K. Huang, R. Yoon, Effect of ζ -Potentials on Bubble-Particle Interactions, Mining, Metall. Explor. 36 (2019) 21–34.

(178) L. Wang, Z. Xu, J.H. Masliyah, Dissipation of film drainage resistance by hydrophobic surfaces in aqueous solutions, J. Phys. Chem. C. 117 (2013) 8799–8805. https://doi.org/10.1021/jp4000945.

(179) D.Y.C. Chan, E. Klaseboer, R. Manica, Film drainage and coalescence between deformable drops and bubbles, Soft Matter. 7 (2011) 2235–2264. https://doi.org/10.1039/c0sm00812e.

(180) B. Liu, R. Manica, X. Zhang, A. Bussonnière, Z. Xu, G. Xie, Q. Liu, Dynamic Interaction between a Millimeter-Sized Bubble and Surface Microbubbles in Water, Langmuir. 34 (2018) 11667–11675. https://doi.org/10.1021/acs.langmuir.8b01202.

(181) B. Liu, R. Manica, Q. Liu, E. Klaseboer, Z. Xu, Coalescence or Bounce? How Surfactant Adsorption in Milliseconds Affects Bubble Collision, J. Phys. Chem. Lett. 10 (2019) 5662–5666. https://doi.org/10.1021/acs.jpclett.9b01598.

(182) B. Liu, R. Manica, Q. Liu, E. Klaseboer, Z. Xu, G. Xie, Coalescence of bubbles with mobile interfaces in water, Phys. Rev. Lett. 122 (2019) 1–5. https://doi.org/10.1103/PhysRevLett.122.194501.

(183) V. V. Yaminsky, S. Ohnishi, E.A. Vogler, R.G. Horn, Stability of aqueous films between bubbles. Part 1. the effect of speed on bubble coalescence in purified water and simple electrolyte solutions, Langmuir. 26 (2010) 8061–8074. https://doi.org/10.1021/la904481d.

(184) I.U. Vakarelski, R. Manica, X. Tang, S.J. O'Shea, G.W. Stevens, F. Grieser, R.R. Dagastine, D.Y.C. Chan, Dynamic interactions between microbubbles in water, Proc. Natl. Acad. Sci. U. S. A. 107 (2010) 11177–11182. https://doi.org/10.1073/pnas.1005937107.

(185) R.G. Horn, L.A. Del Castillo, S. Ohnishi, Coalescence map for bubbles in surfactant-free aqueous electrolyte solutions, Adv. Colloid Interface Sci. 168 (2011) 85–92. https://doi.org/10.1016/j.cis.2011.05.006.

(186) R. Manica, B. Liu, M. Li, Z. Chen, Q. Liu, Hydrodynamic collisions involving bubbles and mineral particles, Can. J. Chem. Eng. (2021) 1–18. https://doi.org/10.1002/cjce.24347.

(187) X.H. Zhang, A. Khan, W.A. Ducker, A nanoscale gas state. Physical review letters. 98(13) (2007) 136101.

(188) X. Wang, X Yin, J. Nalaskowski, H. Du, J.D. Miller, Molecular features of water films created with bubbles at silica surfaces. Surf. Innovations. 3 (1) (2015) 20-26.

(189) A.S.D. Freitas, E. Matiolo, R.T. Rodrigues, Effect of calcium concentration on calcite flotation from apatite using carbonic gas. REM-Int. Eng. J. 73 (2020) 253-259.

(190) E.R. Bobicki, Q. Liu, Z. Xu, Microwave heating of ultramafic nickel ores and mineralogical effects. Miner. Eng. 58 (2014) 22-25.

(191) B.N. Ndlovu, E. Forbes, M. Becker, D.A. Deglon, J.P. Franzidis, J.S. Laskowski, The effects of chrysotile mineralogical properties on the rheology of chrysotile suspensions. Miner. Eng. 24(9) (2011) 1004-1009.

(192) M. Xu, Z. Dai, J. Dong, F. Ford, A. Lee, Fibrous minerals in ultramafic nickel sulphide ores, In Proceedings of the 49th Conference of Metallurgists 2010, Vancouver, BC, Canada. October, 3-6. (2010).

(193) G.W.C. Kaye, T.H. Laby, Tables of physical and chemical constants, 15th Ed., Longman, NY. (1986) p. 219.

(194) L. Ji, H. Yu, B. Yu, R. Zhang, D. French, M. Grigore, S. Zhao, Insights into carbonation kinetics of fly ash from Victorian lignite for CO_2 sequestration, Energy & Fuels. 32(4) (2018) 4569-4578.

(195) B. Averill, P. Eldredge, [eTextbook] General Chemistry: Principles, Patterns, and Applications. (2011).

(196) K.S. Lackner, D.P. Butt, C.H. Wendt, Progress on binding CO_2 in mineral substrates, In ~ Pergamon Energy Com'ers. Mgmt. Vol. 38 (1997).

(197) N. Ishida, T. Inoue, M. Miyahara, K. Higashitani, Nano bubbles on a hydrophobic surface in water observed by tapping-mode atomic force microscopy, Langmuir. 16(16) (2000) 6377-6380.

(198) S. Ljunggren, J.C. Eriksson, The lifetime of a colloid-sized gas bubble in water and the cause of the hydrophobic attraction, Colloids and Surfaces A: Physicochemical and Eng. Aspects. 129 (1997) 151-155.

(199) B. Albijanic, O. Ozdemir, A.V Nguyen, D. Bradshaw, A review of induction and attachment times of wetting thin films between air bubbles and particles and its relevance in the separation of particles by flotation, Advances in Colloid and Interface Sci. 159(1) (2010) 1-21.

(200) W. Gong, J. Stearnes, D. Fornasiero, R. Hayes, J. Ralston, The influence of dissolved gas on the interactions between surfaces of different hydrophobicity in aqueous media, Phys. Chem. Chem. Phys. 1 (1999) 2799-2803.

(201) D.R.E. Snoswell, J. Duan, D. Fornasiero, J. Ralston, Colloid stability and the influence of dissolved gas, J. Phys. Chem. B. 107 (13) (2003) 2986−2994.

(202) S.R. German, X. Wu, H. An, V.S.J. Craig, T.L. Mega, X. Zhang, Interfacial nanobubbles are leaky: Permeability of the gas/ water interface, ACS Nano. 8 (2014) 6193−6201.

(203) B. Klein, M. Pawlik, Rheology modifiers for mineral suspensions, Mining, Metallurgy & Exploration. 22(2) (2005) 83-88.

(204) Z. Dai, J.A. Bos, P. Quinn, A. Lee, M. Xu, Flowsheet development for Thompson ultramafic low-grade nickel ores, In Proceedings of the 48th Annual Conference of Metallurgists of CIM. (2009) 217-228.

(205) P. Bonnissel-Gissinger, M. Alnot, J. Ehrhardt, P Behra, Surface oxidation of pyrite as a function of pH, Environ. Sci. Technol. 32 (1998) 2839−2845.

(206) R.F. Tabor, D.Y.C. Chan, F. Grieser, R.R. Dagastine, Anomalous stability of carbon dioxide in pH-controlled bubble coalescence. Angew. Chem. 123 (2011) 3516−3518.

(207) K. Fujisaki, M. El-Zahar, Flotation of waste activated sludge by use of carbon dioxide gas, In Proceedings of ENVIRO Conference (2002).

(208) J.F. Abrego, Carbon dioxide (CO_2) dissociation and capture by means of ultrasound and flotation cell, Journal of Applied Sciences Research. 6(5) (2010) 469-72.

(209) T. Kempka, M. Waschbüsch, T.M. Fernandez-Steeger, R. Azzam, Sorptive storage of CO_2 on coal dust and flotation waste from coal processing in abandoned coal mines, In EUROCK. (2006) 69-74.

(210) R.R.T. Dananjayan, P. Kandasamy, R. Andimuthu, Direct mineral carbonation of coal fly ash for CO_2 sequestration, J. of Cleaner Production 112 (2016) 4173-4182.

(211) C. Siriruang, P. Toochinda, P. Julnipitawong, S. Tangtermsirikul, CO_2 capture using fly ash from coal fired power plant and applications of CO_2-captured fly ash as a mineral admixture for concrete, J. of Environ. Management. 170 (2016) 70-78.

(212) K.S. Lackner, C.H. Wendt, D.P. Butt, E.L. Joyce Jr, D.H. Sharp, Carbon dioxide disposal in carbonate minerals, Energy. 20(11) (1995) 1153-1170.

(213) V. Núñez-López, E. Moskal, Potential of CO_2-EOR for near-term decarbonization, Frontiers in Climate, 1 (2019) 5.

(214) E.R. Bobicki, Q. Liu, Z. Xu, Effect of microwave pre-treatment on ultramafic nickel ore slurry rheology, Miners. Eng. Jun 1;61 (2014) 97-104.

(215) S. Khan, O.B. Wani, M. Shoaib, J. Forster, R.N. Sodhi, D. Boucher, E.R. Bobicki, Mineral carbonation for serpentine mitigation in nickel processing: a step towards industrial carbon capture and storage, Faraday Discussions. 230 (2021) 172-86.

(216) S. Yang, R. Pelton, C. Abarca, Z. Dai, M. Montgomery, M. Xu, J.A. Bos, Towards nanoparticle flotation collectors for pentlandite separation, Int. Journal of Miner. Processing. Sep 10;123 (2013) 137-44.

(217) E.R. Bobicki, Q. Liu, Z. Xu, Microwave treatment of ultramafic nickel ores: heating behavior, mineralogy, and comminution effects, Minerals. 8 (11) (2018) 524.

(218) P. Patra, T. Bhambhani, D. Nagaraj, P. Somasundaran, Impact of pulp rheological behavior on selective separation of Ni minerals from fibrous serpentine ores, Colloids Surf., A. 411 (2012) 24–26.

(219) Y. Yu, L. Ma, M. Cao, Q. Liu, Slime coatings in froth flotation: A review, Miner. Eng. Dec 1;114 (2017) 26-36.

(220) S. Uddin, S.R. Rao, M. Mirnezami, J.A. Finch, Processing an ultramafic ore using fiber disintegration by acid attack, Int. Journal of Miner. Processing. Jan 25;102 (2012) 38-44.

(221) R.C. Santana, J.A Ribeiro, M.A Santos, A.S. Reis, C.H. Ataíde, M.A. Barrozo, Flotation of fine apatitic ore using microbubbles, Separation and Purification Techno. Sep 19;98 (2012) 402-9.

(222) S.G. da Cruz, A.J. Dutra, M.B. Monte, The influence of some parameters on bubble average diameter in an electroflotation cell by laser diffraction method, Journal of environmental chemical engineering. Sep 1;4(3) (2016) 3681-7.

(223) C. Li, L. Dong, L. Wang, Improvement of flotation recovery using oscillatory air supply, Miner. Eng. Jan 15;131 (2019) 321-4.

(224) R. Ahmadi, D.A. Khodadadi, M. Abdollahy, M. Fan, Nano-microbubble flotation of fine and ultrafine chalcopyrite particles, Int. Journal of Mining Science and Technology. (2014) Jul 1;24(4) 559-66.

(255) F.C. Nogueira, O.M. Rodrigues, S.D. Nogueira, C.A. Pereira, Hydrophobic aggregation of galena fine particles. (2020).

(226) J. Rubio, H. Hoberg, The process of separation of fine mineral particles by flotation with hydrophobic polymeric carrier. International journal of mineral processing. Jan 1;37(1-2) (1993) 109-22.

(227) A. Makara, M. Smol, J. Kulczycka, Z. Kowalski, Technological, environmental and economic assessment of sodium tripolyphosphate production–a case study, Journal of Cleaner Production. Oct 1;133 (2016) 243-51

(228) N. Wang, H. Gao, J. Zhang, L. Li, X. Fan, X, Diao, Anticorrosive waterborne epoxy (EP) coatings based on sodium tripolyphosphate-pillared layered double hydroxides (STPP-LDHs), Progress in Organic Coatings. Oct 1;135 (2019):74-81.

(229) Y. Hu, L. Zhang, Y. Yi, I. Solangi, L. Zan, J. Zhu, Effects of sodium hexametaphosphate, sodium tripolyphosphate and sodium pyrophosphate on the ultrastructure of beef myofibrillar proteins investigated with atomic force microscopy, Food Chemistry. Feb 15;338 (2021) 128146.

(230) K. Gan, J. Xu, Y.J Gai, J.M. Wu, S.J. Li, Y.J. Lu, W.L Huo, X.Y. Zhang, J.L. Yang, In-situ coagulation of yttria-stabilized zirconia suspension via dispersant hydrolysis using sodium tripolyphosphate. Journal of the European Ceramic Society. (2017) Dec 1;37(15):4868-75.

(231) F. Rashchi, J.A. Finch, Polyphosphates: a review their chemistry and application with particular reference to mineral processing, Miner. Eng. Sep 1;13(10-11) (2000) 1019-35.

(232) I. Choi, Q. Zhong, Physicochemical properties of skim milk powder dispersions prepared with calcium-chelating sodium tripolyphosphate, trisodium citrate, and sodium hexametaphosphate, Journal of dairy science. Nov 1;103(11) (2020) 9868-80.

(233) Y. Wang, G. He, D. Abudukade, K. Li, T. Guo, S. Li, Z. Xiao, J. Wang, S. Nie, Selective inhibition of sodium tripolyphosphate on calcite in the process of magnesite flotation, Journal of Molecular Liquids. Jan 1;345 (2022) 117412.

(234) X. Wang, W. Jia, C. Yang, R. He, F. Jiao, W. Qin, Y. Cui, Z. Zhang, W. Li, H. Song, Innovative application of sodium tripolyphosphate for the flotation separation of scheelite from calcite. Minerals Engineering. Aug 15;170 (2021) 106981.

(235) J. Yao, B. Yang, K. Chen, H. Sun, Z. Zhu, W. Yin, N. Song, Q. Sheng, Sodium tripolyphosphate as a selective depressant for separating magnesite from dolomite and its depression mechanism, Powder Technol. Apr 1;382 (2021) 244-53.

(236) J.R. Van Wazer, C.F. Callis. Metal complexing by phosphates, Chemical Reviews. Dec 1;58(6) (1958) 1011-46.

(237) L. Zhang, X.Y. Guo, Q.H. Tian, D. Li, S.P. Zhong, H. Qin, Improved thiourea leaching of gold with additives from calcine by mechanical activation and its mechanism. Miner. Eng. 178 (2022) 107403.

(238) Y. Chen, G. Zhang, Q. Shi, S. Yang, D. Liu, M. Wang, Utilization of trisodium phosphate to eliminate the adverse effect of Mg2+ on the flotation of pyrite. Miner. Eng. May 1;150: (2020) 106281.

(239) S. Tan, Bruker D8 Discover XRD User's Guide. NanoScale, Fabrication, and Characterization Facility, University of Pittsburgh, US. (2009) 1-2.

(240) Malvern Zetasizer Nano User Manual. Malvern Instruments Ltd., Malvern United Kingdom. April (2013) MAN0485 Issue 1.1.

(241) iCAP 6000 Series ICP-OES Spectrometer Hardware Manual v3.5, Thermo Fisher Scientific. (2010).

(242) iCAP 6000 Series ICP-OES Spectrometer User Guide v2.0, Thermo Fisher Scientific. (2010).

(243) D.A. Skoog, F.J. Holler, S.R. Crouch, Atomic Emission Spectrometry: Chapter 10 in Principles of Instrumental Analysis, 6th Edition, Eds. Belmont, CA, USA. (2007) Pgs. 254-280.

(244) Y. Chen, G. Zhang, Q. Shi, S. Yang, D. Liu, Utilization of tetrasodium iminodisuccinate to eliminate the adverse effect of serpentine on the flotation of pyrite. Miner. Eng. May 1;150: (2020) 106235.

(245) Krotos Axis Ultra XPS description, XPS (Kratos Axis Ultra) General Experimental Parameters, The nanoFAB, University of Alberta.

(246) M. Alvarez-Silva, A. Uribe-Salas, K.E. Waters, J.A. Finch, Zeta potential study of pentlandite in the presence of serpentine and dissolved mineral species, Miner. Eng. Jan 1;85: (2016) 66-71.

(247) F.E. Bo, Y.P. Lu, Q.M. Feng, D.I. Peng, L.U. Na, Mechanisms of surface charge development of serpentine mineral. Transactions of Nonferrous Metals Society of China. Apr 1;23(4): (2013) 1123-8.

(248) M. Hodgson, G.E. Agar, Electrochemical investigations into the flotation chemistry of pentlandite and pyrrhotite: process water and xanthate interactions, Can. Metall. Q. 28 (3) (1989) 189–198.

(249) A.M. Kusuma, Q. Liu, H. Zeng, Understanding interaction mechanisms between pentlandite and gangue minerals by zeta potential and surface force measurements, Miner. Eng. Dec 1;69 (2014) 15-23.

(250) G. Zhao, X. Fang, Y. Zhang, Selective flotation of pyrite from serpentine using phytic acid as the depressant. Colloids and Surfaces A: Physicochemical and Engineering Aspects. Feb 5;658 (2023) 130703.

(251) J. Huang, Enhancing gold recovery from Nevada double refractory gold ores using a novel dual bubble generator (2018).

(252) P. Chen, X. Wu, J. Lin, K.L Tan, High H2 uptake by alkali-doped carbon nanotubes under ambient pressure and moderate temperatures. Science. Jul 2;285(5424) (1999) 91-3.

(253) X. Wang, Carbon dioxide assisted paraffinic froth treatment. Master Thesis, University of Alberta. (2020).

Appendix 1

CasaXPS data used to produce XPS plots for both the baseline and STPP case.

Quantification Report

/c:/Ultra/data/24374-Sep27_Nzube.dset — Sun Oct 8 22:27:45 2023

State : Angle Name : s1

Peak	Type	Position BE (eV)	FWHM (eV)	Raw Area (cps eV)	RSF	Atomic Mass	Atomic Conc %	Mass Conc %
Fe 2p	Reg	710.500	5.293	12079.7	2.957	55.846	0.79	2.46
O 1s	Reg	530.500	3.153	250099.4	0.780	15.999	59.65	53.03
C 1s	Reg	283.500	3.065	25940.0	0.278	12.011	16.08	10.73
Si 2p	Reg	101.500	2.821	18839.4	0.328	28.086	9.80	15.29
Mg 2p	Reg	48.500	2.678	13499.3	0.168	24.312	13.68	18.48

State : Angle Name : s2

Peak	Type	Position BE (eV)	FWHM (eV)	Raw Area (cps eV)	RSF	Atomic Mass	Atomic Conc %	Mass Conc %
Fe 2p	Reg	711.000	5.139	11715.8	2.957	55.846	0.72	2.26
O 1s	Reg	530.500	3.088	277087.8	0.780	15.999	62.11	55.79
C 1s	Reg	283.500	3.046	26465.9	0.278	12.011	15.42	10.40
Si 2p	Reg	101.500	2.760	18112.5	0.328	28.086	8.83	13.92
Mg 2p	Reg	48.500	2.724	13567.0	0.168	24.312	12.92	17.64

State : Angle Name : s3

Peak	Type	Position BE (eV)	FWHM (eV)	Raw Area (cps eV)	RSF	Atomic Mass	Atomic Conc %	Mass Conc %
Fe 2p	Reg	711.500	4.189	10831.2	2.957	55.846	0.91	3.00
O 1s	Reg	530.500	3.115	215807.3	0.780	15.999	65.64	62.25
C 1s	Reg	283.500	3.307	25171.5	0.278	12.011	19.30	14.16
Si 2p	Reg	101.500	2.492	7137.3	0.328	28.086	4.72	7.86
Mg 2p	Reg	48.500	2.607	6837.7	0.168	24.312	8.84	12.74

State : Angle Name : s4

Peak	Type	Position BE (eV)	FWHM (eV)	Raw Area (cps eV)	RSF	Atomic Mass	Atomic Conc %	Mass Conc %
Fe 2p	Reg	711.500	5.017	11259.5	2.957	55.846	1.06	3.33
O 1s	Reg	530.500	3.095	191957.8	0.780	15.999	65.75	59.22
C 1s	Reg	283.500	2.858	15597.3	0.278	12.011	13.88	9.59
Si 2p	Reg	101.500	2.871	10263.3	0.328	28.086	7.64	12.08
Mg 2p	Reg	48.500	2.588	8016.4	0.168	24.312	11.67	15.97

State : Angle Name : s5

Peak	Type	Position BE (eV)	FWHM (eV)	Raw Area (cps eV)	RSF	Atomic Mass	Atomic Conc %	Mass Conc %
Fe 2p	Reg	712.000	4.036	11608.8	2.957	55.846	1.01	3.23
O 1s	Reg	530.500	3.117	215956.2	0.780	15.999	68.09	62.68
C 1s	Reg	284.000	3.016	18459.2	0.278	12.011	15.13	10.45
Si 2p	Reg	101.500	2.762	10513.2	0.328	28.086	7.21	11.64
Mg 2p	Reg	48.500	2.671	6398.1	0.168	24.312	8.57	11.99

State : Angle Name : s6

Peak	Type	Position BE (eV)	FWHM (eV)	Raw Area (cps eV)	RSF	Atomic Mass	Atomic Conc %	Mass Conc %
Fe 2p	Reg	711.500	6.666	14800.8	2.957	55.846	0.92	2.86
O 1s	Reg	530.500	3.084	265290.9	0.780	15.999	60.21	53.45
C 1s	Reg	284.000	3.030	26696.8	0.278	12.011	15.75	10.50
Si 2p	Reg	101.500	2.777	19559.0	0.328	28.086	9.65	15.04
Mg 2p	Reg	48.500	2.775	13957.2	0.168	24.312	13.46	18.16

Appendix 2

CasaXPS data used for the XPS results of CO_2 case.

Quantification Report

/c:/Ultra/data/24374-Sep27_Nzube.dset Sun Oct 8 22:31:03 2023

State : Angle Name : s7

Peak	Type	Position BE (eV)	FWHM (eV)	Raw Area (cps eV)	RSF	Atomic Mass	Atomic Conc %	Mass Conc %
Na 1s	Reg	1070.000	1.887	1896.5	1.685	22.990	0.23	0.32
Fe 2p	Reg	711.000	6.418	13348.7	2.957	55.846	0.80	2.73
O 1s	Reg	530.500	3.252	215870.0	0.780	15.999	47.31	45.94
C 1s	Reg	284.000	3.379	62873.1	0.278	12.011	35.82	26.11
Si 2p	Reg	101.500	3.014	14100.8	0.328	28.086	6.72	11.45
Mg 2p	Reg	48.500	2.940	9784.3	0.168	24.312	9.11	13.45

State : Angle Name : s8

Peak	Type	Position BE (eV)	FWHM (eV)	Raw Area (cps eV)	RSF	Atomic Mass	Atomic Conc %	Mass Conc %
Na 1s	Reg	1070.000	2.663	7357.5	1.685	22.990	0.84	1.08
Fe 2p	Reg	712.500	4.740	12419.9	2.957	55.846	0.71	2.21
O 1s	Reg	530.500	3.143	278539.6	0.780	15.999	57.53	51.56
C 1s	Reg	284.000	3.323	34016.5	0.278	12.011	18.26	12.29
Si 2p	Reg	101.500	2.816	21026.6	0.328	28.086	9.44	14.85
Mg 2p	Reg	48.500	2.652	15067.9	0.168	24.312	13.22	18.01

State : Angle Name : s9

Peak	Type	Position BE (eV)	FWHM (eV)	Raw Area (cps eV)	RSF	Atomic Mass	Atomic Conc %	Mass Conc %
Na 1s	Reg	1070.500	3.124	9367.0	1.685	22.990	0.98	1.24
Fe 2p	Reg	710.500	5.878	18215.2	2.957	55.846	0.94	2.32
O 1s	Reg	530.500	3.126	307093.2	0.780	15.999	57.32	51.36
C 1s	Reg	284.000	3.138	34940.4	0.278	12.011	17.13	11.40
Si 2p	Reg	101.500	2.854	23807.6	0.328	28.086	9.76	15.19
Mg 2p	Reg	48.500	2.702	16558.5	0.168	24.312	13.27	17.88